PARTICULATE AND GAS PHASE HYDROCARBON EMISSIONS FROM PARTIALLY PREMIXED LOW TEMPERATURE COMPRESSION IGNITION COMBUSTION OF BIODIESEL

by

William F. Northrop

A dissertation submitted in partial fulfillment
of the requirements for the degree of
Doctor of Philosophy
(Mechanical Engineering)
in the University of Michigan
2010

Doctoral Committee:

Professor Dionissios N. Assanis, Co-Chair
Associate Research Scientist Stani V. Bohac, Co-Chair
Professor Volker Sick
Professor Phillip E. Savage
Patrick G. Szymkowicz, General Motors Corporation

2010

ACKNOWLEDGMENTS

As with most achievements in life, the work required to complete a doctorate requires help from many people and forces. My successful journey though the process has been assisted greatly first from the mentorship and support of my advisor and co-chair Professor Dennis Assanis. I greatly appreciate his confidence in my work which gave me the freedom to explore research topics on my own while maintaining overall attention to my decisions. I would also like to acknowledge my co-chair and friend Dr. Stani Bohac. With his day-to-day guidance, I was able to more smoothly navigate the waters of university research. Stani's attention to detail has been a fantastic counter-point to my more broad perspective allowing our collaborative work to develop into the high quality research presented in this dissertation. My colleagues in the WE Lay Auto Lab have also provided support, friendship and camaraderie during my tenure. I would like to especially recognize Praveen Madathil for his direct help in the laboratory during the taking of crucial data needed for this study.

I would like to acknowledge the General Motors and University of Michigan Collaborative Research Laboratory (CRL) for the financial support required for my research. The feedback of the General Motors R&D Diesel Team has also been crucial for guiding my work technically. Specifically, Patrick Szymkowicz has been consistently helpful in both developing my research direction and in critiquing my results. Additional support for the research presented in this dissertation came from the University of

Michigan, School of Public Health. The research group of Prof. Stuart Batterman helped to develop methods for measurement of organics on particulate and in concentrating extracted samples from the Soxhlet procedure. Also, thanks goes to the US-EPA National Vehicle and Fuel Emissions Laboratory in Ann Arbor for allowing me to use their micro-balance and clean room for conducting the gravimetric analysis presented in this study.

I'd like to recognize my family for supporting me both materially and emotionally during my doctoral work. My parents, Jim and Linda Northrop were instrumental in helping me get through difficult personal times in pursuit of my degree. My brother Ben and sister-in-law Leah have also been incredibly supportive throughout. My dog Owen deserves special recognition as he has been a constant source of companionship and unwavering positivity during my graduate studies. I would finally like to acknowledge my wife Alyssa whom I met during the course of my time at University of Michigan. Our shared love and deep commitment to learning has given me a new appreciation of life and my work considerably more meaning.

TABLE OF CONTENTS

LIST OF FIGURES

LIST OF TABLES

ABBREVIATIONS

ATDC	After Top Dead Center
B__	__% by volume biodiesel
B50SWE	50% by volume biodiesel mixed with SWE
B50ULSD	50% by volume biodiesel mixed with ULSD
BC	Black Carbon
BMEP	Brake Mean Effective Pressure
BSFC	Brake Specific Fuel Consumption
BTDC	Before Top Dead Center
CA	Crank Angle
CA__	Crank Angle of __% Mass Fraction Burned
CN	Cetane Number
DCM	Dichloromethane
DMS	Differential Mobility Spectrometer
DOC	Diesel Oxidation Catalyst
DR	Dilution Ratio
EC	Elemental Carbon
ECU	Electronic Control Unit
EGR	Exhaust Gas Recirculation
EI	Emissions Index
ELPI	Electrical Low-Pressure Impactor
ELTC	Early injection Low Temperature Combustion
FAME	Fatty Acid Methyl Ester
FE	Fuel Economy
FID	Flame Ionization Detector
FSN	Filter Smoke Number
FT-IR	Fourier Transform Infra-Red
GC-FID	Gas Chromatograph using a Flame Ionization Detector
GHSV	Gas Hourly Space Velocity
HC	Hydrocarbon
HCCI	Homogeneous Charge Compression Ignition
IMEP	Indicated Mean Effective Pressure
LHC	Light Hydrocarbons
LHV	Lower Heating Value
LLTC	Late injection Low Temperature Combustion
LOF	Light Organic Fraction of gaseous THC
LTC	Low Temperature Combustion
LTHR	Low Temperature Heat Release
MEP	Mean Effective Pressure

MPG	Miles per gallon
NMOG	Non-Methane Organic Gases
NO_X	Nitrogen Oxides (NO + NO2)
OC	Organic Carbon
OCEC	Organic Carbon versus Elemental Carbon
PAH	Polycyclic Aromatic Hydrocarbons
PM	Particulate Matter
RFS	Renewable Fuels Standard
RME	Rapeseed-derived Methyl Ester
RoHR	Rate of Heat Release
SME	Soybean-derived Methyl Ester
SOC	Start of Combustion
SOF	Soluble Organic Fraction of PM
SOI	Start Of Injection
SWE	Swedish diesel fuel
TDC	Top Dead Center
THC	Total Hydrocarbons
TOA	Thermal Optical Analyzer
TOF	Total Organic Fraction of PM
UHC	Unburned Hydrocarbons
ULSD	Ultra Low Sulfur Diesel fuel
US-EPA	United States Environmental Protection Agency
VGT	Variable Geometry Turbine
VOC	Volatile Organic Compounds

ABSTRACT

The research presented in this document examines the results of melding three diesel engine emissions reduction methodologies: partially premixed low temperature combustion (LTC); the use of alternative, biodiesel fuel; and aftertreatment using a diesel oxidation catalyst (DOC). It shows how alternative fuels and novel combustion strategies complement each other on one hand and create new emissions challenges on the other.

Partially premixed LTC simultaneously reduces soot and NO_X emissions for both biodiesel and petroleum diesel fuels. The use of biodiesel in LTC has added benefits of lowering total hydrocarbon (THC) and CO emissions and reducing soot emissions to near undetectable levels. Light hydrocarbon species like ethylene emitted from biodiesel LTC as a fraction of THC are higher independent of ignition delay indicating that biodiesel burns more completely and results in less unburned hydrocarbon (UHC) emissions than petroleum diesel. However, the generally higher gas-phase UHC emissions from LTC compared to conventional combustion results in excessive particulate matter (PM) for biodiesel due to heterogeneous condensation of methyl esters onto soot particles after dilution with atmospheric air. In the work presented here, this condensation process resulted in over an order of magnitude increase in PM emissions for B100 in a late injection LTC condition (LLTC) compared to petroleum-derived fuels. For an early injection LTC (ELTC) condition, PM emissions were almost 100 times higher than the diesel fuels tested. Low vapor pressure methyl esters making up biodiesel have a near

95% conversion from the gas to the particle phase with an undiluted exhaust UHC concentration of 1000 ppm for a 10:1 dilution ratio and 47°C collection temperature.

Although the use of biodiesel in LTC increases PM emissions significantly following dilution of the raw exhaust, the results of this work indicate that 80% of UHC in the exhaust is oxidized by a standard DOC with inlet temperature of 240°C. Unfortunately, the remaining unburned biodiesel left unconverted still significantly contributes to the PM following dilution. Methyl esters were found to be the primary species contributing to the higher total organic fraction (>90%) on the PM for biodiesel compared with diesel LLTC following a DOC.

CHAPTER ONE

INTRODUCTION

1.1 Motivation

Internal combustion engines are a ubiquitous force in the everyday life of humanity as we know it today. The conversion of stored chemical energy contained in fuels through heat to produce mechanical work allows the mechanization of society at power levels in Watts from one to one million. Although their practical use has been well established for well over one hundred years, the complexity of engines provides an ongoing challenge to scientists and engineers to this day.

With inherently high thermal efficiency, ability to burn heavier fuels than gasoline, excellent durability and high torque capability, diesel-fueled compression ignition engines have a multitude of practical uses. In 2008, the United States consumed over 60 billion gallons of diesel fuel (EIA, 2009) in diverse applications such as agriculture, construction, industrial, marine, and on-highway applications. Projections are that diesel fuel use will continue to grow, especially if more passenger cars start to utilize diesel engines to improve fuel economy.

Scientists in recent years have concluded that the increasing atmospheric concentration of anthropogenic carbon emissions from sources including fossil fuel-

burning engines have a direct impact on the climate of the earth (IPCC, 2007). Logically, partially replacing gasoline engines with more efficient diesel engines would help in the global effort to reduce CO_2 emissions from engine-related sources, particularly in the transportation sector. However, concerns over high emissions of species like oxides of nitrogen (NO_X), volatile organic compounds (VOCs), CO and particulate matter (PM) have restricted more widespread growth of diesel engines. Such species are harmful to both humans and the environment and are therefore regulated by agencies like the United States Environmental Protection Agency (US-EPA).

NO_X includes the chemical species NO and NO_2 produced at high temperatures in the combustion chamber from both N_2 in the air used by the engine and sometimes from fuel-borne nitrogen. In the atmosphere, NO and NO_2 are in thermodynamic equilibrium depending on the amount of solar irradiation. NO_X reacts with moisture in the air and other species to eventually form nitric acid, one of the most water soluble gases found the atmosphere thus contributing to acid rain. NO_X also reacts with VOCs via the OH radical in the atmosphere in the presence of sunlight to make troposphere ozone, more commonly known as smog. Ground level ozone has been definitively linked with respiratory disease in humans.

VOCs are organic chemical compounds that have high enough vapor pressures under normal conditions to significantly vaporize and enter the atmosphere. They are also defined by having low water solubility. The US-EPA defines a VOC as “any organic compound that participates in atmospheric photochemical reactions except those designated by the EPA as having negligible photochemical reactivity” (US-EPA 40 CFR Part 51.100). Important gaseous species from diesel combustion related to incomplete

combustion that fall outside the definition include hydrocarbons like methane (CH_4) and ethane (C_2H_6), inorganic carbon species like carbon monoxide (CO) and carbon dioxide (CO_2), and hydrogen (H_2). These unregulated species are also investigated in this work. All organic species with low carbon number including CH_4 and VOCs are termed light hydrocarbons (LHC) for the purposes of this study.

Not only do some LHCs originating from incomplete combustion in diesel engines photochemically react with NO_X in the atmosphere to form smog, they can be harmful in their own right. They are generally produced by diesel engines as a byproduct of incomplete combustion of fuel or from the engine lubricant. Methane is the most common LHC in the atmosphere and is known to be an efficient greenhouse gas. Benzene, a cyclic hydrocarbon byproduct of combustion is a known human carcinogen. Other LHCs from diesel combustion like formaldehyde and 1,3 butadiene are probable human carcinogens according to the California Air Resources Board (Seinfeld, 1996, pp. 110).

CO is not defined as a VOC since it is not considered to be photochemically reactive though it is formed from similar processes in diesel engines. However, it is toxic to humans where it forms a stable complex of carboxyhemoglobin in red blood cells, prohibiting the delivery of oxygen to the body. Concentrations of 600 ppm can cause death in humans in as little as ten hours of exposure (Seinfeld, 1986, pp.85).

PM includes all solid and liquid-phase compounds, except water, in the atmosphere. Diesel engines emit PM as both carbonaceous soot and organic species forming mainly from rich partial combustion processes and from collection on established particle nuclei

in the exhaust. The health effects of particulates are many and sometimes proceed through complex pathways. Although PM from engines is generally regulated on a mass basis, its health effects are more dependent on the size of the particle. The size ranges of particles are defined in many different ways. Figure 1.1 graphically shows how different types of particles compare in terms of their size in a figure adapted from Eastwood (2008, pp. 26). In the discussion of PM emissions, the terminology PM2.5 and PM10 are generally used to define particles of size 2.5 μm and smaller and 10 μm and smaller respectively. Nanoparticles are defined as those with diameters less than 100 nm. High pressure diesel fuel injectors generate particles from 1 to over 200 μm, orders of magnitude larger than the PM created by the combustion process they enable.

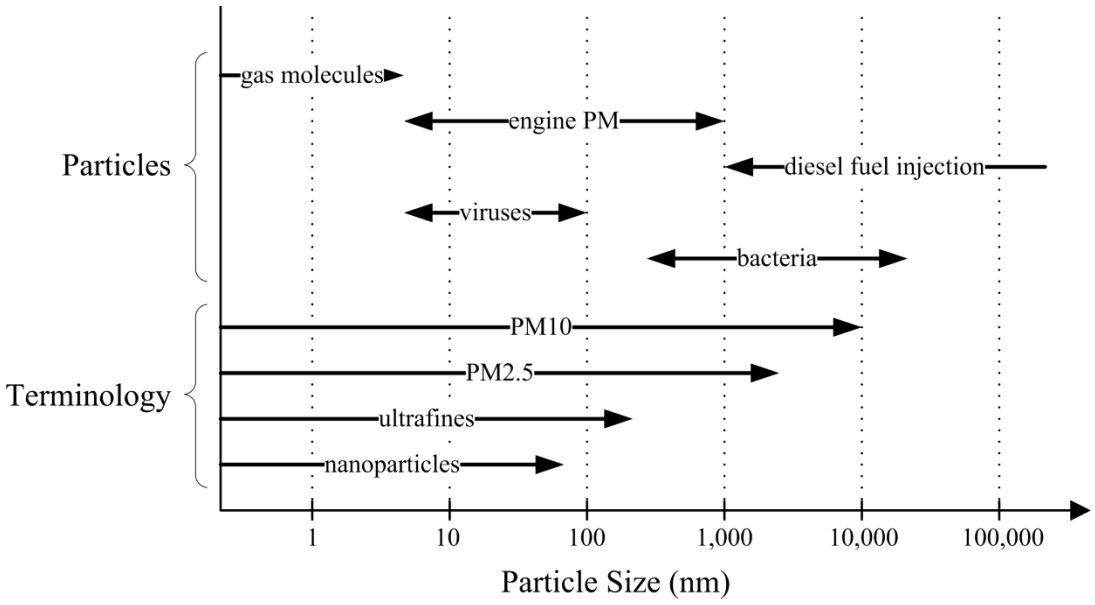

Figure 1.1: Terminology of particle size ranges and sizes of common PM compared with electromagnetic wavelengths adapted from Eastwood (2008, pp. 26).

Risk to human health from PM depends heavily upon the point of deposition in the respiratory tract. Smaller particles like ultrafines are generally deposited via diffusion and larger particles by sedimentation or inertia (Eastwood, 2008) leaving a middle region of

particle size from about 100 – 1000 nm where less deposition occurs. Smaller particles generally go deeper into the respiratory system where they have been shown to have mutagenic effects. Larger particles which deposit in the upper respiratory tract have been proven to contribute to bronchitis and asthma among other ailments. PM from diesel engine emissions has also been implicated in cardiovascular illness (Seaton et al., 1995) prompting investigation into further reduction in ultrafine particles.

Regulations have been enacted worldwide to enforce the limitations on the amount of NO_X, VOCs, CO and PM that can be emitted by vehicles. The US-EPA Tier 2 Bin 5 emissions rule in effect for passenger car vehicles from the model year 2007 is an example of such a regulation. Jacobs (2005) summarized the allowed emissions levels succinctly by expressing the regulated grams of pollutant, i per mile (S_i) in terms of emissions index (EI_i) given in grams of pollutant emitted per kilogram of fuel used in an engine as given in Equation 1.1.

$$EI_i\left(\frac{g}{kg\text{-}fuel}\right)=S_i\left(\frac{g}{mile}\right)FE\left(\frac{mile}{gallon}\right)\frac{1}{3.785}\left(\frac{gal}{liter}\right)\frac{1}{\rho_{fuel}}\left(\frac{L}{kg}\right) \quad (1.1)$$

Based on Equation 1.1, the regulated emissions in EI for various vehicle fuel economy (FE) values in miles per gallon (MPG) are shown in Table 1.1 for the Tier 2 Bin 5 regulation. Although meeting government emissions targets is not the goal of this work, the values in Table 1.1 are useful numbers for putting emissions data presented later into a more practical perspective. For this regulation, total hydrocarbon (THC) emissions are categorized as non-methane organic gases (NMOG). This captures all hydrocarbons excluding methane for which no significant human health effects have been reported.

Table 1.1: Regulated EI emissions based on the US-EPA Tier 2 Bin 5 standards per vehicle fuel economy from Equation 1.1 with ρ_{fuel} = 0.81 kg/liter.

MPG	NMOG	CO	NO_X	PM
25	0.72	33.45	0.56	0.08
30	0.86	40.14	0.67	0.10
35	1.00	46.83	0.78	0.11
40	1.15	53.52	0.89	0.13
45	1.29	60.22	1.00	0.14

Harmful emissions reductions in diesel engines can be achieved in three primary ways: by eliminating them from the exhaust using aftertreatment systems; by reducing the formation of species during combustion; or by using an alternative fuel. Installing catalytic aftertreatment devices in the exhaust of spark-ignited engines has proven to be a simple and relatively cost effective method for emissions reduction. Since the advent of the three-way catalyst, only one reactor is needed to eliminate NO_X, THC and CO simultaneously provided the engine fuel to air mixture remains approximately stoichiometric. Diesel engines inherently operate fuel-lean of stoichiometric and cannot utilize a three-way catalyst. Current technology requires a series of reactors to remove the desired species. One example of such a system used by engine manufacturers includes a diesel oxidation catalyst (DOC) which can be used to convert hydrocarbon species and CO, a urea selective catalytic reduction reactor can then be installed to reduce NO_X to N_2 and finally a diesel particulate filter can be used to remove PM. Many variations of aftertreatment systems have been proposed (Majewski and Khair, 2006) and some have been implemented in production vehicles with considerable success though they have proven to be quite costly to implement in practice.

As an alternative to treating the exhaust, eliminating or reducing the production of harmful species during combustion is an attractive option for emissions reduction. Advanced technologies like high-pressure injection systems, optimized combustion chamber design, cooled exhaust gas recirculation (EGR) and turbocharging have enabled the exploration of novel combustion regimes not possible in the early days of diesel engines. Partially premixed low temperature combustion (LTC), the methodology described in this work, utilizes recent advancements in engine design to simultaneously reduce NO_X and PM. LTC is not without downsides since CO and THC emissions are generally higher than for conventional combustion and the speed and load range of operation is limited.

Utilizing alternative fuels is a third method for reducing harmful emissions from diesel engines. Biodiesel, the fuel explored in this work, is a fatty acid methyl ester (FAME) produced from natural oil sources and has been shown to reduce many pollutants from diesel engines such as CO, THC and PM (Agarwal,2006, Lapuerta et al., 2008). Most reductions in emissions from the use of biodiesel are assumed to be due to the oxygen contained in the fuel providing oxidant in fuel rich areas of the combustion chamber. Biofuels, including biodiesel, have an additional benefit of reducing overall CO_2 emissions of an engine since a portion of the fuel can be made from renewable sources.

Government regulations have been put in place to encourage the production of biofuels. In the United States, the Renewable Fuels Standard (RFS) originally established by Congress in 2005 and later expanded in 2007 (US-EPA 40 CFR Part 80) requires that 13 billion gallons of renewable fuels be blended into petroleum motor vehicle fuels,

including diesel and gasoline-like products by 2019 increasing to 36 billion gallons in 2022 which accounts for almost 25 percent of fuel production in the United States based on today's consumption levels (EIA, 2009). A revision to the RFS was proposed in 2009 (US Federal Register Vol. 74 No. 99) to better define the renewability of biofuels meeting the standard. Under this new standard, "biomass-based diesel" includes biodiesel and is mandated to reduce greenhouse gas emissions by 50% from the baseline petroleum diesel fuel it replaces. The impetus for a revised standard reveals a disadvantage of biodiesel as it is currently produced since considerable energy from non-renewable sources is required in its manufacture. Current studies place biodiesel between 22% reduction in GHG emissions from the baseline fuel (EPA, 2009) to 80% (Biodiesel Board, 2009). Regardless of how it is manufactured, biodiesel use is increasing. The revised RFS mandates fuel suppliers in the US blend 0.71% biodiesel into diesel fuel by 2010 accounting for approximately 426 million gallons of total biodiesel use based on 2008 consumption figures. Europe has also adopted aggressive goals to implement renewable fuels. Current standards mandate reaching a minimum of 5.75% biofuels by 2010 of which most is estimated to be biodiesel (Bozbas, 2008) since over 50% of European passenger cars are diesel-powered (Palmen, 2007).

The work presented in this dissertation examines the results of melding the three emissions reduction methodologies described above. In implementing biodiesel with partially premixed LTC strategies and aftertreatment, this research examines how an alternative fuel and novel combustion strategies complement each other on one hand and create new emissions challenges on the other. The work shows that the development of new fuels cannot be considered completely independently of the engine they enable. As

Lyle Cummins eloquently states in *Internal Flame* (Cummins, 1989), engine researchers face a “challenge in a real liquid fuel energy shortage that will come within the lifetime of many now living. As we plunge into the seeking of solutions to our dilemma, we must never forget that an engine and the fuel it consumes are inseparable partners; the one cannot progress without the full cooperation from the other."

1.2 Conventional Diesel Combustion

The ideal constant pressure engine cycle was conceived by Rudolf Diesel more than 100 years ago. Unlike previous engine concepts, Diesel's "Rational Motor" was designed entirely using thermodynamic principles before a prototype was constructed. By utilizing near constant pressure combustion in the expansion stroke, Diesel hoped to more closely realize the ideal Carnot Cycle (Diesel, 1897) to improve the thermal efficiency of engines. To achieve this goal, a slow diffusion burn process was conceived where fuel is injected into the cylinder as combustion occurs.

The progression of conventional diesel engine combustion can be described in the following manner. First, fuel is injected into the combustion chamber near top dead center of the compression stroke there mixing with the surrounding air and residual combustion products from the last cycle. This fuel is highly atomized and partially vaporizes. Since the surrounding gases are near or above the auto-ignition point of the fuel-air mixture, combustion begins within a few crank angle degrees. The combustion and continuing compression of the gases in the cylinder further evaporate the fuel spray and fuel continues to mix and burn. All of the fuel proceeds through injection, mixing and combustion until it is completely expended.

There are many advantages of the diesel process with comparison to that of spark-ignited engines. Firstly, there is no knock limitation since fuel is injected very shortly before combustion begins. Therefore, higher compression ratios can be used in diesel engines increasing thermal efficiency. Also, since the desired load of the engine is controlled by the amount of fuel injected per cycle, the mass of air in the cylinder for a given engine speed is almost constant. This requires lower pumping work at part load compared with spark-ignited engines which use a throttle to lower the mass of premixed fuel and air allowed into the cylinder to control load.

Diesel engines are also more suited towards turbocharging due to the elimination of the throttle valve thus more effectively increasing cycle efficiency. Naturally aspirated diesel engines are limited in maximum mean effective pressure (MEP) due to the limited time available to completely combust large quantities of fuel. If the injection process lasts too long, smoke emissions will increase. Increasing cylinder pressure by turbocharging allows a higher rate of mixing and more fuel to be burned thus directly altering the torque output of the engine. Finally, since the diesel engine always operates with globally lean equivalence ratio, the effective value of the ratio of specific heats (λ) over the expansion process is larger than for spark ignited engines. This has the effect of increasing fuel conversion efficiency for a given expansion ratio.

Achieving rapid mixing is the most difficult challenge of diesel engines since this controls the burning rate of the fuel. At maximum rated power, the mean piston speed of large and small diesel engines is approximately the same. Thus for a fixed crank angle interval allowed for combustion, the time required for mixing is proportional to the

stroke. In small direct injection engines, the mixing is greatly enhanced by creating swirl in the combustion chamber and by increasing the injection pressure to improve atomization of the fuel to account for the shorter allowable time.

The diesel combustion process can be described by four primary events (Heywood, 1988). Ignition delay describes the time from the start of injection (SOI) of fuel into the cylinder to the start of combustion (SOC). For the work described here, SOC is defined as the crank angle degree that the apparent rate of heat release (RoHR) crosses the x-axis of a heat release rate versus crank angle plot. The second stage is the premixed combustion phase. During this time in the cycle, fuel that has mixed with air within flammability limits combusts. This is generally a rapid event and, for conventional diesel combustion, occurs faster than the time required to mix the remaining fuel. This leads to the third stage of combustion, the diffusion burn or mixing-controlled phase. The rate of combustion here is primarily controlled by the rate at which fuel is vaporized and mixes with air. The late combustion phase is when residual fuel pockets continue to burn and soot created in the earlier stages oxidizes. As the temperature of the gases fall during expansion, the rate of late combustion decreases.

Dec et al. (1997) in often-cited work further solidified understanding of the stages of diesel combustion using optical methods. In their work, they identified when the formation of soot and oxides of nitrogen (NO_X) occurred in the diesel flame. By looking at the period from the time fuel injection began to when it ended, they were able to gain new insight into ignition delay and premixed combustion through the early stages of diffusion burn. They devised a schematic, shown in Figure 1.2 that illustrates where soot

and NO_X creation zones are located. During premixed combustion both just as the injected fuel begins to burn and also during any premixed burning occurring during the mixing controlled phase of combustion, the mixture has a very high equivalence ratio and therefore does not tend to generate NO_X by either thermal or prompt mechanisms. However, NO_X is formed on the periphery of the diffusion flame where temperatures are high due to near-stoichiometric combustion as shown in the figure.

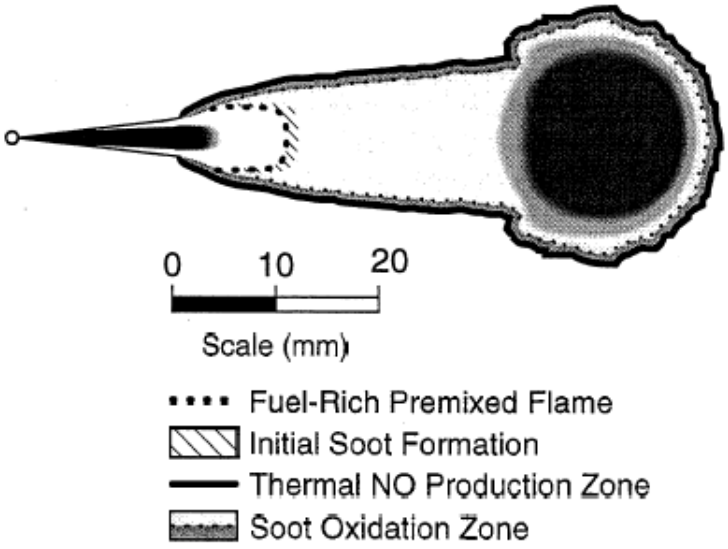

Figure 1.2: Illustration from Dec et al. (1997) showing the regions of soot and NO_X production in diesel combustion

Soot formation occurs downstream of the standing premixed flame just behind the fuel jet. Here, rich combustion products break down into precursor species leading to the inception of carbonaceous particles. Soot oxidation is also thought to occur during the diffusion burn phase along the outside of the flame where oxygen is present and temperatures are high enough to promote pyrolysis reactions.

HC and CO are created as a result of incomplete combustion and are mainly created in over-lean and over-rich zones of the flame (Turns, 1996, pp.488). Fuel lean areas located on the periphery of the diffusion flame have O_2 concentrations greater than the flammability limits and therefore do not burn completely. Over-rich areas in the center of the diffusion flame have inadequate O_2 to consume all the fuel, creating products of partial oxidation.

Fuel properties have a significant impact on diesel combustion. Density, vaporization range, and viscosity are among the important factors. Since the processes described above all depend on the mixing of the injected fuel with the air and residual gases present in the cylinder, the penetration, spray particle size distribution and volatility of the fuel can impact ignition and the resulting combustion processes. It is desirable to have consistent properties of fuels such that engine performance and emissions do not suffer.

Fuel chemical composition is even more important than physical properties when considering the ignition characteristics of a fuel. Large straight-chain paraffins, like n-alkanes have the highest ignition quality which increases with hydrocarbon chain length. Aromatic species like benzene and alcohols lower the ignition quality (Gülder et al., 1985).

The cetane number (CN) is a useful property that indicates the ignition quality of a fuel. It is determined by comparing the ignition delay of a fuel to a primary reference fuel on a standardized test engine. Using this single metric the CN is a concise parameter for categorizing the ignition characteristics of a fuel taking into account its diverse chemical makeup.

1.3 Premixed Low Temperature Combustion

One classical feature of diesel combustion is the soot-NO_X tradeoff. Soot and NO_X are the primary emissions from conventional diesel combustion as mentioned in Section 1.2 and arise primarily during the mixing controlled phase. In conventional combustion, it is generally found that any decrease in NO_X emissions leads to an increase in soot emissions and vice versa. For example, advancing injection timing tends to increase the premixed burn portion of combustion thus creating higher temperature conditions needed for NO_X formation. This increased premixing however lowers the fraction of over fuel-rich areas in combustion, reducing soot formation.

As a more complex example of this tradeoff, increasing EGR increases the heat capacity of the mixture in the combustion chamber and reduces the overall combustion temperature, decreasing NO_X. Further, ignition delay is increased with increasing EGR allowing more mixing which alone would cause a lowering of local equivalence ratios. However, dilution with EGR lowers O_2 concentration and tends to counter that effect where mixing-controlled combustion is still present. This can raise local equivalence ratios creating more soot. Recent work has shown that by extending ignition delay such that the mixing controlled phase is eliminated, the soot versus NO_X tradeoff can be largely avoided (Jacobs, 2007). This concept sets the foundation for diesel premixed low temperature combustion (LTC).

Kamimoto and Bae (1996), in shock-tube experiments, explored the dependency of soot and NO_X on temperature and local equivalence ratio (φ) opening up the idea that diesel combustion could have simultaneously low soot and NO_X. In their work, they

showed that soot formation does not occur due to active fragmentation at temperatures over 2600 K. They also found that there is a high temperature, fuel-rich regime in which thermal NO_X is not produced due to lack of oxygen. By looking at diesel combustion in a φ-T space it is possible to identify regions where neither soot nor NO_X are present. Figure 1.3 shows a φ versus temperature plot adapted from Kook et al. (2005) where the shaded region 1 is the high temperature diesel combustion mode identified by Kamimoto and Bae.

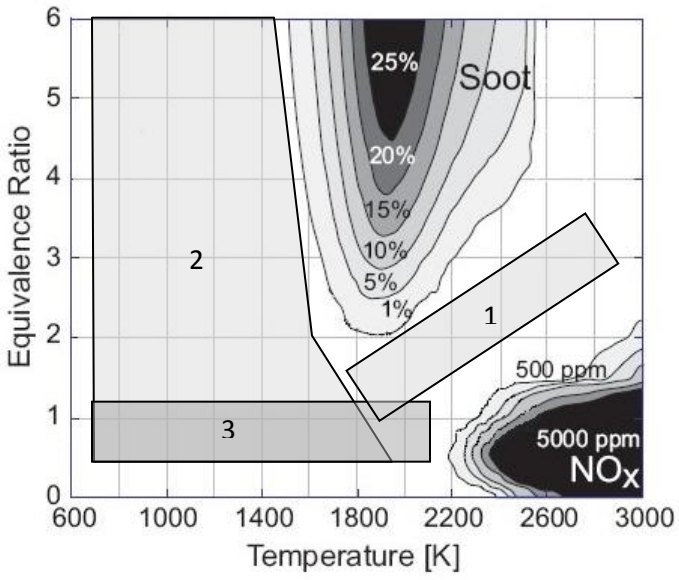

Figure 1.3: Local φ versus temperature plot with soot and NO_X islands adapted from Kook et al. (2005). Numerical values from Kitamura et al. (2002) from numerical simulation of n-heptane and air at 6 MPa and a residence time of 2 ms. Region 1- high temperature smokeless combustion from Kamimoto and Bae (1996), Region 2- Premixed low temperature combustion, Region 3 – HCCI combustion

Other researchers like Akihama et al. (2001) and Kimura et al. (2001) experimented with a region of combustion at lower temperature. They found that by increasing the EGR rate and retarding injection timing, ignition delay increased and combustion was primarily premixed with little diffusion burn. The increased ignition delay helped to

improve air and fuel mixing prior to combustion and to avoid high flame temperature regions. The high dilution caused by heavy EGR also contributed to lower temperature combustion. Region 2 in Figure 1.3 shows the premixed low temperature combustion region on the φ versus temperature plot. Akihama et al. deduced that this mode of combustion can be achieved at a wide range of global equivalence ratios. Jacobs et al. (2005) experimented with both lean and rich premixed low temperature strategies and maintained simultaneously low soot and NO_X for both.

Homogeneous charge compression ignition (HCCI) engines can also operate in a region where soot and NO_X are simultaneously reduced. This type of combustion premixes fuel and air in the intake manifold or injects fuel into the combustion chamber early in the compression stroke, allowing fuel and air adequate time to completely mix. It results in a very narrow band of φ in the fuel-lean regime during combustion and a wide range of temperature as is shown in region 3 on Figure 1.3. By advancing fuel injection timing very early in the compression stroke, Kimura et al. (1999) showed that a NO_X could be reduced by 98% compared with conventional diesel combustion at low load. Disadvantages of the early injection strategy include extremely high HC and CO emissions compared with the late injection strategy due to fuel wall wetting (Shimazaki et al., 2007) and practical limitations on load due to excessive combustion noise and the potential of diesel knock.

Modes of LTC discussed here are centered on those illustrated by region 2 in Figure 1.3 where fuel is injected in the range of top dead center (TDC) to 40° BTDC. Early strategies within this range like that described by Lechner et al. (2005) allow for a greater

amount of mixing before combustion occurs but have less control over the location of peak pressure, limiting the maximum load they can attain. With injection timing retarded to near TDC, more control over combustion phasing can be attained. Late LTC strategies like those developed by Kimura et al. (2001) utilize high injection pressures and lowered compression ratio to slow ignition delay such that adequate premixing can occur.

The criteria for developing premixed LTC, although appearing simple from Figure 1.3, are complex in practice since local temperatures and φ in the cylinder are not typically measured. EGR rate is the key enabler of LTC development and is an easier parameter to measure using standard emissions equipment. One way to identify the LTC region is to observe the trends in soot and NO_X emissions as EGR changes. LTC is identified by observing that both species decrease with an increase in EGR rate, thus defeating the soot versus NO_X tradeoff.

A more concise criterion for the development of premixed LTC is to control ignition delay to be longer than injection duration (Kimura et al, 2002). By accomplishing this, the diffusion burn portion is generally reduced considerably and combustion is primarily premixed. Ignition delay and premixed combustion can be easily identified on a rate of heat release and injection current versus crank angle plot.

The use of early and late LTC strategies is limited by engine load. The early LTC condition is restricted to low loads since as fueling rate increases, peak cylinder pressure and temperature become very high near TDC and danger of incurring diesel knock occurs. Late injection LTC can be used at higher loads since combustion is more retarded away from TDC. As the fueling rate continues to increase for a given speed, late LTC is

more difficult to attain since it becomes impossible to set the ignition delay longer than the injection duration. As this limit approaches, more diffusion burn is present thereby reinstating the soot versus NO_X tradeoff. Knafl et al. (2006) explored the load limits of premixed LTC in a 4 cylinder DI diesel engine at 1500 rpm and found that an early injection strategy almost completely eliminated soot and NO_X at brake mean effective pressures (BMEP) less than 200 kPa. A late premixed strategy was chosen for loads above 200 kPa. It was found that soot emissions and combustion noise increased with load and the maximum load achieving suitably low emissions was 700kPa.

LTC has other disadvantages when compared to conventional diesel combustion in addition to load limitations. One issue is higher CO and THC emissions due primarily to unburned and partially combusted fuel escaping the premixed burn process from over-lean pockets in the combustion chamber. These emissions are generally not high in conventional combustion due to the extended time allowed for combustion to occur. Jacobs et al. (2005) reported about two times the THC emissions and 20 times the amount of CO on an emissions index basis for a late premixed LTC condition versus a best brake specific fuel consumption (BSFC) conventional case with no EGR at the same fueling rate in a 4 cylinder DI diesel engine operating at 1500 rpm. A related disadvantage to higher THC and CO emissions is higher BSFC due lower combustion efficiency.

Although LTC exhibits mainly premixed combustion, fuel is still injected directly into the cylinder which leads to some degree of stratification regardless of the time of injection. Using optical methods Musculus et al. (2009) devised an analogous concept for LTC to that shown in Figure 1.2 for conventional combustion. In comparing this

illustration to that shown in Figure 1.4, the concept for LTC combustion is quite different.

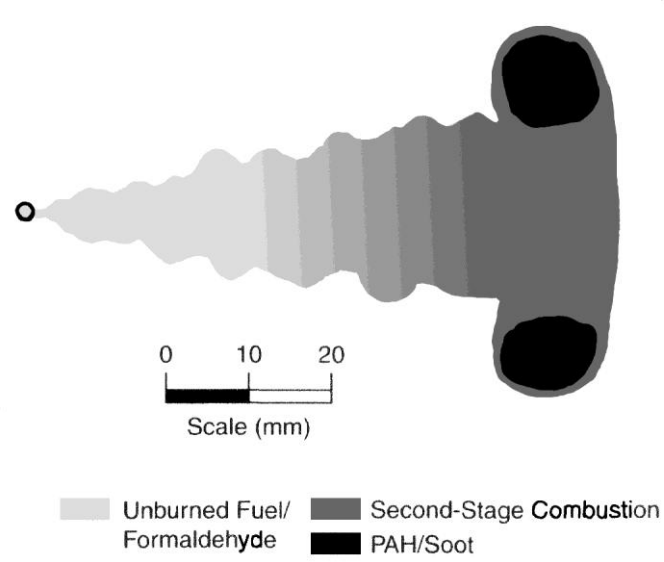

Figure 1.4: Graphical representation of diesel premixed low temperature combustion adapted from Musculus et al. (2009)

One interesting feature of the scheme is that remnants of the fuel spray are still evident as combustion occurs. Since for most LTC conditions, the injection event is complete by ignition, the fuel spray shape is allowed to penetrate the combustion chamber and create a fuel rich zone downstream as shown in the figure. Genzale et al. (2008) in an optical study of a late-injection LTC condition found that equivalence ratios in this region reached approximately 1.4 and decreased rapidly back towards the injection point. Near the injector, the fuel from the end of the injection event is over mixed. Much of the unburned hydrocarbon emissions from LTC are assumed to originate from this very lean region near the injector (Musculus et al., 2007).

1.4 Biodiesel

Vegetable-based fuels as a substitute for petroleum diesel were proposed very early in the history of diesel engines. In fact, it is commonly purported that Rudolf Diesel ran an engine in the 1900 Paris Exhibition on peanut oil (Knothe, 2001). Although this engine was designed to operate on mineral fuel, it was able to run on vegetable oils without any alterations. The desire to run engines on fuels other than those from petroleum sources was mostly motivated by recognition of the finite availability of petroleum. Diesel himself stated, "In any case, they make it certain that motor-power can still be produced from the heat of the sun, which is always available for agricultural purposes, even when all of our natural stores of solid and liquid fuels are exhausted."

Today the same goal of reducing the use of fossil sources of energy along with added motivations to reduce global CO_2 emissions and diversify fuel sources due for political reasons has re-invigorated research into bio-derived fuels for engines. Although not a new process, the production of alkyl-esters from bio-oils is a way to create a fuel that is very similar to petroleum diesel. The use of neat triglycerides in modern diesel engines introduces complications which are mitigated by the use of their esters. Viscosities of pure oils are an order of magnitude higher than petroleum diesel which strongly affects injection characteristics. Neat oils also have a high cloud point creating practical difficulties for their use in colder climates.

Biodiesel is the result of the transesterification of triglycerides with an alcohol usually in the presence of a base catalyst like NaOH, resulting in an alkyl ester as shown in Figure 1.5. Fatty acid methyl esters have more similar viscosity to diesel fuel than

straight oil and are better adapted to production engines. Glycerol is a byproduct of the manufacture of biodiesel and can be used for soaps and other industrial products.

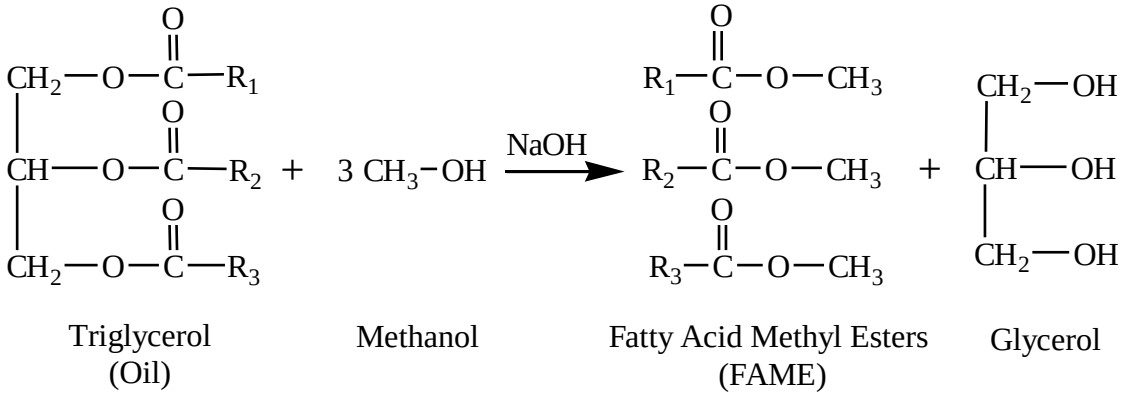

Figure 1.5: Transesterification of oil to a fatty acid methyl ester and glycerol

The use of biodiesel in engines is not new. Walton (1938) in a study of multiple types of bio-oils in a diesel engine recognized the advantages of only using the fatty acids from the oil. He claimed that "to get the utmost value from vegetable oils as a fuel it is academically necessary to split off the triglycerides and to run on the residual fatty acid." Although he did not report any data substantiating his claim, the use of "biodiesel" was reported prior to his publication in a Belgian patent in (Chavanne, 1937).

The manufacture of biodiesel and other biofuels like ethanol also has costs and their environmental impact must be weighed before blanket statements can be made about the benefits of their expanded use. For example, one reason that biofuels are being investigated is due to their potential to reduce global CO_2 emissions since they are derived from renewable sources. Methanol is the most economic material for use in industrial transesterification operations and comes primarily from fossil sources. Its use in biodiesel production erodes the renewability of the fuel. Furthermore, the planting,

fertilization, harvesting, and transporting of biofuels also generate carbon emissions and use non-renewable sources of energy. It has been further shown that a "carbon debt" is acquired as a result of biofuels production due to the clearing of established natural lands to plant fuel crops (Fargione et al., 2008). An additional complication in the use of biofuels is a result of competition for food production. It is estimated by researchers that global food prices will continue to rise as a result of increased use of cropland for energy production (Ragauskas et al., 2006).

Aside from potential pitfalls, there are still benefits of using biodiesel for fueling diesel engines. It is still partially renewable since a portion of its feedstock comes from a renewable source. Every fraction of renewability in fuels humans use reduces global CO_2 emissions. Biodiesel also has other benefits for use in engines (Knothe, 2005). It can be derived from local sources, is biodegradable, has reported reductions in exhaust emissions like smoke and hydrocarbons and has higher lubricity than petroleum diesel. Its high lubricity is due to oxygenated species and tends to increase with the degree of unsaturation in the fuel (Knothe, 2003).

In terms of fluid properties, biodiesel has some crucial differences from petroleum diesel. Petroleum diesel consists of many long chain paraffins and aromatic species. In comparison, as stated above, biodiesel consists of a small number of alkyl esters. Due to this more homogeneous composition, biodiesel exhibits a very narrow boiling range instead of a long distillation curve like diesel. This boiling point is generally around the 100% recovery point for petroleum diesel. Table 1.2 shows the distillation curve and boiling point of a low sulfur diesel and a soy methyl ester taken from Sharp et al. (2000).

The reported methyl ester, a soy-derived methyl ester (SME) has a boiling range of 11°C whereas the boiling range of the reference petroleum diesel is 160°C. This difference in volatility as a function of temperature may create a difference in ignition quality compared with the reference fuel used in the cetane number test.

Table 1.2: Distillation ranges from Sharp et. al (2000) for soy methyl ester and a petroleum diesel. IBP- Initial boiling point, FBP- Final boiling point, all values in °C

Distillation	SME	Diesel
IBP	331	192
10%	333	226
50%	336	266
90%	341	321
FBP	342	352

Other property differences between biodiesel and petroleum diesel include higher viscosity and surface tension which have the effect of prolonging the breakup of atomized fuel in the cylinder. Biodiesel also has a higher bulk modulus; the reduction of liquid volume when subjected to elevated pressure. Tat et al. (2000) reported that biodiesel has 5-10% higher bulk modulus than a number 2 diesel fuel. This has the effect of advancing the actual start of injection depending on the type of fuel injection system used. Monyem et al. (2001) reported a 2.3° advance in injection timing. Boiling range, viscosity and bulk modulus differences change the start of combustion in engines significantly which has effects on engine emissions and performance. When common rail injection systems are used however, the effect of differences in bulk modulus is not as great because injection pressure is already established before injection (Fang et al., 2008).

Performance and emissions from diesel engine operation on various types of biodiesel is well known and is reviewed by Agarwal (2006) and others although reported results have varied according to engine, fuel injection strategy, and emissions measurement technique. In general, engine operating characteristics of biodiesel are very similar to petroleum diesel and sometimes their differences fall within the statistical error of measurement techniques. Table 1.3 shows a selection of results from a selection of ten different engine studies performed comparing biodiesel with a reference petroleum diesel fuel.

In Table 1.3 the CN of the neat biodiesel is shown to be higher than the reference petroleum diesel in some cases and lower in others. Studies conducted in Europe and Asia use a reference diesel that has low aromatic content which raises its CN whereas those conducted in the United States use a reference fuel with higher aromatic content and lower CN. Among the biodiesel fuels shown, there is also a range of CN reported even though most are made from the same feedstock. This variation could be due to the error of the testing method or could be due to a different oxidation state of the fuel. It has been shown that biodiesel that is oxidized yields a much higher CN when tested than fresh fuel (Monyem et. al, 2001). The oxidative stability of soy methyl ester is generally lower than that of rapeseed or other esters due to its high degree of unsaturation (Knothe, 2005). Furthermore, it has been shown that the cetane test is not a completely appropriate measure of the ignition quality of fuels like biodiesel that are significantly different in chemical makeup than the primary reference fuels used in the test (Siebers, 1985).

Table 1.3: Comparison of ten published studies of convention combustion of biodiesel and petroleum diesel; References - 1) Zhang et al., 1996, 2) Senatore et al., 2000, 3) Scholl et al., 1993, 4) Patterson et al., 2006, 5) Sharp et al., 2000, 6) Szybist et al., 2005, 7) Akasaka et al., 1997, 8) Choi et al., 1999 9) Alam et al., 2006 10) Monyem et al., 2001; N/R- Not reported, SME- Soybean methyl ester, RME-Rapeseed methyl ester, M-Mechanical injection, CR- Common rail injection, FTP- Federal Test Cycle, D13-Japanese heavy duty test cycle

Reference	1	2	3	4	5	6	7	8	9	10
Fuels										
Diesel CN	47	48	N/R	54	43.3	48.2	53.9	46.3	47.3	47.4
Biodiesel	SME	RME	SME	SME	SME	SME	SME	SME	SME	SME
Biodiesel CN	59	52	N/R	59	47.5	51.8	48.7	N/R	61.0	51.1
Max. Blend	50%	100%	100%	100%	100%	100%	50%	40%	100%	100%
Engine										
Displacement (L)	4.5	1.9	3.0	2.3	5.9	N/R	7.9	2.4	5.9	4.5
Cylinders	4	4	4	4	N/R	1	6	1	6	4
Breathing	T	T	N.A.	N.A.	T	N/R	T	T	T	T
Inj. Type	M	CR	M	M	M	M	M	CR	M	M
Comp. Ratio	16.8	19.8	16.5	18.5	N/R	N/R	18.0	16	16.3	16.8
Speed (rpm)	1400	3000	1800	2000	FTP	3600	D13	1600	1800	1400
Load	100%	var.φ	3 bar BMEP	100%	FTP	75%	D13	φ=0.5	10%	100%
Performance and Emissions										
BSFC	↑	↑	N/R	N/R	↑	N/R	N/R	N/R	↑	N/R
Thermal Eff.	≈	≈	≈	≈	N/R	N/R	N/R	N/R	≈	N/R
BS-CO	↓	≈	↓	N/R	↓	N/R	↓	↓	↓	↓
BS-THC	↓	N/R	↓	N/R	↓	N/R	↓	N/R	↓	↓
BS-NO_X	↑	↑	≈	↓	↑	↑	↑	≈	↑	↑
Smoke No.	N/R	↓	↓	↓	N/R	N/R	N/R	N/R	N/R	↓
Total PM	↓	N/R	N/R	N/R	↓	N/R	↓	↓	N/R	N/R
SOF Fraction	↑	N/R	N/R	N/R	↑	N/R	↑	≈	N/R	N/R
Ign. Delay	↓	↓	≈	↑	N/R	↓	N/R	N/R	↓	N/R
Actual SOI	N/R	←	←	→	N/R	←	N/R	N/R	←	N/R

BSFC of biodiesel is generally reported to be lower than that of diesel fuel since the caloric value of biodiesel is lower. However, brake thermal efficiency is reported to be the same. Most studies keep speed and load consistent between fuels either at steady state points or through a transient drive cycle.

Carbon monoxide and THC emissions are generally reported to be lower for biodiesel than for petroleum diesel. As reviewed in Lapuerta et al. (2008), reasons for lower THC emissions include fuel property differences like high levels of oxygenation and higher CN leading to more advanced combustion. Work done by Rakopoulus et al. (2004) shows that additional oxygen present either in the intake air or contained in the fuel as oxygenated species contribute to lower CO and HC emissions in DI diesel engines.

It is commonly reported that NO_X emissions are higher for engines running on biodiesel than petroleum diesel. Suggested reasons for this vary and are reviewed in Cheng et al. (2006). Changing start of combustion, higher premixed burn fraction, higher diffusion burn temperature and combustion chemistry are given as possible explanations. In Table 1.3 most of the studies reporting NO_X emissions found that NO_X stays approximately constant or increases for biodiesel. One exception is the work done by Patterson et al. (2006) in which it was found that NO_X decreased for the same engine settings at a constant load. When comparing to other studies, it is apparent that the actual start of injection in this study was retarded significantly when 100% biodiesel was used. This caused combustion phasing to be later and thus reduced NO_X. Reasons for this change in actual SOI were not given though the correlation between combustion phasing and NO_X emissions is interesting. As reported by Scholl et al. (1993) and Szybist et al.

(2005) changing NO_X emissions with biodiesel was found to be primarily a function of combustion phasing. Scholl plotted the brake specific NO_X emissions versus location of peak cylinder pressure and found no differences between fuels tested. Szybist plotted brake specific NO_X versus crank angle location of maximum heat release rate and came to a similar conclusion. However, Cheng et al. (2006) found that NO_X emissions are not purely dependent on start of combustion or premixed burn fraction.

Filter smoke number (FSN), primarily a measure of visible carbon generated during combustion is generally lower for biodiesel than for petroleum diesel as shown in Table 1.3. Studies such as Mueller et al. (2003) show that the presence of oxygenates in fuels contribute to lower formation of soot in the combustion process. In this and other studies like Upatnieks et al. (2004), it is found that the oxygen content in the fuel is not the only factor in reducing carbon formation but that molecular structure of the fuel also plays a part. They also found that oxygen in the fuel is more effective at reducing soot formation than enhancing oxygen entrainment into the flame. The presence of oxygen in the rich regions of combustion aids the soot oxidation process in the diffusion burn portion of combustion.

Emissions of total PM are also lower for the loads and conditions shown in Table 1.3. However, if the percentage of soluble organic fraction (SOF) is reported, it is usually found to be higher. This SOF consists mainly of unburnt biodiesel fuel due to the low volatility of the esters found in the fuel. It was concluded in Zhang et al. (1996) that any increases in total PM for biodiesel is due to SOF increases especially at light loads. Chang et al. (1998) also found SOF to increase in a study of SME in a four cylinder

direct injected diesel engine. In his work, he also found that the collection conditions like filter temperature and dilution ratio had a large effect on the SOF of biodiesel exhaust due to the high boiling range of the unburned fuel on the soot particles. Also in this work, Chang found that the standard sample temperature of 190°C for the gaseous sample system also changed the amount of THC measured by a flame ionization detector (FID) analyzer due to condensation and adsorption of esters on the walls. This could compromise the actual readings of THC for any of the studies reported in Table 1.3.

Overall THC emissions from operating diesel engines on biodiesel have been reported to contain higher concentrations of vapor phase aldehydes and other volatile oxygenates created during the combustion process. Hansen et al. (1997) found that combustion of RME in a 6 cylinder direct injected bus engine at moderate speeds and loads resulted in higher formaldehyde and acetaldehyde emissions with comparison to a reference diesel fuel. They also found that poly aromatic hydrocarbons (PAH) in the PM decreased for 100% RME and that most of the SOF contained in the PM was unburnt fuel. Corrêa et al. (2006) also saw a reduction in PAH in PM emissions from a 6 cylinder direct injected engine at moderate load and 1500 rpm when operating on 20% SME with comparison to diesel.

Particulate size distribution has been reported for biodiesel operation in diesel engines with comparison to petroleum diesel. Jung et al. (2006) used a dilution system and a scanning mobility particulate scanner (SMPS) with a medium-duty four cylinder direct injection engine set at constant speed and load. They found that the PM had a smaller size distribution for biodiesel primarily due to the lower formation of carbonaceous species

during combustion as mentioned above. The SOF was not measured in this study. Tsolakis (2006) also reported smaller particles when running a single cylinder direct-injected engine at constant speed and load on rapeseed-derived methyl ester (RME) using an electrical low-pressure impactor (ELPI). Using a correlation for mass density of the particles, Tsolakis also calculated that the biodiesel PM had a lower mass than the reference low sulfur diesel.

1.5 Biodiesel use with Premixed LTC

1.5.1 Previous work on Biodiesel LTC

Using biodiesel in the premixed LTC mode has recently sparked interest as both are becoming desired capabilities of modern diesel engines. However, little literature exists exploring this combination. Zheng and coworkers in a series of papers (Zheng et al., 2006, Zheng et al. 2007, Zheng et al., 2008) have shown that it is possible to achieve LTC combustion with biodiesel in both the HCCI-like, early LTC strategy and with a late-injection LTC strategy. In their first paper, they explored early combustion modes using a single-cylinder DI engine at 1400 rpm with a heated fuel injection system in the intake. In this work, they found a shorter ignition delay with the biodiesel due to its higher cetane number and that due to biodiesel's low volatility and higher viscosity, intake manifold injection and atomization was a challenge.

Zheng et al. (2008) more recently experimented with running a biodiesel derived from various sources in a 4-cylinder direct-injected diesel engine with a compression ratio of 18.2:1 at a speed of 1500 rpm and 8 bar indicated mean effective pressure (IMEP). They varied SOI over a 20CA° range and ran EGR rates from 0% to 70%. In

their work, they found that compared with conventional diesel fuel, biodiesel had comparable NO_X emissions and that CO and THC emissions were lower at a fixed injection timing. They also found that biodiesel was able to better sustain high EGR rates and LTC combustion due to its higher cetane number than the reference diesel and accessible fuel oxygen. Confirming these findings Cheng et al. (2007) found that oxygenated fuels are capable of sustaining more dilute combustion.

Karra et al. (2008) compared B100 and B20 with a No. 2 diesel fuel under a single and dual injection LTC condition at 1400 rpm and 7.11 bar BMEP in a medium-duty multi-cylinder diesel engine. In their study, they found that NO_X emissions were higher for B100 for a given injection timing and FSN was lower. Since fuel injection conditions were maintained constant Karra et al. assumed that increases in NO_X emissions for LTC were not due to variations in fuel injection conditions as had been reported in earlier literature for other injection systems.

Fang et al. (2008) also experimented with both early and late LTC strategies with biodiesel and petroleum diesel in an optical single cylinder direct-injected engine at 1500 rpm and 2 bar IMEP. They found that SME had a longer ignition delay than their reference diesel which is indicative of the CN of the fuels tested. As mentioned above, European diesel fuel has very low aromatic content and therefore can have a higher CN than biofuels. In the LTC regime, Fang et al. also found similar NO_X emissions for SME compared with diesel fuel for fixed injection timing. In the case of LTC, since the thermal NO_X formation island shown on Figure 1.3 is avoided, it may be assumed that

any formation of NO_X is then by the prompt mechanism (Plee et al. 1981) in which the initial fuel composition may have little effect.

1.5.2 Preliminary Study on Biodiesel LTC

Research done at University of Michigan in a preliminary study of a late-injection LTC strategy and blends of soy methyl ester with two different petroleum diesel fuels further expanded the knowledge of the combination and was published in Northrop et al. (2009). Insight gained through the study provided the impetus and direction for the deeper research presented in this dissertation. A brief outline of the preliminary study and its results are summarized in this section.

The purpose of the preliminary study was to broadly observe trends when operating a 1.7 liter displacement high speed passenger car diesel engine on biodiesel in the LTC regime. Instrumentation included an emissions analyzer, smoke meter, cylinder pressure-based combustion diagnostics and a differential mobility particle spectrometer (DMS).

A test plan was executed which centered on a baseline operating condition using a US-specification ultra low sulfur diesel (ULSD) fuel. The condition was selected to be a representative medium speed and load of steady state vehicle operation. From the baseline condition, data for two fuel injection timing settings and two fuel injection pressure settings were taken while maintaining a constant speed, load, and EGR rate. Other fuels selected for the study included a soy-based methyl ester biodiesel and a low-aromatic Swedish diesel fuel. Two blends of ULSD and biodiesel were also tested, a 20% (B20) and 50% (B50) by volume biodiesel. To eliminate the effects of combustion

phasing between fuels at the baseline operating condition, the 50% fuel mass fraction burned point (CA50) was kept constant by adjusting the fuel injection timing. Table 1.4 shows the operating conditions of the engine for the baseline condition.

Table 1.4: Engine conditions for baseline LTC condition and variation of injection pressure and timing for preliminary study from Northrop et al. (2009)

Condition	Baseline LTC
Engine Speed (rpm)	1500
BMEP (kPa)	400
EGR Rate (%)	50
Injection Pressure (bar)	800,**1000**,1200
Injection Timing (°BTDC)	5,**7**,9
Air/Fuel Ratio	20.8
Intake Manifold Pressure (kPa)	107
Intake Manifold Temperature (°C)	47
Coolant Temperature (°C)	85

The preliminary study revealed some interesting findings concerning LTC of biodiesel compared with petroleum diesel. Firstly, a given fuel's CN is a better indicator of the duration from SOI to CA50 than of the ignition delay defined by the duration of SOI to SOC. This is mainly due to an altered ignition region of combustion for biodiesel at a given CA50. Given that observation, it was concluded that examining engine emissions and efficiency as a function of CA50 is a good way to compare fuel performance independent of combustion phasing. Two examples of this from the work were brake fuel conversion efficiency (η_f) and NO_X. When plotted versus injection timing, NO_X was statistically higher for B100, consistent with the findings of Karra et al (2008). When plotted versus CA50 however, NO_X and η_f showed no differences between

fuels to the statistical error of the measurements. It was therefore concluded that NO_X emissions in the premixed LTC regime are strongly tied to combustion phasing regardless of fuel. Based on this finding and that from the literature, the biodiesel NO_X effect shown by other researchers applies to neither LTC nor conventional combustion so long as phasing is taken into account.

Brake fuel conversion efficiency also was also found to be the same for all fuels tested as a function of CA50. It therefore concluded that any differences in fuel consumption reported in the literature for biodiesel is mainly due to differing fuel lower heating values and not combustion quality so long as combustion phasing is maintained constant.

Differences did appear among the tested fuels when comparing CO and THC versus CA50. Both the high cetane Swedish diesel and B100 had statistically lower CO and THC emissions. The lower amount of these products of incomplete combustion for Swedish could be explained by its shorter ignition delay for a given CA50 leading to less over-leaning in the cylinder during combustion. B100 however had a longer ignition delay than the Swedish diesel which begs the question of whether some of the THC in the exhaust was missing from the measurements or whether fuel chemistry plays a more direct role in lowering the emission of partially reacted species in biodiesel combustion.

Although smoke emissions as measured by FSN were nearly zero for B100 and higher for the petroleum fuels, the particle size distribution as measured by the DMS indicated a significantly higher mass of PM for B100 than the other fuels. This finding

led to the conclusion that the organic content of the PM from biodiesel LTC may be been greater for B100. Further work as outlined in this dissertation, takes the story from there.

1.6 Research Goals and Dissertation Outline

Like all research, the work presented in this document stands on the shoulders of already established results. Owen Chamberlain, a Nobel Prize winning physicist once said, “The whole structure of science gradually grows, but only as it is built upon a firm foundation of past research”. Both partially premixed LTC of petroleum diesel and conventional biodiesel combustion have been investigated thoroughly. However, based on the prior work described in the above section, three primary research goals form the focus of the current investigation.

The first goal is to explain why the gaseous HC and CO emissions from biodiesel LTC decrease compared to petroleum diesel fuels by exploring the distribution of light hydrocarbons within the THC measurement. To accomplish this, a breakdown of the THC is made by speciation of light HCs in the exhaust gases using a Fourier Transform infra-red (FT-IR) analyzer. Relative concentrations of such volatile species can be indicators of over-lean and over-rich portions of the cylinder, allowing induction of the relative differences in local equivalence ratio and thus gain further insight into the combustion process.

The second research goal is to prove the hypothesis that the organic fraction of the PM mass is greater for biodiesel in premixed LTC and to determine the primary species that contributes to this increase. To accomplish this, the mass emission of both

carbonaceous soot and PM must first be measured. Then, it is necessary to extract and identify the organic species contained within the PM structure.

As a third goal, this work looks to identify whether a DOC can oxidize organic species in the exhaust that contribute to increased PM mass emitted from a vehicle tailpipe using biodiesel in the LTC mode. Measurements of THC and LHC contained therein are taken and compared to reductions in PM mass. Conversion of primary organics found on the PM is measured from diluted samples taken before and after the DOC.

An experimental study is described in this work which seeks to meet these goals and to seek deeper understanding into underlying physical and chemical mechanisms. The dissertation is organized as follows. Following this introduction, Chapter Two describes the experimental methodologies used in the study. Instrument specifications, key calculations used in presenting results and measurement uncertainty are discussed. The development of three engine combustion conditions used in the study is explained in Chapter Three. Engine performance, combustion parameters and general emissions are used to characterize these conditions.

The following three chapters are each dedicated to the proof and exploration of the three main thrusts outlined above. Chapter Four examines the emissions of gaseous hydrocarbon and inorganic carbon emissions in LTC for biodiesel and compares the results to conventional combustion. In Chapter Five, PM and the role of unburned HCs plays in those particulates is explored. As an extension of the work of the previous two chapters, Chapter Six discusses the performance of a standard DOC in the conversion of

organic species which normally would be found on the PM for biodiesel LTC. Finally, Chapter Seven provides a summary of the conclusions of the work and discusses recommended next steps to further advance the research presented here.

CHAPTER TWO

EXPERIMENTAL METHODS

2.1 Engine Test Cell

Two major types of experimental platforms are typically used in engine research. Single cylinder engines eliminate cylinder-to-cylinder variability and thus ensure that the bulk exhaust from combustion emanates from one source. Generally, optical diagnostic and other detailed combustion studies are performed using these platforms. One drawback of single cylinder engines is that they do not accurately produce intake and exhaust conditions found in the actual engines they resemble. Exhaust temperatures are lower due to higher heat losses and flows have higher magnitudes of pulsation. Multi-cylinder engines are useful for understanding systemic trends in actual working engines and are useful for bulk emissions studies. Since exhaust flows are higher and combustion products are essentially the average of multiple cylinders, larger gas and particulate samples can be taken. This is especially important for measuring PM from engines operating in low soot-producing conditions like partially premixed LTC where sufficient loading on filters for gravimetric analysis can take significant time. Further, since exhaust flows and temperatures are higher with less pulsation, aftertreatment studies are more readily correlated with expected performance of catalysts in practice.

A multi-cylinder engine test platform is best suited for meeting the goals of this study. Measuring the combined effect on bulk emissions of fuel, combustion strategy and aftertreatment is more easily correlated to engine performance on an actual diesel engine and DOC used in practice.

2.1.1 Test Engine

The experimental study to investigate premixed LTC of biodiesel fuels was conducted using a production 4-cylinder diesel engine designed by Isuzu Advanced Engineering Center in Japan and manufactured in cooperation with General Motors. The engine has been produced under many different configurations and is used in vehicles marketed in Europe and Asia. The engine used in the study has the technical specifications given in Table 2.1. The production version, manufactured in 2002, is capable of producing 100 hp at 4400 rpm, a suitable size for powering a small to mid-sized passenger vehicle.

The engine uses a common rail fuel injection system designed and developed by the Robert Bosch Corporation. This configuration decouples the generation of injection pressure and the fuel injection process. Fuel is injected by pressurizing a common manifold with a positive displacement pump from which a solenoid allows high pressure fuel to enter the injector. Advantages of common rail include extremely fast actuation time allowing multiple injections per engine cycle. The injection system also allows sustained and controllable injection pressures between 100 and 1400 bar. High pressures are essential for LTC as they enhance mixing prior to combustion.

Table 2.1: Specifications of the engine used in the experimental study

Type	Direct Injected Diesel
Manufacturer	Isuzu
Cylinders	4
Displacement (L)	1.7
Bore (m)	0.079
Stroke (m)	0.086
Connecting Rod Length(m)	0.134
Wrist Pin Offset (m)	0.0006
Compression Ratio	16.0
Piston Geometry	Bowl-in-Piston
Valves/Cylinder	4
Injection System	Common Rail
Injector Location	Centrally Mounted
Injector Holes	6
Injector Nozzle Spray Angle (°)	150
Injector Nozzle Flow (cc/30-s)	320

Creation of high levels of cooled EGR, up to 60% by mass of the intake gases, is also critical for premixed LTC as it both extends ignition delay and reduces the temperature of combustion by diluting the fuel-air mixture. The engine used in the study has a high pressure EGR system in which recycled exhaust from the high pressure side of the turbocharger is mixed with the relatively lower pressure gas in the intake manifold. A diagram of the system is given in Figure 2.1. A variable geometry turbocharger (VGT) utilizes controllable vanes to optimize upstream pressure of the turbine in the exhaust while a throttle valve in the intake runner after the compressor controls the differential

pressure needed to create EGR. Typically throttle-less operation is a key advantage of diesel engines over spark-ignited engines since reduction in intake air pressure has a negative impact on pumping work. For this reason, the throttle valve was kept completely open for the conditions used in the study. EGR was controlled by changing the VGT for large changes in flow between engine conditions and an EGR valve for small adjustments at a given engine setting. An EGR cooler using engine coolant as the cold medium allowed EGR to be maintained to a constant temperature. Cooling EGR and reducing the intake air temperature using an intercooler is important in diesel engines for maintaining high intake charge density for a given speed and load.

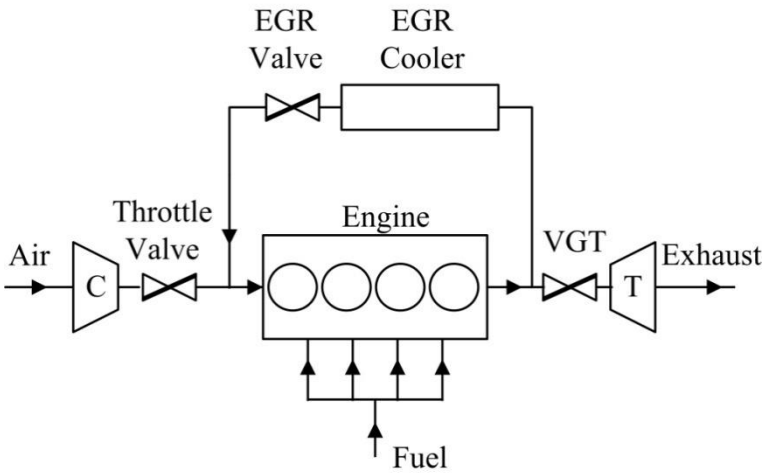

Figure 2.1: Test engine flow diagram showing cooled EGR system

The engine used in the study was modified from the production specifications in a number of ways to both make it more suitable for the laboratory environment and to better operate in the partially premixed combustion regime. First it was modified to have a lower compression ratio than the stock engine such that premixed combustion could be achieved over a wider load range. To accomplish this, the design of the bowl located in

the piston crown was enlarged to lower the geometric compression ratio from the stock 19:1 to 16:1.

Another change made to the engine was the replacement of the production EGR cooler with one of larger capacity for accommodating the larger quantities of cooled EGR to be used in premixed LTC. To maintain a constant temperature of gas at the outlet of the EGR cooler, a separate coolant boost pump was installed to increase the flow. The original EGR valve was also replaced with a throttling ball valve for more precise control of EGR flow.

2.1.2 Engine Control

The load and speed of the engine is controlled by a General Electric direct current dynamometer connected to the flywheel of the engine. Torque is measured by a load cell mounted to the dynamometer and speed is measured by a hall-effect type sensor.

The engine is equipped with a programmable version of the engine electronic control unit (ECU) of that in production. A digital throttle controller from Dyne-Systems is used to provide the fueling input to the controller through an ETAS ETC interface. This interface also allows independent control of all parameters set by the ECU using the INCA software package. These parameters included injection timing, injection pressure, VGT position, throttle position, and swirl vane position. Setting of different engine settings during testing was done by altering maps for each parameter and was changed while the engine was operating. Other engine settings including EGR Valve actuation, engine coolant temperature and DOC inlet temperature are changed externally to the engine ECU using lab-based PID controllers.

2.1.3 Diesel Oxidation Catalyst

A production DOC is mounted in the exhaust stream of the engine following the turbine. It is the standard size and formulation meant to meet EURO IV emissions regulations for the production version of the test engine. Catalyst formulation and other specifications of the DOC are shown in Table 2.2.

Table 2.2: Known physical specifications of DOC catalyst used in the study

Monolith length/diameter (mm)	93/74
Fraction engine swept volume	23.5%
Cell density (cm^{-2})	62
Substrate material	Cordierite ($Mg_2Al_4Si_5O_{18}$)
Washcoat materials	Alumina, Silica, Zeolite
Total washcoat loading (g/in^3)	2.32
Active metal loading (g/ft^3)	Pt – 88.63
	Pd – 29.15

The DOC was de-greened prior to the study to ensure steady state activity over the testing period. This process involved maintaining the catalyst at a temperature of 160°C in an air and 10% water environment for 16 hours.

Three primary factors control the performance of catalytic reactors in exhaust aftertreatment applications; space velocity, catalyst temperature and composition. In the study, only the effects of changing exhaust composition into the DOC per fuel at a given engine condition is desired. Since a constant engine condition produces a near-constant flow rate, temperature of the inlet of the catalyst is set to a constant value. For this

purpose, a co-flow gas to gas heat exchanger was installed in the exhaust prior to the DOC. Forced cooling air is provided by a centrifugal blower. The heat exchanger has the capability to lower the temperature by 15°C from a baseline value which is suitable for maintaining constant DOC inlet temperature over the tested fuels for a given operating condition.

2.1.4 Low Speed Data Acquisition

In the experimental test setup, measurement of temperatures and pressures are made independent of the production engine control system and are recorded using a low speed data acquisition system. This system uses a Measurement Computing PCI card with 32 analog input channels. The signals are processed, viewed and controlled by a National Instruments LabVIEW software interface at a rate of approximately 1 Hz. Signals measured by the low speed system include intake manifold temperature and pressure, oil pressure, turbine inlet and outlet temperature and pressure, DOC inlet, outlet and substrate temperature, coolant temperature, intake air temperature and humidity and engine speed and load. Temperatures are measured using K-type thermocouples and pressures by piezoresistive transducers both manufactured by Omega Engineering. Fuel flow is accurately measured using a Coriolis mass flow meter and is recorded by the system. Data from the online emissions measuring equipment is also processed through the low speed data acquisition system. For each low speed sample taken in the experimental study, 50 points of data were taken.

2.1.5 Combustion Analysis

Cylinder pressure is measured in each of the four cylinders by water-cooled Kistler 6041A piezo-electric pressure transducers. They were installed in place of the glow plugs normally used for cold start in the production engine. Fuel injector current for cylinder number 1 is measured by an inductive current sensor. Start of injection (SOI) was assumed to occur at 50% of the initial rise in the signal from the transducer. An AVL 365C crank angle encoder set at a resolution of 0.25 CA° fitted to the front of the engine is used to time the pressure and injection data.

The high speed signals are measured by a Redline CAS II data acquisition system manufactured by A&D Technology Inc. The CAS system has 16 analog input channels and an 8 million sample raw data memory. Along with cylinder pressure and injector current, the CAS system also has inputs for engine speed, engine load, and intake manifold pressure. The system also incorporates a real-time combustion processing module to calculate parameters like rate of heat release and mass fraction of fuel burned. For each steady state data point, the CAS system records and averages 100 cycles at a 0.25 CA° resolution.

In the experimental study, high speed pressure data was post-processed using UMHR, an internal program developed at The University of Michigan (Depcik, 2005). This program combines low speed data and the high speed pressure trace from cylinder one to calculate the rate of heat release, fuel mass fraction burned and mean cylinder temperature using the first law of thermodynamics for an open system. Constant mass during the cycle was assumed for the analysis neglecting changes due to fuel injection,

blow-by or crevice flows. Thermodynamic properties are calculated using the correlations of Krieger and Borman (1966). Hohenberg's correlation (Hohenberg et al., 1979) for heat transfer from the cylinder during combustion is assumed.

In the experiments, it was found that for the point of 50% fuel mass fraction burned (CA50), the real time combustion analysis using the CAS system never deviated more than 0.2 CA° away from the more accurate value calculated by the post-processed heat release program. Therefore, it was deemed acceptable to use the real-time CA50 value for real-time engine control as well as for plotting the results of the study.

Fuel injection timing was estimated by using the crank angle of 50% rise of the injector signal pulse. Though this metric measures timing to be slightly before the actual injection event, it was deemed acceptable for the purposes of this study.

2.2 Emissions Measurement

The results from emissions measurement including both gaseous species and particulate phase species is the primary focus of this work. A phalanx of analytical instruments was applied to gather as much data as in pursuit of the research goals. Figure 2.2 shows a flow diagram of the instrumentation used both during the operation of the engine and that used in post-processing.

For gaseous emissions, an analyzer bench for measuring the five primary species from diesel combustion is used in concert with an FT-IR analyzer for HC speciation and an H-Sense H_2 analyzer. Particle emissions are measured by a smoke meter for carbonaceous species, DMS for particle size distribution and a partial flow dilution tunnel

for collecting aerosol samples on filters. From the particulate filters, PM mass was measured before removing the organic species using Soxhlet extraction. Extracts were speciated using a gas chromatograph with flame ionization detector (GC-FID). Organic versus elemental carbon analysis is conducted from quartz filters taken using the dilution tunnel. The following sections provide more detailed description of the instruments used in the emissions analysis.

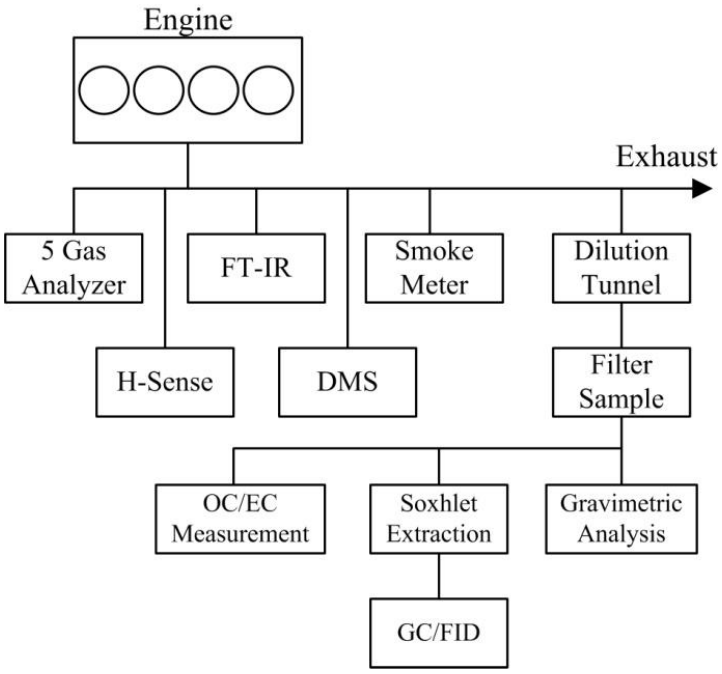

Figure 2.2: Emissions measurement flow diagram for experimental study

2.2.1 Analyzer Bench

The primary gaseous emissions from both the engine and the outlet of the DOC are measured by an AVL CEB II emissions bench. The analyzer bench utilizes non-dispersive infra-red (NDIR) detectors for measurement of CO and CO_2, a paramagnetic detector for O_2, a dual channel FID for THC and CH_4 and a chemiluminescence detector for measurement of NO_X consisting of NO and NO_2. Each analyzer has the capability of

multiple measurement ranges to increase the accuracy of measurement. For the measurement of NO_X and HC the sample line is heated to 190°C from the sampling point on the engine exhaust line to each detector. Two heated glass micro fiber filters with 95% efficient retention for particles of 0.03 micron diameter of are mounted in the heated sample line to remove PM and other solid material before the analyzer. The O_2, CO, and CO_2 emissions are measured on a dry basis with a cooler to drop out any water from the sample prior to the analyzers.

Calibration of the analyzer on each range of detection was performed before each day of testing along with a leak check of the vacuum system to ensure atmospheric air did not enter the sample lines at any point. Linearization of all analyzers was accomplished once at the beginning of the experimental study and two subsequent linearization checks were run during the course of the testing period. Heated filter elements were also changed after every day of testing. The analyzers were regularly purged with ultra-high purity nitrogen during the course of each testing run.

2.2.1.1 Gaseous Emissions-Based Calculations

In measuring the majority of species contained in engine exhaust, the analyzer bench data were used to calculate other parameters useful for the study of emissions and engine performance. First, species measured on a dry basis like CO and CO_2 were calculated on a wet basis using the well established methods in Stivender (1971) such that all emissions data in the study were comparable.

Emissions Index (EI) is a near dimensionless parameter used to show the mass flow of a species in the exhaust with respect to the mass flow of fuel into the engine. In this

way, emissions can be compared between engine conditions independent of dilution in the exhaust stream or efficiency of the combustion process. Using wet concentrations, the emissions index for each species was found using Equation 2.1 (Stivender, 1971).

$$EI_j = X_j \left[\frac{MW_j}{MW_f \left[X_{CO} + X_{CO2} + X_{THC1} \right]} \right] \tag{2.1}$$

Where:

EI_j:	Emissions index of species j in g/kg-fuel
X_j:	Wet mole fraction of species j
MW_j:	Molecular weight of species j
MW_f:	Molecular weight of fuel per atom of carbon
THC_1:	Total hydrocarbons per atom of carbon

Equation 2.1 is slightly different for hydrocarbons assuming a representative molecular weight defined by the US-EPA as 83.25 and divided by 6 to account for the US-EPA reporting method for hydrocarbons on a C_6 basis as shown in Equation 2.2.

$$EI_{THC} = \frac{X_{THC1}}{6} \left[\frac{83.25}{MW_f \left[X_{CO} + X_{CO2} + X_{THC} \right]} \right] \tag{2.2}$$

Emissions data were also used to calculate the mass air to fuel ratio (AFR) using wet concentrations and a mole balances based on the methods described in Stivender (1971). Values for AFR were calculated both using an oxygen balance and a carbon balance as shown in Equations 2.3 and 2.4. By dividing the stoichiometric value of AFR for a given fuel by the mean of the two calculations, the equivalence ratio can be obtained.

$$AFR_O = 4.774 \frac{MW_{air}}{MW_{fuel}} \cdot \frac{\left(X_{CO2} + X_{O2} + 0.5 \left(X_{H2O} + X_{CO} + X_{NO} \right) \right)}{\left(X_{CO} + X_{CO2} + X_{THC} \right)} \tag{2.3}$$

$$AFR_C = \frac{MW_{air}}{MW_{fuel}} \cdot \left(\frac{100+1.5X_{H2O}+3(1.5y-1)X_{THC}-0.5X_{CO}}{(X_{CO}+X_{CO2}+X_{THC})} - \frac{y}{2} \right) \quad (2.4)$$

Where:

AFR_O: Mass air to fuel ratio based on oxygen mole balance
AFR_C: Mass air to fuel ratio based on carbon mole balance
MW_{air}: Molecular weight of air (28.96)
y: Atomic hydrogen to carbon ratio in the fuel

The EGR rate on the test engine is measured using a separate CO_2 analyzer sampling from the intake manifold. The mass fraction of EGR in the total intake charge was calculated by comparing the mole fraction of CO_2 in the intake with that of the exhaust according to the correlations found in Stivender et al. (1971) and given in Equations 2.5 and 2.6.

$$EGR = \frac{100}{1+\frac{MW_{air}}{MW_{exh}}\left(1+\frac{1}{AFR_{avg}}\right)\left(\frac{100}{m}-1\right)} \quad (2.5)$$

$$m = 100\frac{(100+X_{H2O})X_{CO2\text{-}int}}{X_{H2O}X_{CO2\text{-}int}+100X_{CO2\text{-}exh}} \quad (2.6)$$

Where:

EGR: Mass fraction of EGR in intake
AFR_{avg}: Mean value of AFR_O and AFR_C
MW_{exh}: Molecular weight of exhaust (29.06)

Combustion efficiency, a measure of available energy contained in the exhaust gas compared with the total energy contained in the fuel, was also calculated using the

gaseous emissions data (Stivender, 1971). Equation 2.7 gives the relationship for η_c assuming that the THC in the exhaust has the same heating value as the fuel.

$$\eta_c = 100 - \left(\frac{100}{X_{CO}+X_{CO2}+X_{THC1}}\right)\left(\frac{254X_{CO}+217X_{H2}}{h_{LHV,f}MW_f}+X_{THC1}\right) \quad (2.7)$$

Where:

η_c: Combustion efficiency
$h_{LHV,f}$: Lower heating value of fuel (MJ/kg)

2.2.2 Hydrogen Analyzer

Diatomic hydrogen is not typically measured in engine studies as it is generally assumed to be proportional to the concentrations of CO, H_2O and CO_2 according to a pseudo-water gas shift reaction relationship (D'Alleva, 1936). However, this relationship has been shown to break down in the lean LTC regime (Northrop, 2009). To more accurately report H_2 and for use in the emissions-based calculations described in the previous section, it is measured in this study using a sector-field mass spectrometer manufactured by V&F Instruments. The sector field mass spectrometer uses a high speed turbo pump to separate H_2 from the other heavier gases in the exhaust. Then by ionizing and collecting molecules according to charge, the instrument measures the quantity of hydrogen molecules in the gas stream.

The gas sample for the mass spectrometer is taken after the same filter as the emissions analyzer and flows through a heated line to the instrument in a heated line controlled to 190°C. The sample is then cooled in an internal chiller to remove water before analysis. Therefore, the H_2 measurement is made on a dry basis and was corrected

to a wet basis using the methods described in a previous section before converting to EI using Equation 2.1.

The H-Sense analyzer was calibrated before every day of testing by setting a zero using ultra-high purity nitrogen and an upper span of 3000 ppm H_2. Linearization of the instrument is not recommended by the manufacturer and thus was not checked during the course of the experiments.

2.2.3 FT-IR

An FT-IR analyzer was used to measure more detailed composition of LHC and other species. The specific instrument used was a 2030-HS Multigas Analyzer manufactured by MKS Instruments Inc. It has the capability to detect species from ppb levels to percent concentration in a gas stream. Identification of specific molecules is accomplished by measuring the absorption spectrum emitted by that species when exposed to an infrared beam in a gas cell. The spectral frequencies and intensity are unique based on the number and strength of chemical bonds among atoms contained in a given molecule. Most gases in engine exhaust are infrared detectable with exception of diatomic gases like O_2, H_2 and N_2. The concentration of gas is determined by comparison of magnitude of the signal compared with pre-loaded calibrations.

During the testing, a range of calibrations were loaded into the FT-IR software to look for desired species. Table 2.3 gives the species detected. Some redundancy exists between the emissions bench and the FT-IR for detection of species like CO, CO_2, NO and NO_2. This is an advantage however for further confirmation of experimental accuracy. Although the FT-IR is capable of detecting most hydrocarbon species found in

engine exhaust, it was not used to measure THC since pre-loaded calibrations of all expected organic components from the different fuels used in the study would introduce too many errors. The value for THC was taken only from the FID incorporated into the analyzer bench. For expected LHC species like ethylene and formaldehyde however, the FT-IR is an invaluable tool for identifying light organic components within the THC.

Table 2.3: Gas species with pre-loaded calibrations in the FT-IR used in the experimental study

Species	Formula	Species	Formula
1,3-Butadiene	C_4H_6	Fulminic Acid	HCNO
Acetaldehyde	CH_3CHO	Methane	CH_4
Acetylene	C_2H_2	Nitrogen Dioxide	NO_2
Ammonia	NH_3	Nitrogen Oxide	NO
Carbon Dioxide	CO_2	Nitrous Oxide	N_2O
Carbon Monoxide	CO	Propane	C_3H_8
Ethane	C_2H_6	Propylene	C_3H_6
Ethylene	C_2H_4	Water Vapor	H_2O
Formaldehyde	H_2CO		

Since water and therefore condensable HC was measured with the FT-IR, sampling was accomplished though a heated sample line maintained at 190°C. When recording from the FT-IR, data were collected at a rate of 5 Hz for two minutes, of which the last minute was logged and averaged. Values for concentration were measured directly on wet basis and EI values were calculated using Equation 2.1. Since hydrocarbons are measured by the FT-IR directly and not on a carbon number basis like with a FID, concentrations were multiplied by the number of carbons in the molecule and the

molecular weight used in equation 2.1 normalized per atom of carbon. In this way, the data collected by the FT-IR could be directly compared with the THC value from the FID.

The gas cell was maintained at a temperature of 191°C, the path length was 5.11 m and the pressure was maintained constant at 1 atm. The FT-IR background gas was set twice per day of testing by sending ultra-high purity nitrogen into the gas detection cell for 15 minutes to allow complete purging. Residual spectra were checked along with other system checks before setting the background spectra. Calibration of the FT-IR using a span gas is not recommended by the manufacturer and therefore was not done during the course of the experimental study.

2.2.4 Smoke Meter

Smoke emissions from the engine were measured by an AVL 415S variable sampling smoke meter. In this device, a known volume of exhaust gas is drawn through a filter paper and the degree of darkening is measured by an optical sensor. The paper blackening (P_B) measured by this device approximates the black carbon in the exhaust stream hereto referred to as soot and is measured on a linear scale between black and white according to Equation 2.8.

$$P_B = 10 \times \left(1 - \frac{R_G}{R_W}\right) \tag{2.8}$$

Where:

R_G: Reflectivity of blackened filter paper
R_W: Reflectivity of white filter paper

The filter smoke number (FSN) is a function of both the paper blackening and the volume of gas that is drawn through the filter. It is therefore a measurement of the mean soot mass over a sampling time. The mass of soot per volume of exhaust gas at 1 atm pressure and 25°C (C_{FSN}) can be approximated with the FSN using a correlation found in Christian et al. (1993) given in Equation 2.9.

$$C_{FSN}[\,mg/m^3] = \frac{1}{0.405} 4.95\,FSN\,e^{(0.38\,FSN)} \tag{2.9}$$

The emissions index of filter soot (EI-FSN) is calculated by using Equation 2.10.

$$EI_{FSN} = C_{FSN} \frac{T_{std}\overline{R}}{P_{std}MW_{exh}} \left(AFR_{avg}+1\right) \tag{2.10}$$

Where:

EI_{FSN}:	Emissions index of soot (g/kg-fuel)
T_{std}:	Standard temperature (298 K)
P_{std}:	Standard pressure (101,000 Pa)
$\overline{R}$:	Ideal gas constant (8.314 J/mol-K)

When taking FSN samples using the smoke meter for the experimental study, 3000 ml of gas was passed through the filter and three samples were acquired and consequently averaged per engine condition.

2.2.5 Differential Mobility Spectrometer

For measuring PM size distribution, a differential mobility spectrometer (DMS) was used in the experimental study. The DMS500 fast particulate spectrometer manufactured by Cambustion Inc. provides a real-time size distribution of particles. The instrument has an internal air dilution system to more accurately simulate PM concentrations at exhaust

outlet conditions. A mass dilution ratio of air to exhaust gas of 5:1, the maximum allowable by the DMS500, was used for the testing. When taking samples from the DMS, 30 seconds of data were acquired at a sampling rate of approximately 10 Hz and consequently averaged per engine condition.

The principle of detection of the DMS is based on ionized particles traversing a classifier column at sub-atmospheric pressure. The diluted sample is drawn through a conductive rubber tube, sent through an impactor to remove particles of size greater than 1000 nm and subsequently exposed to a corona charger to ionize the remaining particles. The charged particles then flow within a flow of laminar air where they are carried in a predictable manner. They are then repulsed from a high voltage center rod towards grounded electrometer rings where they land based on their charge and momentum. Since their charge is only a function of particle size and not material composition, the measurement of current from each ring is based on numbers of particles that fall within a classification of size.

The output of the DMS500 is given in terms of particle size number distribution $n(D_p)$ where D_p is the equivalent particle diameter. Thorough explanation of different definitions of particle diameter and types of size distributions can be found in various texts including Seinfeld (1996) and Eastwood (2008). The number of particles per unit volume of gas can be expressed as a function of particle size as given in Equation 2.11.

$$N = \int_0^{\infty} n\left(D_p\right) dD_p \tag{2.11}$$

It is useful to normalize $n(D_p)$ by N such that the range dD_p expresses the fraction of particles within the entire population. Since within a population of particles in the atmosphere or engine exhaust sizes vary over a few orders of magnitudes (10-1000 nm), it is also common to express number distribution in terms of a log function $n(\log D_p)$. With this new independent variable, the total number of particles N can be expressed as given in Equation 2.12.

$$N = \int_{-\infty}^{\infty} n(\log D_p)\, d\log D_p \tag{2.12}$$

The number of particles within a range of diameters dD_p is the same as the number within $d\log D_p$. Therefore, the number of particles dN does not depend on which way the distribution is expressed as shown in Equation 2.13.

$$dN = n(D_p)dD_p = n(\log D_p)d\log D_p \tag{2.13}$$

Rearranged, this equation becomes:

$$\frac{dN}{d\log D_p} = n(\log D_p) \tag{2.14}$$

In words, $dN/d\log D_p$ is a way of expressing the number distribution of the log of particle diameter. Particle size distributions are expressed in this way in plotting the experimental data of this experimental study. One key advantage of plotting number distributions in this way is that the total number of particles in any given size range is proportional to the area under the curve within that size range.

A similar procedure as outlined in Equations 2.12 through 2.14 can be accomplished to find the mass distribution $m(D_p)$. In general, the number distribution is useful for looking at the smallest particles and the mass distribution for the larger particles in a poly-disperse aerosol since the smaller particles have a disproportionately smaller mass as illustrated by Equation 2.14. Further, just as the number distribution can be integrated to yield N, the area under the mass distribution gives the total mass, M of the particles per unit volume of gas.

2.2.6 Particulate Filter Analysis

A critical part of the experimental study of PM from partially premixed LTC of biodiesel and petroleum diesel fuels was the collection and analysis of particles collected on filters after a dilution process. Dilution allows for the simulation of conditions just as the exhaust leaves the tailpipe of a vehicle and enters the relatively cooler atmospheric environment. Where FSN can be correlated to the mass concentration of soot generated by combustion, diluted filter collection and subsequent gravimetric analysis is direct measurement of total particulate mass per unit volume of engine exhaust gas. Current governmental emissions regulations, as described in Chapter One, limit the emissions of particulate on a mass basis though particle size is becoming an important metric for evaluation since smaller particles have an arguably greater health effect on humans. In the experimental study presented here, the collection of engine PM on filters in a controlled environment allowed for the scientific comparison of mass, composition and morphology of engine particulate for different fuels and engine conditions.

2.2.6.1 Dilution Tunnel

The partial flow dilution tunnel used in the study extracts a small fraction of the exhaust gas and mixes it with a known quantity of filtered ambient air before sending the mixture to a filter collection housing. Advantages of a partial flow dilution system over one that dilutes the entire engine exhaust are that equipment size is greatly reduced and capital and use costs are lower. The particular dilution tunnel used was a BG-2 manufactured by Sierra Instruments Inc. It was designed and implemented in accordance with the standard ISO/DIS 16183. Figure 2.3 shows the configuration of the dilution tunnel and its installation in the test cell system.

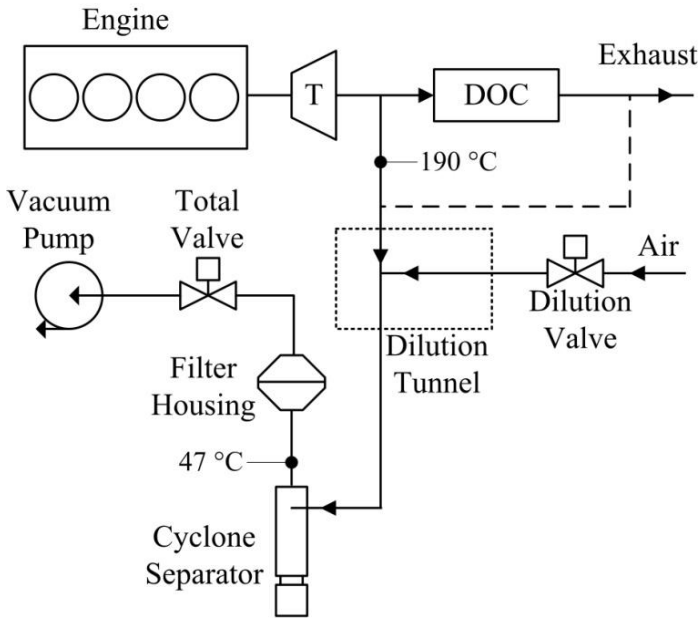

Figure 2.3: Flow diagram for the partial flow dilution tunnel system used in the study

The BG-2 controls the relative quantity of air and exhaust using two mass flow controllers, one for the total diluted sample and one for the dilution air. In this way the

volumetric air flow at standard conditions of the sample flow can be calculated according to the expression given in Equation 2.15.

$$\dot{V}_s = \dot{V}_t - \dot{V}_d \quad (2.15)$$

Where:

$\dot{V}_s$: Volumetric flow rate of exhaust sample into dilution tunnel (std-l/min)
$\dot{V}_t$: Volumetric flow rate of total diluted sample (std-l/min)
$\dot{V}_d$: Volumetric flow rate of dilution air (std-l/min)

The dilution ratio (DR) is the ratio of standard volumetric or mass flow of dilution air divided by the total flow. The filter face velocity (V_f), exposed filter diameter (D_f), filter temperature (T_f), and filter pressure drop (dP_f) are also important parameters for accurate measurement of PM using dilution tunnel methods. Table 2.4 gives a summary of the pertinent constant dimensions and settings used in taking dilution tunnel filter measurements. The set parameters are within the allowable limits according to ISO-DIS 16183 and consistent with the US-EPA 40 CFR Part 1065 Engine Testing Procedures. Using the control software of the BG-2, the constant settings for V_f and DR were converted to volumetric flow commands to the two mass flow controllers.

The BG-2 required daily calibration of both total air and dilution air mass flow controllers. Calibration was done by matching the range of desired flow set points to the flow expected based on the factory setpoints.

Table 2.4: Dilution tunnel constant settings and dimensions for the experimental study compared with allowable values from ISO-DIS 16183

Parameter	Allowable	Setting
D_f (mm)	39	39
T_f (°C)	47±5	45
V_f (cm/s)	35-100	100
DR	NA	10:1
dP_f (kPa) *maximum*	25	20

2.2.6.2 Particulate Collection and Filter Handling

Collection of particulate from engines using filters requires precise and consistent procedures to ensure accurate data. In the experimental study, both filter handing and collection of filters as well as additional analysis like gravimetric and extraction were done with extreme care to reduce errors.

In collecting engine PM on filters, the guidelines under US-EPA 40 CFR Part 1065 were followed. Prior to sampling, the diluted exhaust gas passed through a 2000-30ES stainless steel cyclone separator manufactured by URG Corporation to separate out particles greater than 10 µm. These particles were not of interest since they were assumed to not be from the combustion process but rather from debris from the exhaust system carried downstream.

PM was collected using a stainless steel filter holder with 12.5° tapered inlet provided by Sierra Instruments. Within the holder, filters were held in place using removable filter cassettes. Cassettes were loaded with fresh filters before every day of testing. Special care was taken to not touch the filter face during any part of the process. The entire

separator and filter holder assembly was heated using controlled heating tape purchased from Omega Engineering such that the desired T_f was achieved for each sample taken.

For gravimetric analysis, Whatman 7592 ring supported 100% PTFE membrane filters with 2 μm pore size were used. All filter handing was done inside an atmospherically controlled clean room with specifications given in the EPA test standard. Fresh filters were pre-conditioned by exposing them to the clean room environment in partially open glass Petri dishes for a minimum of 2 hours before pre-weighing. They were then loaded into the cassettes within 12 hours of use. Before removing from the clean room, filter cassettes were wrapped in Parafilm and stored in individual metal containers. These containers were stacked in a sealed tube which was used to transport them to the test location. Figure 2.4 shows a photograph of the filters, cassettes and associated containers used.

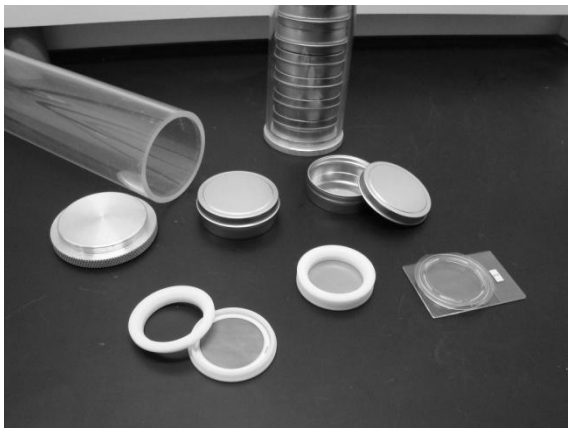

Figure 2.4: Filters, filter cassettes and associated containers

During loading as mentioned in the previous section, DR and V_f were maintained constant. Since different conditions had varying amounts of PM, the sample time (τ_s) was changed such that the maximum allowable dP_f given in Table 2.3 was not reached. For

the tests conducted in this study, τ_s varied between 30 seconds and 10 minutes to reach an adequate PM loading at different conditions.

After PM loading during a test, the filter cassettes were re-wrapped in Parafilm, placed back in their metal tins and taken back to the clean room within ½ hour of the testing day. There they were exposed in opened Petri dishes for a minimum of 12 hours to condition before weighing and additional analysis.

Filter cassettes and metal tins were cleaned between tests using de-ionized water in an ultrasonic bath for 30 minutes and subsequently air dried. Petri dishes were cleaned using a combination of de-ionized water and isopropyl alcohol.

2.2.6.3 Gravimetric Analysis

Determining the mass of PM on filters was done using a Mettler Toledo XP6U microbalance with accuracy of 0.1 μg. The balance is located in the clean room environment discussed previously. If the room fell out of the environmental conditions required, no data was collected until the room was allowed to re-equilibrate for 1 hour. The procedure for weighing filters was accomplished using the US-EPA 40 CFR 1065 regulations as a guideline. The microbalance was calibrated and leveled at the beginning of each weighing session and re-zeroed after every 3 filters weighed. Before weighing filters for a test, a blank reference filter of known mass was checked. If the reference filter was more than 20μg from the known original value, the calibration procedure was repeated.

A grounding strap was worn and statically resistive tweezers were used to handle filters when weighing. The filter was exposed to a radioactive Polonium source to eliminate static charge to ±2.0 V of neutral. Weighing occurred in an enclosed chamber and was automatically recorded using computer software.

The mass of PM on a filter was taken to be the mass of a filter after PM loading subtracted from the mass before PM loading as shown in Equation 2.16.

$$m_p = 1000(m_{f,post} - m_{f,pre}) \tag{2.16}$$

Where:

m_{pm}: Mass of PM on filter (μg)
$m_{f,post}$: Mass of filter after PM loading (mg)
$m_{f,pre}$: Mass of filter before PM loading (mg)

Since atmospheric pressure was not controlled in the clean room, a buoyancy factor was applied to m_p per the calculation outlined in US-EPA 40 CFR 1065.690.

To calculate the mass concentration of PM for a given filter and dilution tunnel sampling time Equation 2.17 was applied.

$$M_{pm} = \frac{m_{pm} \cdot 60}{\tau_s \cdot \dot{V}_s} \tag{2.17}$$

Where:

M_{pm}: Mass concentration of PM in exhaust gas (mg/std-m^3)
m_{pm}: Mass of PM on filter (μg)
$\dot{V}_s$: Volumetric flow rate of exhaust sample into dilution tunnel (std-l/min)
τ_s: Dilution tunnel sample time (s)

The emissions index for PM was then calculated using engine AFR according to Equation 2.18.

$$EI_{pm} = M_{pm} \cdot \frac{T_{std}\overline{R}}{P_{std}MW_{exh}}\left(AFR_{avg}+1\right) \tag{2.18}$$

Where:

EI_{pm}: Emissions index of PM (g/kg-fuel)

For each engine condition for which a PM mass was taken, three particulate filters weights were taken. The data reported for the experimental study was the mean of the three values.

2.2.6.4 Total Organic Carbon Analysis

Quartz fiber filters were used in the dilution tunnel during the experimental study to determine the organic carbon versus elemental carbon (OCEC) of the engine PM. These quartz filters were also handled only in a clean room environment like the PTFE filters for gravimetric analysis described above. After removal from their sampling cassettes, they were packaged in sealed Petri-dishes and stored in a laboratory refrigerator controlled to 5°C for later analysis.

The OCEC value for the quartz filters was determined by the methods described in NIOSH 5040 and in Birch et al. (1996) using a thermal optical analyzer (TOA) manufactured by Sunset Laboratory Inc. In the TOA, a 1.5 cm diameter punch of the PM-loaded filter is placed into a sealed chamber and is taken through two primary steps. The first is to heat the filter in a He environment over a period of minutes up to approximately

850°C. This step evolves organic carbon (OC) from the surface, catalytically oxidizes it to CO_2 through a bed of MnO_2 granules then converts it to CH_4 in a Ni/firebrick methanator. The CH_4 is then measured using a FID. In the second step, the temperature is lowered and the filter is heated again in a He/O_2 environment to evolve the elemental carbon (EC) from the surface. The EC portion is then quantified in the same way as the OC.

The primary output of the TOA is the mass of EC and OC per square centimeter. In the experimental study, these values were multiplied by the total exposed area of the filter to yield the mass of EC and OC (m_{ec}, m_{oc} respectively). The total carbon (TC) mass reported was the sum of EC and OC. To determine the mass concentration and EI of EC and OC in the exhaust, Equations 2.17 and 2.18 were applied.

Calibration of the OCEC method was done according the NIOSH 5040 method. This calibration procedure uses a known quantity of carbon loaded onto a quartz filter and analyzes it multiple times to correlate the FID output to a mass measurement. Repeatability was established by running at least one duplicate sample per day of analysis.

2.2.6.5 Soxhlet Extraction

To characterize the organic matter from the PM-loaded PTFE filters, Soxhlet extraction was used. In this method, developed in 1879 by Franz von Soxhlet, a specially designed glass extractor is used to dissolve species from a sample into a solvent. The apparatus comprises a heated flask containing solvent, an extraction section and a condenser. The sample is generally loaded into a thimble and placed in the sample

chamber within extractor. As the solvent in the flask evaporates, it travels up a distillation arm to the condenser section which is cooled with room temperature water. The condensed solvent condenses and slowly fills the sample chamber. As the chamber fills, the desired compounds dissolve into the solvent. When the chamber is almost full, it is automatically emptied by siphon side arm and carried back into the flask. The cycle is repeated for as many times as necessary to concentrate the solvent with the desired compounds. The advantage of the Soxhlet method is that only fresh solvent is exposed to the sample each cycle allowing the maximum extraction to occur in the chamber. Three Soxhlet apparatus were used in parallel in the as shown in the photograph in Figure 2.5 to facilitate faster analysis time.

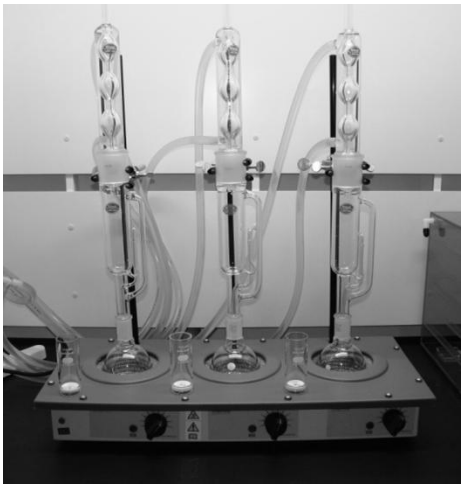

Figure 2.5: Soxhlet extraction apparatus used in the experimental study

The extraction of diesel particulate using Soxhlet has been a standard procedure for many years. However, the choice of solvent has been the subject of much debate. Benzene was the solvent of choice for extracting ambient particulate for many years until concerns regarding its carcinogenic nature inspired the search for safer alternatives. It is

known that the polarity of solvents is important for the extraction selectivity of a desired species; polar solvents tend to attract polar molecules and non-polar attract non-polar species. Grosjean (1975) presented a detailed analysis of the extraction efficiency of different solvents compared to benzene for organic matter from particulate collected from the ambient air. In the analysis, dichloromethane (DCM), a slightly polar molecule, had a higher efficiency in extraction of organic molecules than benzene alone. The overall analysis suggested that for best extraction of polar and non-polar organic species within a sample, a two component solvent be used. Non-polar solvents have the ability to extract polar molecules to a certain extent. Some have experimented with combinations of benzene and DCM and found the mixture of the two, when mixed in the correct ratio, to have higher extraction efficiency than either of them alone (de Lucas et al., 1999).

For the experimental study reported here, extraction of major species contained in the fuels used from the PM was of primary interest. Straight alkanes, found to high concentration in low sulfur petroleum diesel and fatty-acid methyl esters contained in biodiesel have all shown high extraction efficiency using DCM (Lapuerta et al., 2003). It has also been a standard for extraction of diesel PM from filters for many years (Funkenbusch et al., 1979; Wall et al., 1984). Based on these reasons and its relative safety compared with benzene, DCM was used as the sole solvent for extraction of organics from diesel PM in this study.

In the Soxhlet extraction procedure, all glassware was first cleaned by triple rinsing with DCM, then with acetone and finally with de-ionized water. The glassware was then dried in a convection oven at 150 °C for at least 12 hours. Pyrex thimbles for holding the

PM filters were additionally cleaned in an ultrasonic bath of acetone for 30 minutes before rinsing with de-ionized water and dried.

Once cleaned, all glassware was handled with gloves to reduce contamination and filters were inserted into thimbles using stainless tweezers. The flasks were filled with 200 mL of DCM and 1 ml of internal standard mixture for each filter extraction. During one run, 3 filters were extracted at a rate of 6 minutes per cycle for 15 hours to yield approximately 150 total cycles. After extraction, the saturated solvent was transferred to clean glass jars and stored in a laboratory refrigerator controlled to a temperature of 5 °C. The solvent was then concentrated using a vacuum rotary evaporator to a volume of approximately 1.5 ml for use in the GC analysis.

2.2.6.6 Gas Chromatography Methods for Extracted Particulate

The use of GC methods for analyzing organic species from particulate filters has been well established. A Shimadzu GC-17A gas chromatograph with flame ionization detector GC-FID was used in the study. Details of the setup and program of the GC used are shown in Table 2.5.

Although many published studies use GC with mass spectrometry as the detection method, GC-FID as the chosen analysis technique is appropriate for the experimental work presented here. This detector cannot conclusively detect species a priori, especially those with overlapping retention times which is a key disadvantage. However, it can be extremely accurate when concentrations of a desired species in a sample are high and when a known standard of the species have been established using the chosen instrument

and program. Both qualitative and quantitative methods have been well established for GC-FID (McNair and Miller, 1997) and are used in the work presented here.

Table 2.5: GC specification and program for speciation of extracted PM samples

Gas Chromatograph	Shimadzu GC-17A	
Column	Restek RTX-1, 60 m, 0.53 mm, 2.5 μm	
Carrier Gas	Ultra-high purity He	
Injection	Temperature = 300 °C, Split Ratio = 8:1	
Program	Temperature:	Pressure:
	40 °C for 0 min	126 kPa constant
	10 °C/min to 185 °C	
	185 °C for 14 min	
	10 °C/min to 300 °C	
	300 °C for 15 min	
Detector	Temperature = 320 °C	

In analyzing the extracted PM, solvent samples were injected into the GC-FID using a 1μl plunger-in-needle syringe. Before running a sample, pure DCM was injected using the same program to ensure that residual contamination in the syringe, injection port or column did not exist. The sample was then run using the program outlined in Table 2.5. The syringe was cleaned by flushing 10 times with acetone and 10 times with DCM followed by baking in a syringe oven at 300 °C for 30 minutes.

As mentioned in the previous section, internal standards were mixed into the solvent flask prior to the extraction process. Qualitatively, the standards species of known retention time and with higher concentration than the species in the sample allow relative identification of peaks. For quantitative analysis, the peak area of a known mass of a

standard species prior to extraction can be correlated to the mass of like species dissolved and concentrated in the solvent sample. Three standard species were chosen, tetradecane ($C_{14}H_{30}$), nonadecane ($C_{19}H_{40}$), and methyl heptadecanoate, a saturated C_{17} methyl ester (C17:1) not found in biodiesel. A mass of 400 μg of each standard species was mixed into the solvent for each filter extraction. To calculate the mass of identified species in a solvent sample, Equation 2.19 was applied.

$$m_i = \frac{m_{ISTD} f_i A_i}{f_{ISTD} A_{ISTD}} \tag{2.19}$$

Where:

m_i:	Mass of species with identified species i
m_{ISTD}:	Known mass of internal standard
f_i:	Response factor for identified species i
A_i:	Peak area of species with identified species i
f_{ISTD}:	Relative response factor for internal standard
A_{ISTD}:	Peak area of internal standard

In Equation 2.19, relative response factors (f_i) allow compensation for non-linearity in the relationship between peak area from a given detector and the mass of a species relative to another molecule. It is generally advisable to determine response factors specifically for use in one instrument and program. Literature values were used instead however since for n-alkanes they can be predicted to good accuracy. The FID is particularly linear for n-alkanes because their molecular weight is linear as a function of carbon number. Scanlon and Willis (1985) give an analytic expression for the calculation of hydrocarbon response factors for FID using what they termed the effective carbon response. This expression is given as Equation 2.20.

$$f_i = \left[\frac{\left(\left(MW_C N_{C,i} \right) + \left(MW_H N_{H,i} \right) \right)}{N_{C,i}} \right] \cdot \frac{0.7487}{MW_C} \quad (2.20)$$

Where:

MW_C:	Molecular weight of carbon (12.011)
MW_H:	Molecular weight of hydrogen (1.008)
$N_{C,i}$:	Number of carbon atoms in species i
$N_{H,i}$:	Number of hydrogen atoms in species i

Equation 2.19 was not used for fatty acid methyl ester (FAME) components which make up biodiesel however since the response of oxygenated molecules are generally more unpredictable. Alcohols and other oxygen containing molecules generally have a measured carbon deficiency where the FID detects less than the actual number of carbon atoms present. Therefore, these oxygenated compounds result in a response factor greater than 1. The FID response factors for FAME components used in the study are from Ulberth et al. (1999). They found that for high molecular weight esters like those found in biodiesel, response is surprisingly linear and near the value of 1 meaning that all carbon atoms are measured irrespective of the oxygen present. They speculate that the full carbon response for large methyl esters may be due to the particular breakdown sequence of the ester component in combustion. Table 2.6 shows the response factors for relevant compounds for the experimental study.

Table 2.6: Values used for FID response factors of n-alkanes (Scanlon and Willis, 1985) and FAME compounds (Ulberth et al., 1999)

n-Alkane	F	FAME	f
$C_{14}H_{30}$	0.883	C16:0	0.992
$C_{15}H_{32}$	0.882	C18:0	1.000
$C_{16}H_{34}$	0.882	C18:1	0.987
$C_{17}H_{36}$	0.881		
$C_{19}H_{40}$	0.881		

In the implementation of Equation 2.19 to determine the mass of extracted components, the response factor for the internal standard (f_{ISTD}) $C_{14}H_{30}$ was used for species eluting earlier than $C_{14}H_{30}$. The f_{ISTD} for $C_{19}H_{40}$ was used in estimating the mass of all heavier species than $C_{14}H_{30}$ with exception to known FAME components. For these a standard response factor of 1.00 was used given the linearity of FAME response as illustrated in Table 2.6.

2.3 Tested Fuels

The primary fuels used in this work were a mid-cetane US-specification ultra-low sulfur diesel (ULSD) certification fuel, a soy-based methyl ester (SME) biodiesel and Swedish Environmental Class 1 (SWE) diesel fuel. The ULSD fuel was blended by the supplier to have a cetane number in the middle of the range 40-50. The SWE fuel is a light distillation blend with low aromatics. It was chosen to represent an upper bound of CN and for relevance in comparison with past studies conducted at the University of Michigan.

As discussed in Chapter One, when the combustion characteristics of biodiesel were compared with a petroleum diesel, ignition delay and therefore combustion phasing and NO_X emissions correlated strongly with CN. Studies choosing a low aromatic diesel showed different trends than studies using a diesel fuel higher in aromatic species. By selecting two petroleum diesels with CN bounding that of the biodiesel used, this study attempted to see this effect more clearly.

Along with the two diesels and 100% SME (B100), two 50% by volume blends of biodiesel mixed with ULSD and Swedish (B50ULSD and B50SWE) were tested. In this way, a matrix of fuels with a progression of CN was used as shown in Table 2.7. The table also shows other measured properties for all the fuels tested in the study from an analysis carried out by Paragon Laboratories Inc. Due to the instability of the SME due to oxidation as was mentioned in Chapter One, all fuel analyses were carried out within the month before testing began.

Table 2.7: Properties of fuels tested in the preliminary study.

Fuel	ULSD	B50ULSD	B100	B50SWE	Swedish
Cetane	45.7	48.1	50.1	51.2	55.9
LHV (MJ/kg)	42.97	39.98	37.35	40.22	43.54
Kin. Viscosity (mm^2/s)	2.35	3.02	3.93	2.65	1.84
Oxygen (Wt %)	0.0	5.6	10.9	5.7	0.0
H/C ratio	1.86	1.86	1.83	1.93	2.00

Trends in lower heating value (LHV) were as expected. The two petroleum fuels had very similar values whereas B100 has the lowest energy content per unit mass. Viscosity

was similar to values found in the literature with B100 having a slightly higher value than ULSD and Swedish diesel, a lower viscosity than ULSD. Sulfur was less than 15ppm in all fuels tested as required by federal regulations.

SME was obtained from Peter Cremer Inc., a biodiesel manufacturer in Illinois, and was used within 3 months of transesterification. The standard ASTM 6751 outlines limits of properties required for biodiesel sold in the United States. It is a compilation of tests defined by separate standards. The results of the tests performed by Midwest Laboratories Inc. according to this standard are shown in Table 2.8.

Table 2.8: Additional properties of biodiesel used in the study as part of ASTM 6751, n.d.-not detected

Property	Level	Detection Limit	Method
Oxidation Stability (hrs @110°C)	5.8	0.1	EN14112
Flashpoint (°C)	143	4	ASTM D93
Water and Sediment (% Vol.)	n.d.	0.010	ASTM D2709
Kinematic Viscosity (mm^2/s)	3.920	1.000	ASTM D445
Sulfated Ash (% mass)	n.d.	0.01	ASTM D874
Sulfur (ppm mass)	n.d.	0.5	ASTM 5453
Cloud Point (°C)	5.0°C		ASTM D2500
Carbon Residue (% mass)	n.d.	0.020	ASTM D4530
Acid Number (mg KOH/g)	0.19	0.05	ASTM D664
Free Glycerin (% mass)	0.008	0.001	ASTM D6584
Total Glycerin (% mass)	0.020	0.001	ASTM D6584
Boiling Point/100% Dist. Temp. (°C)	343	1	ASTM D1160

The boiling point of the B100 fuel was measured to be about the same as that found in Sharp et al. (2000) as shown in Table 1.2 and it may be assumed that the initial boiling point was about 10°C lower than the value shown. For comparison, the distillation curve of ULSD and the Swedish diesel used in this study is shown in Table 2.9. Both exhibited almost identical distillation ranges although the 50% point is 20°C higher for Swedish than for ULSD. All fuels have a final boiling point within 8°C of each other.

Table 2.9: Distillation ranges of unmixed fuels used in the study, IBP- Initial boiling point, FBP- Final boiling point, * IBP not measured for B100, all values in °C

Distillation	ULSD	SWE	B100
IBP	183	181	≈330 *
10%	208	216	
50%	242	262	
90%	309	308	
FBP	332	333	340

Table 2.10: Significant fatty acids contained in the biodiesel used in the study

Fatty Acid	Concentration
Linoleic (C18:2)	52.3%
Oleic (C18:1)	22.4%
Palmitic (C16:0)	11.2%
Alpha Linolenic (C18:3)	8.28%
Stearic (C18:0)	4.53%
Arachidic (C20:0)	0.34%

Another important set of properties to measure for biodiesel is the fatty acid profile. This analysis shows the percentages of different fatty acid groups paired with methyl

groups in the fuel. Table 2.10 shows the most significant fatty acids contained in the B100 used in this study in order from highest to lowest. The profile test was also done by Midwest Laboratories Inc.

Linoleic acid was the primary fatty acid found and is consistent with expected values for a soy feedstock. This poly-unsaturated species is more prone to oxidation than mono-unsaturated and saturated species like oleic acid and stearic acid, also found in high concentration in the SME tested. Biodiesels produced from other sources like rapeseed oil contain more oleic acid and therefore have higher oxidative stability.

2.4 Experimental Uncertainty

To establish the uncertainty of the data taken in the study, three primary categorizations of error are considered. First the accuracy of the data is evaluated based on the systemic error, or design-stage uncertainty (u_o). It is estimated by tallying the error associated with different measurement devices and techniques. The second step is the estimation of uncertainty based on the single test repeatability of the data taken (u_m). In this case, the u_m of a given data sample is evaluated solely on the variability of that engine operating condition at the time of sampling. The third element of the uncertainty analysis is the repeatability uncertainty (u_r) based on the three samples taken per fuel and operating condition. The repeatability based on repeated days of testing was confirmed qualitatively and is not included in the error bars reported in the results shown. To combine u_o, u_m and u_r in estimating overall uncertainty (u_t), the root-sum-squares (RSS) method is used as shown in the Equation 2.21(Figliola and Beasley, 2006, pp.151).

$$u_t = \sqrt{u_o^2+u_m^2+u_r^2} \tag{2.21}$$

The RSS method assumes variations of an error over repeated measurements tend to follow a Gaussian distribution. Although a straight algebraic addition of errors would yield a higher overall uncertainty, it assumes that all errors occur at their worst possible state which is not realistic. All errors in this study were calculated to a 95% confidence interval. For a given sample size this is equivalent to ±2 standard deviations (σ).

2.4.1 Systemic Uncertainty

The u_o for each of the raw variables measured is shown in Table 2.11. The emissions analyzer bench uncertainty is shown along with the measurement ranges in Table 2.12. In most cases, the data were provided by the manufacturer of the equipment used. In the case of the emissions uncertainty, both the full scale accuracy and the accuracy of the calibration span gas (SG) were combined using the RSS method.

Table 2.11: Analyzer bench measurement ranges and uncertainty, * Span gas error was 1% of span gas concentration

Species		Range	Span Gas	FS Error	Inst. Error	SG Error*	u_o
Units	Range	(ppm)	(ppm)	(%/100)	(ppm)	(ppm)	(ppm)
CO	1	1200	989	0.014	17	10	19
	2	11000	10200	0.014	154	102	185
	3	70000	50070	0.014	980	501	1101
$CO_{2\text{-exh}}$	1	80000	70300	0.014	1120	703	1322
	2	200000	145400	0.014	2800	1454	3155
O_2	1	60000	50000	0.014	840	500	978
	2	250000	210000	0.014	3500	2100	4082
$CO_{2\text{egr-int}}$	1	40000	30080	0.014	560	301	636
	2	80000	70300	0.014	1120	703	1322
NOx	1	65	60	0.018	1	1	1
	2	450	398	0.018	8	4	9
THC	1	500	412	0.014	7	4	8
	2	2600	2334	0.014	36	23	43
CH_4	1	200	100	0.014	3	1	3

Table 2.12: Instrument uncertainty of other variables measured from the engine

Smokemeter (FSN)	0.1
Pressure (kPa)	4.1
Combustion Noise (dB)	1
Thermocouples (K)	2.2
Torque (n-m)	1.5
Speed (rpm)	5
Fuel Flow (%/100)	0.0005

The uncertainty associated with fuel properties used in calculations is also accounted for and is shown in Table 2.13. Each is found from the ASTM standard used to measure the property. When calculating the overall u_o for these variables, the repeatability and reproducibility were combined using the RSS method.

Table 2.13: Uncertainty associated with fuel properties used in calculations for this study

	Standard	Range/Average	Repeatability	Reproducibility
LHV (MJ/kg)	ASTM D 240		0.13	0.40
Carbon (Wt %)	ASTM D 5291	75 to 87	(x+48.48)*0.0072	(x+48.48)*0.018
Hydrogen (Wt %)	ASTM D 5291	9 to 16	(x^0.5)*0.1162	(x^0.5)*0.2314
Oxygen (Wt %)	ASTM D 5622	1.0 to 5.0	0.06	0.26
Oxygen (Wt %)	ASTM D 5622	40 to 50	0.81	0.81
Cetane No.	ASTM D 613	40-56	0.01*x+0.42	0.125*x-2.2
Viscosity @40C (mm^2/s)	ASTM D 445	1 to 13	0.0043*(x+1)	0.0082*(x+1)

For measurement of FT-IR samples, the instrument uncertainty was assumed to be 1% of the full scale range of concentration for a given species spectral calibration. No systemic uncertainty was assessed for the gravimetric measurement of PM, soxhlet extraction, or GC-FID analysis because it was assumed that measurement uncertainty due to repeated samples was much greater than errors introduced by instrument inaccuracies. Furthermore, for the purposes of the experimental study, the accuracy of the PM measurements are not as important as the precision between samples conducted using the same methods and equipment.

2.4.2 Measurement Uncertainty

To find the uncertainty associated with measurement variability for a given trial (u_m), twice the standard deviation (σ) of all samples taken for that data point was used to represent a 95% confidence interval. For the low speed data samples like engine speed and load for example, u_m was 2σ of the 50 data points taken at 1Hz for a given engine condition. For the FT-IR, u_m was 2σ of one minute of spectral data taken at 1 Hz. In the case of the FSN measurements, u_m is 2σ of the three measurements taken for each fuel and operating condition.

Some calculated values like BMEP or EI emissions are functions of many measured parameters. To find the uncertainty associated with functions of measured parameters each with their own uncertainties, the method of sequential perturbation (Figliola and Beasley, 2006, pp.158) was used. This method is a numerical approach using the finite difference method to approximate solutions to partial differential equations. The procedure was as follows:

1. Calculate the average of a set of each variable, x_i and their relative uncertainties u_{xi}. In our case this is equivalent to 2 standard deviations, $u_{xi} = 2\sigma$.
2. Calculate the desired result, R_o using the average values found where

   $R_o = f(x_1, x_2, ..., x_L)$
3. Increase the independent variables by their respective uncertainties one at a time and recalculate the result.

   $R_1^+ = f(x_1+u_{x1}, x_2, \ldots, x_L)$

   $R_2^+ = f(x_1, x_2+u_{x2}, \ldots, x_L)$

   $R_L^+ = f(x_1, x_2, \ldots, x_L+u_{xL})$
4. Similarly, decrease the independent variables in the same way and recalculate the function, R_i^+
5. Calculate the differences δR_i^+ and δR_i^- for all i=1,2,…,L.

   $\delta R_i^+ = R_i^+ - R_o$

   $\delta R_i^+ = R_i^+ - R_o$
6. Evaluate the approximation of uncertainty contribution from each variable.

   $$\delta R_i = \frac{\delta R_i^+ - \delta R_i^-}{2}$$
7. The uncertainty of the function then is the sum of squares of each contribution.

   $$u_m = \left[\sum_{i=1}^{L} (\delta R_i)^2\right]^{1/2}$$

2.4.3 Repeatability Uncertainty

The repeatability uncertainty (u_r), was represented by twice the σ of the three data sets for emissions, high speed and FT-IR are collected per condition and fuel. It was then added to the overall uncertainty for all the variables. The key assumption made was that given multiple trials of changing engine conditions and consequently coming back to the same conditions for a given fuel test where LTC was established, u_r would be the same for any data point.

For the gravimetric PM analysis, three Teflon fiber filters are collected along with one quartz filter per fuel and condition. The weights of the three Teflon filters are averaged and u_r is twice the standard deviation of the three masses.

On the plots shown in the following chapters, error bars are shown based on the above uncertainty analysis with each error bar being represented by $\pm u_t$. It is noted that for all high-speed variables like CA50, the instrument error was not included and the method for propagation of error was not known since they were calculated using externally developed, and proprietary, software. The uncertainty shown for these are based solely on the variability from the 100 sampled cycles per steady state condition.

CHAPTER THREE

COMBUSTION DEVELOPMENT

3.1 Engine Condition Development

The intent of this chapter is to establish engine operating conditions best suited to achieve the goals set forth in Chapter One. Since a large number of instruments are brought to bear to accomplish this task, single operating points are first developed with the baseline ULSD fuel to ensure that they meet the criteria for the type of combustion they are meant to typify. Identification of constant parameters used for the development of the points and selection of these parameters based on past studies is accomplished. Data taken from sweeps in injection timing and EGR, two primary control parameters, are used to optimize the selection of each condition.

In the second part of the chapter, combustion performance is explored for chosen operating conditions over the range of fuels used in the study. The objective is to see the effect of chosen constant parameters on combustion and to ensure that the emissions data presented in later chapters is from operating conditions best suited to illuminate differences resulting from fuel chemistry rather than those arising from secondary effects from physical fuel characteristics or ignition properties.

3.1.1 Identification of Constant Parameters

This section details constant parameters used for the experimental study chosen such that appropriate comparisons can be made between the selected fuels. In the experimental study, engine speed and load are such variables. Load for multi-cylinder engines is generally indicated using BMEP. In the study, duration of the main fuel injection event is altered to change engine load.

Another parameter that is maintained constant between fuels is the EGR rate. As mentioned in Chapter Two, the throttle is kept completely open to maximize volumetric efficiency, the VGT is used to set an initial EGR and the EGR valve is used to make small adjustments between fuels at an engine condition. In this way, although not specifically controlled, intake manifold pressure is maintained effectively constant for a given engine condition.

As was shown in the preliminary study, removing the effects of combustion phasing between fuels is best accomplished by maintaining a constant CA50 (Northrop et al., 2009). This measure of combustion phasing has also been proven to be an effective parameter of comparison between petroleum fuels of differing cetane numbers (Ickes et al., 2009). To maintain constant CA50 between fuels for a given engine, the timing of the main fuel injection event is advanced or retarded.

3.1.2 Selection of Engine Conditions

3.1.2.1 Overview

Three engine conditions are chosen in the experimental study. For these conditions, the parameters mentioned above are kept constant and comprehensive data are taken to compare detailed HC and PM emissions between the selected fuels. One mode represents a common use of early injection LTC (ELTC) and another represents late injection LTC (LLTC). The third is a conventional diesel combustion condition. The conventional case is selected to both confirm findings found in the established literature and to form a basis for comparison with premixed LTC of biodiesel. For choosing the two premixed LTC points, the work of previous researchers using the same engine as in the current experimental study and discussions with the engine manufacturer are used as guidelines. Table 3.1 shows a summary of the constant engine parameters set in the experimental study for the three operating conditions. The key constant parameters are shown along with their 95% confidence interval uncertainties taken over all data recorded at that condition. The remainder of this chapter is dedicated to characterizing these three chosen test conditions to set the stage for the detailed analysis of HC and PM in later chapters.

Table 3.1: Summary of important parameters for the three chosen engine conditions in the experimental study

Condition	Conventional	LLTC	ELTC
Speed (rpm)	1500 ± 2	1500 ± 1	1500 ± 1
Power (bhp)	17.1 ± 0.2	11.3 ± 0.1	5.7 ± 0.1
BMEP (kPa)	601 ± 7	397 ± 3	201 ± 3
Injections	Pilot/Main	Single	Single
Inj. Pressure (bar)	798 ± 17	1007 ± 11	804 ± 10
Inj. Timing (°BTDC)	≈ 2.2 (13.8)	≈ 5.9 – 7.1	≈ 17.3 – 24.1
CA50 (°ATDC)	10.1± 0.1	10.9 ± 0.1	-0.4 ± 0.1
NO_X Range (ppm)	39 – 65	26 – 35	221 – 239
EGR	24.9% ± 0.2%	45.3% ± 0.4%	55.2% ± 0.3%
Φ	0.57 ± 0.01	0.68 ± 0.02	0.52 ± 0.01
O_2 in Intake	16.9% ± 0.1%	13.6% ± 0.2%	14.4% ± 0.2%
Intake Pressure (kPa)	105 ± 1	101 ± 1	101 ± 1
Coolant Temp. (°C)	85 ± 1	86 ± 1	82 ± 1
Intake Temp. (°C)	53 ± 1	52 ± 1	38 ± 1

3.1.2.2 Engine Speed and Load

As discussed in Chapter One, the LTC regime is limited by both engine speed and load. Typical engine speeds studied for the use of these conditions are in the range of 1000 to 2000 rpm. As engine speed increases, the time allowed for fuel and air mixing decreases thereby limiting the duration of injection and engine load for that speed. For the study, 1500 rpm is chosen since at this speed, it is realistic to operate all three combustion strategies at different loads. Further, this speed was chosen for comparison with past studies using similar engines.

For low load operation, it is possible to yield the maximum benefits of simultaneous low soot and NO_X while maintaining high fuel conversion efficiency with an ELTC strategy. With early fuel injection occurring in advance of 15 CA°, peak cylinder pressures generated by combustion generally occur near TDC since fuel and air are very fuel lean. As load increases, peak pressure becomes too high decreasing durability and generating unacceptable combustion noise. In Knafl et al. (2008) it was found that the maximum load for an early injection strategy at 1500 rpm was 200 kPa BMEP and thus this load was chosen for the experimental study.

Though an ELTC condition is not appropriate for a mid-load condition, LLTC, with injection timing nearer to TDC maintains significant premixing while retarding peak pressures further into the expansion stroke. The LLTC test load was chosen to be 400 kPa BMEP since this was the load used in the preliminary study and as well as in other previous work with the same engine. As load increases in LLTC, the end of injection tends towards the start of ignition, this creating more diffusion burning. Once the diffusion portion of combustion becomes significant, the traditional low soot and NO_X tradeoff returns and the benefits of LTC disappear. Ickes et al. (2009) explored the load limits of a late injection LTC condition in a single cylinder version of the same engine used in the study. For an EGR rate of 45% and injection pressure of 1000 bar, the point of limitation was found to be 570 kPa indicated mean effective pressure (IMEP) which corresponds to just greater than 400 kPa BMEP in the test engine used in this study.

At higher loads, a conventional combustion strategy would typically be used in practice. A BMEP of 600 kPa was chosen to allow close enough comparison to the LLTC condition while increasing the soot concentration, allowing greater differences to appear in the comparison of fuels.

To envision the chosen engine speed and load from a practical perspective, Figure 3.1 shows an illustration of what steady state speed a hypothetical small-sized vehicle using the test engine would travel on level road at the three loads chosen for the experimental study. Road load resistance was calculated assuming only rolling resistance and air resistance. The calculations used in making the vehicle speed estimation are not shown in this document but can be found along with typical values for vehicle coefficient of rolling resistance and drag in the Bosch Automotive Handbook (2000, pp.338).

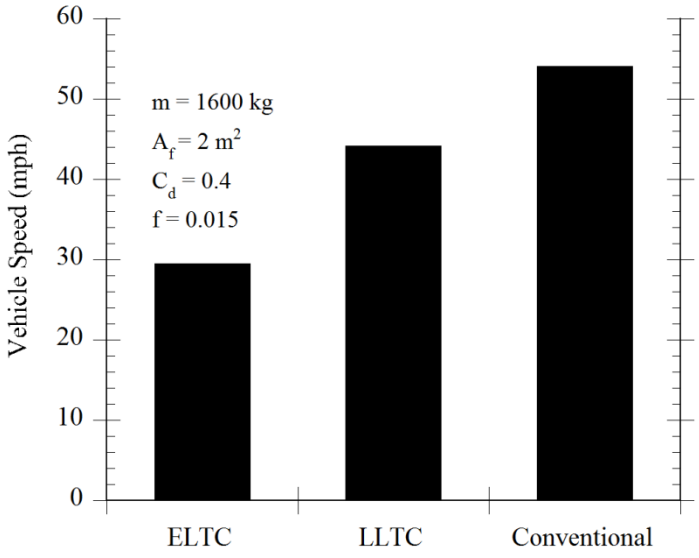

Figure 3.1: Level road vehicle speed for the three engine loads used in the experimental study

3.1.2.3 Injection Pressure and Timing

Premixed LTC strategies depend greatly on fuel injection properties. The pressure and timing of when fuel is injected into the cylinder directly influences mixing and thus ignition delay and burning rate. At the speed and load of the conventional condition, the test engine's stock ECU calibration utilizes a two injection strategy. The small pilot injection is meant to provide a premixed fuel and air region to ignite the larger main injection which occurs around TDC. This injection strategy exhibits a distinct diffusion burning phase since combustion has commenced once the main injection starts. The values of injection pressure, timing and relative duration between pilot and main were taken from the stock ECU calibration.

Injection pressures were set for the ELTC and LLTC conditions according to those from past studies with the same engine and from conversations with the manufacturer of the engine. Although high pressures are advantageous for mixing in LTC, they can have a deleterious effect due to parasitic power losses from the high pressure pump. Therefore, 800 bar injection pressure was chosen for the ELTC low power condition and 1000 bar was selected for the LLTC mid-load condition. Also, since high injection pressure decreases soot formation due to increased mixing and reduction of over-rich zones, lower injection pressure than the maximum allowable pump pressure of 1400 bar is set to enhance soot formation slightly for lower error in the gravimetric PM analysis.

Early injection strategies can be broadly characterized by peak cylinder pressures occurring around TDC and ignition delay longer than 10°ATDC. Such strategies have been developed in the literature with injection timings from 60°BTDC to 20 °BTDC

(Lechner et al., 2005). Even earlier strategies have been investigated in attempts to achieve complete HCCI-like conditions (Hardy et al., 2006, Kimura et al., 1999). The use of very early injection has drawbacks for the current study since it is desired to maintain constant combustion phasing between fuels at the same engine condition. By injecting fuel near intake valve closing, very small deviations in the start of ignition can be affected by large adjustments in injection timing. Therefore, a strategy with timing in the range of 30 °BTDC to 15 °BTDC is chosen to represent a low load premixed LTC condition where CA50 is controlled effectively using injection timing. Figure 3.2 shows how CA50 varies with injection timing for the three conditions used in the study with ULSD fuel over a varying injection timing range and with other parameters from Table 3.1 held constant.

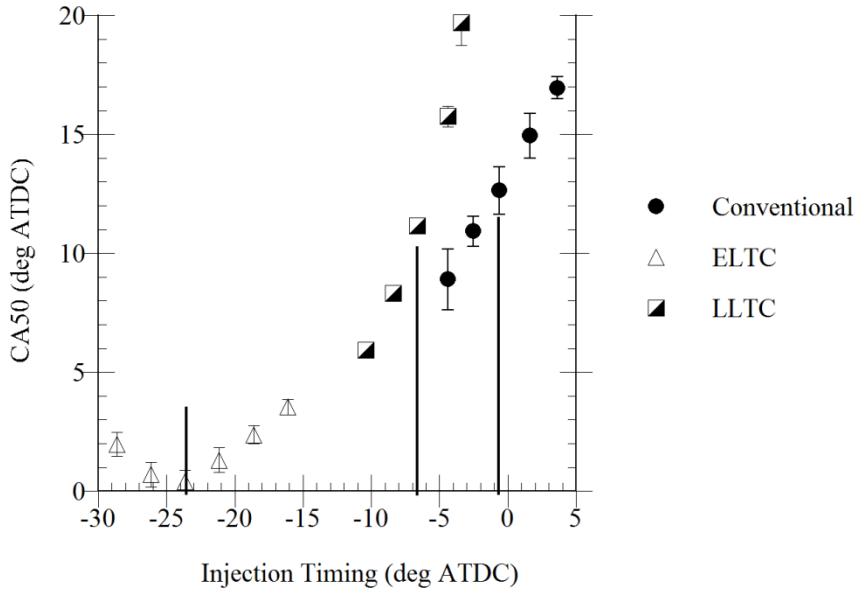

Figure 3.2: CA50 versus injection timing for the conditions tested in the study with ULSD fuel; vertical lines represent chosen conditions from Table 3.1

For all the conditions, CA50 and injection timing have a near-linear relationship with positive slope, a trend that is well known (Northrop et al. 2009, Ickes et al 2009). Interestingly however, CA50 for the ELTC case shows a minimum at the chosen injection timing of 25 °ATDC. Detailed investigation of the trend is beyond the scope of this dissertation. However, one possible reason for the retarding of CA50 with advancing injection timing (ie. increasing ignition delay) from this point is due to changing fuel spray targeting. If fuel droplets begin to miss the piston bowl, they may begin to impact the piston crown and prohibit the mixing essential for ignition to occur. As injection is further retarded, less fuel enters the bowl and exacerbates the mixing deterioration thus extending ignition delay further.

The above explanation is partially verified by Figure 3.3 where the four major pollutant emissions are shown over an injection timing range. When timing is advanced from 25 °BTDC, an inflection point occurs in all the curves. Soot and the other products of incomplete combustion increase while NO_X decreases sharply. One would assume that on either side of the minimum in CA50 for ELTC, NO_X would be similar since the maximum average cylinder temperature is nearly constant. However, if some fuel is deposited on the cylinder crown, more rich zones of combustion are likely. These areas lead to fewer zones where combustion occurs in the bowl leading to more HC and soot emissions.

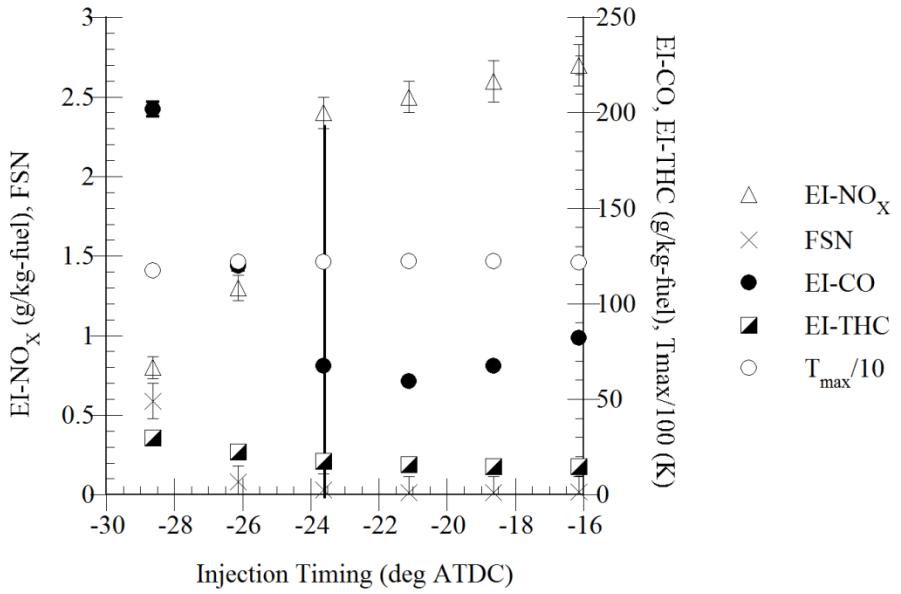

Figure 3.3: EI-NO_X, FSN, EI-CO, EI-THC and maximum mean cycle temperature versus injection timing for the ELTC condition and ULSD fuel

By examining the data, the most optimal point of injection timing for the ELTC condition is 24°BTDC since at this setting, THC and CO are low, FSN is near zero and NO_X is still acceptably low. Further, since all the other test fuels have higher cetane number than ULSD, the injection is retarded from this point to match CA50. Therefore, the limitation on advancing past the optimal point of spray targeting can be avoided for all fuels.

For ELTC, the effects of poor combustion before the 23.6 °BTDC point can be clearly seen in the plot of BSFC versus injection timing given in Figure 3.4 for the three engine conditions. Trends in combustion efficiency, although not shown, follow those of BSFC closely.

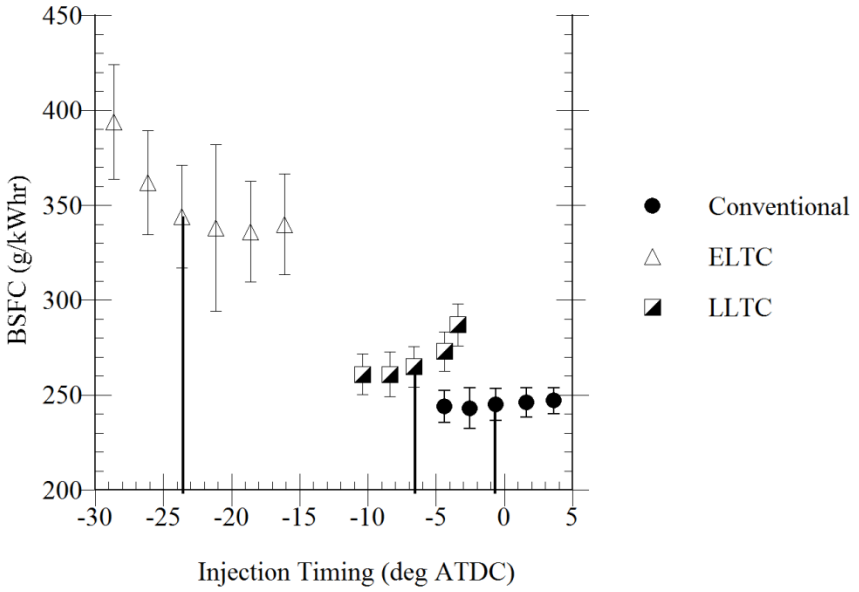

Figure 3.4: BSFC versus injection timing for the three conditions with ULSD fuel; vertical lines indicate chosen conditions from Table 3.1

Late injection strategies are characterized by having injection timing near that of conventional conditions and by combustion occurring after TDC. This is clearly illustrated in Figure 3.2 where CA50 and timing range for both the LLTC and conventional conditions overlap to some degree. The injection timing chosen for the LLTC condition coincides with the preliminary study (Northrop et al., 2009). This condition is also optimized from the perspective of combustion quality. With premixed combustion occurring with CA50 later than approximately 10 °ATDC, fuel and air have less time to burn as the piston travels down through the expansion stroke creating products of incomplete combustion due to quenching. This increases BSFC as shown in Figure 3.4. THC shows a sharp increase at timings more retarded than 6.6 ° BTDC as given in Figure 3.5, also a consequence of lower combustion efficiency. CO increases monotonically through the timing range indicating that zones of incomplete combustion

increase steadily as timing is retarded. NO_X decreases almost linearly with retarded injection timing whereas smoke remains consistently low, showing no evidence of the soot-NO_X tradeoff seen in conventional combustion. The chosen timing for the LLTC condition avoids the area of poorer combustion and also strikes a balance between NO_X and CO emissions.

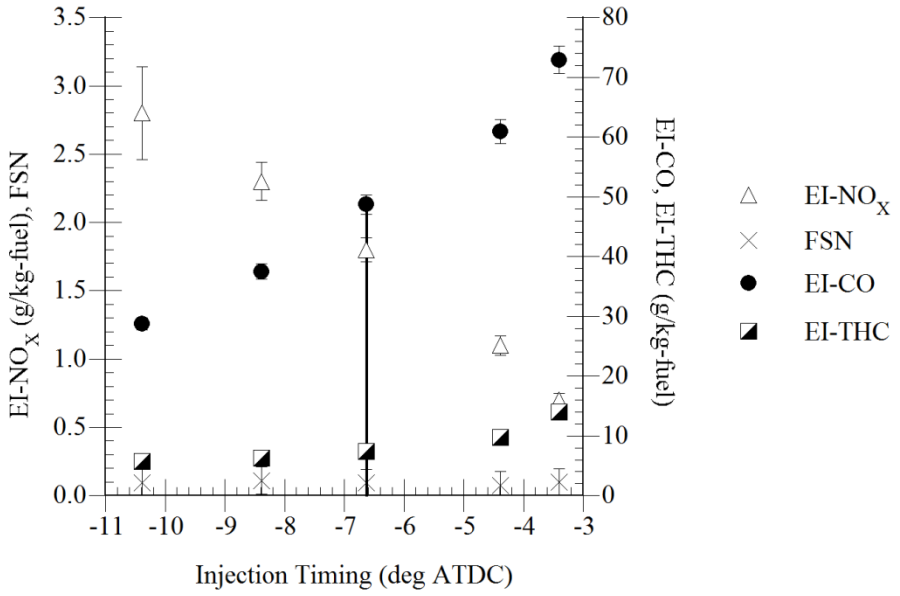

Figure 3.5: EI-NO_X, FSN, EI-CO and EI-THC versus injection timing for the LLTC condition and ULSD fuel

For conventional combustion, BSFC remains essentially constant along in a range of injection timing around the stock ECU setting as shown in Figure 3.4. Emissions for the conventional case are shown in Figure 3.6. Here NO_X decreases and FSN, CO and HC increase with retarded timing. As expected, with more retarded timing, combustion is pushed further back into the expansion stroke and more unburned fuel results. The NO_X emissions also decreases with retarded timing since combustion temperatures are cooling with the retarded combustion phasing. With further retarding of injection timing, smoke

emissions would be expected to rise although this is not seen in the range of timing tested.

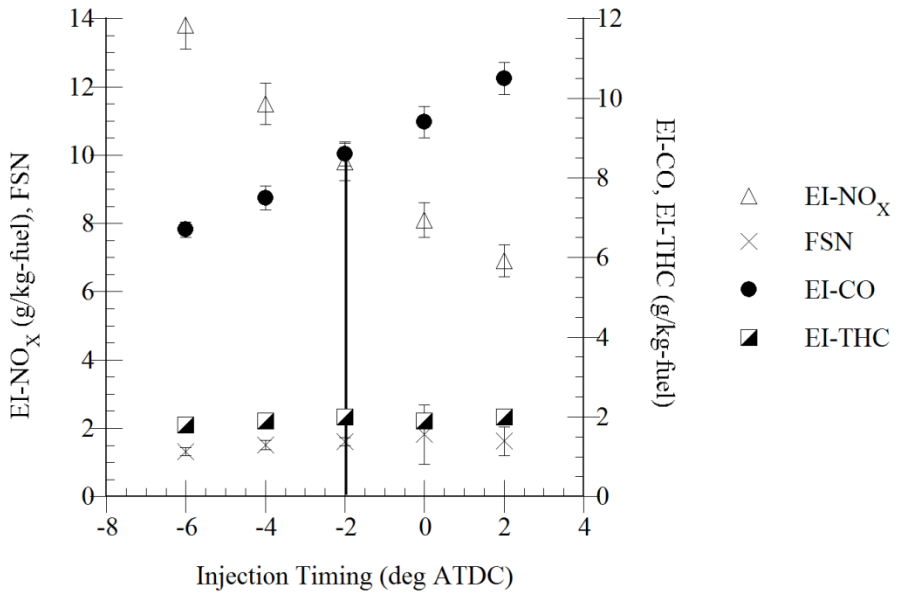

Figure 3.6: EI-NO_X, FSN, EI-CO and EI-THC versus injection timing for the conventional condition and ULSD fuel

3.1.2.4 EGR and Equivalence Ratio

Fueling rate and thus net fuel flow into the engine for the three conditions are dictated by the desired load. The quantity of air and EGR flow into the engine are partially dictated by engine speed though their proportion is chosen independently. High levels of EGR is the key enabling parameter for inducing long ignition delay for LTC and the important factor in reducing peak cylinder temperatures. By setting the fueling rate to achieve the desired load and by controlling the amount of EGR desired using the VGT in combination with the EGR valve as described in Chapter Two, the equivalence ratio is automatically constrained. Further control of φ could be made by using the intake throttle

though it has been shown that creating more boost through the use of a VGT has advantages for both engine efficiency and emissions (Jacobs et al., 2006).

For both the ELTC and LLTC conditions, EGR is set based on the capability of the laboratory EGR cooler to maintain a constant outlet temperature for an extended testing session. One issue limiting the use of LTC strategies in practice is the fouling of EGR coolers over time due to large quantities of cooled exhaust gases passing through them. As engine load increases, demand on cooling duty increases due to higher exhaust temperatures. Therefore, in the case of the experimental study, EGR is 55% for the ELTC and 45% for the LLTC condition. For conventional combustion, 25% EGR is chosen since this represents the estimated value set in the stock ECU calibration at this speed and load.

Emissions of soot and NO_X strongly depend on the choice of EGR rate. Figure 3.7 shows FSN versus EI-NO_X for the three conditions in the study with ULSD as fuel when EGR is varied. Engine speed, load and injection timing are held constant at the values shown in Table 3.1 for the conditions shown in the plot.

For the conventional combustion, the traditional soot versus NO_X tradeoff is clearly illustrated. In the steady state condition chosen for the study, NO_X falls within the middle of the range shown in the plot and the FSN is below 1. For ELTC, no discernable change in FSN is seen as a function of EGR illustrating the defeat of the soot-NO_X tradeoff. NO_X does increase with decreasing EGR due to rising combustion temperatures. Soot remains near zero for ELTC however since the degree of mixing is not changed with changing EGR and formation of hot rich zones of combustion does not occur (Kimura et al. 2001).

For LLTC, the opposite trend appears where soot increases with increasing EGR with only a small change in NO_X.

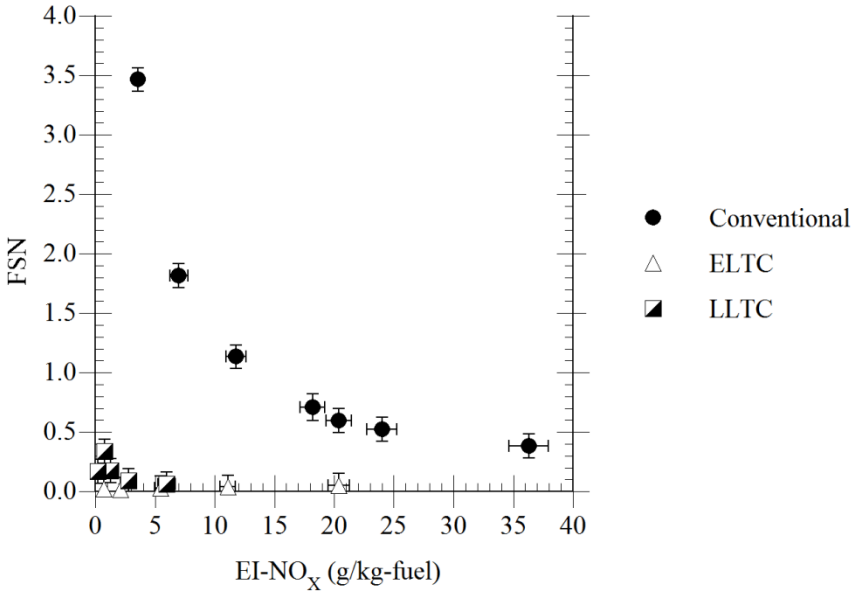

Figure 3.7: FSN versus EI-NO_X for the three chosen conditions with ULSD at varying EGR levels

Increasing EGR for LLTC extends ignition delay thereby retarding combustion further into the expansion stroke. This sharply degrades combustion quality leading to the formation of soot (Jacobs et al., 2007) as illustrated by combustion efficiency versus EGR rate shown in Figure 3.8. In ELTC, combustion efficiency degrades with increasing EGR without the formation of significant soot showing that unburned fuel most likely escapes due to over-leaning and not from fuel-rich zones. Values of η_c are lower in general for ELTC illustrating higher levels of THC for this strategy. In conventional combustion, EGR does not have significant effect on η_c since diesel combustion utilizing a diffusion flame typically yields more complete oxidation of the fuel. For conventional

combustion, EGR is chosen more based on NO_X and soot emissions and less based on combustion quality.

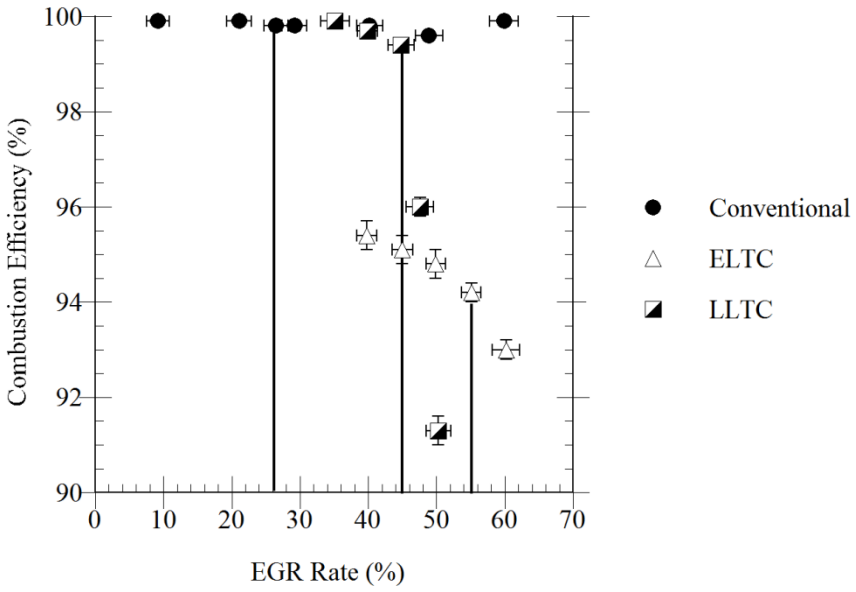

Figure 3.8: Combustion efficiency versus EGR rate for the three chosen conditions with ULSD; vertical lines indicate EGR rates for chosen conditions

3.2 Combustion Comparison Between Fuels

This section examines combustion and engine efficiency differences between fuels for the test conditions outlined in Table 3.1. It provides the proper background for the deeper examination of HC and PM emissions detailed in following chapters.

3.2.1 Test Protocol

In the investigation of the three steady state engine operating points used for the remainder of this dissertation, a specific test protocol was followed to ensure accurate and precise results. For a given fuel the desired operating condition was established and allowed to equilibrate for 45 minutes before data was taken. Then low speed emissions

analyzer data was taken along with high speed combustion data. FT-IR data was then recorded before sampling two filters from the dilution tunnel. A second emissions and high speed data point was then taken prior to a second FT-IR sample. Two more PM filters were then loaded using the dilution tunnel followed by a third round of emissions, high speed and FT-IR data. Total time to collect all data from one fuel and condition was approximately 45 minutes. All data for a given engine condition and all fuels was collected without shutdown of the engine to eliminate day-to-day variability due to atmospheric changes or other laboratory changes.

3.2.2 Conventional Condition

The pilot and main injection strategy used for the conventional combustion condition incorporated both premixed and diffusion burning phases. Results are comparable with those found in the literature reviewed in Section 1.2. This section will show that conventional combustion is very similar among the fuels tested when CA50 and the other parameters are held constant.

Examining the apparent RoHR calculated for conventional combustion, B100 and ULSD show very few differences as illustrated in Figure 3.9. Just following the pilot injection pulse, the RoHR curves dip under the x-axis indicating heat lost to evaporating fuel. At the crank angle where the curve re-crosses the axis with positive slope, the SOI is defined. Since the pilot injection is just 5.5% of the total fuel injected, most of the liquid is evaporated and the first spike in RoHR is mostly premixed as evidenced by its symmetrical shape.

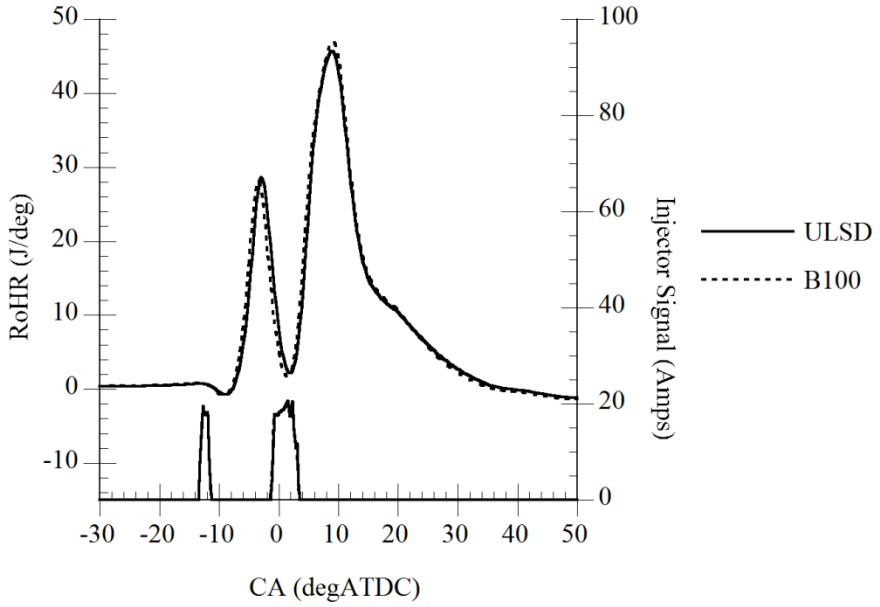

Figure 3.9: RoHR of ULSD and B100 for conventional combustion

The second, main injection occurs at the tail end of the pilot RoHR. The second spike in heat release corresponding to the main injection has a maximum but is not symmetrical. The long "tail" of the main heat release is indicative of a diffusion burning period leading to the eventual burnout phase (Heywood, 1988).

The other three fuels exhibit the same trends and differences between their RoHR curves are insignificant. These are not shown in Figure 3.9 to improve clarity. In examining the pilot region more closely for the neat fuels tested, Figure 3.10 shows that ULSD has a slightly retarded peak pilot RoHR due to its lower cetane number. All other fuels have identical pilot RoHR to the SWE and B100 cases.

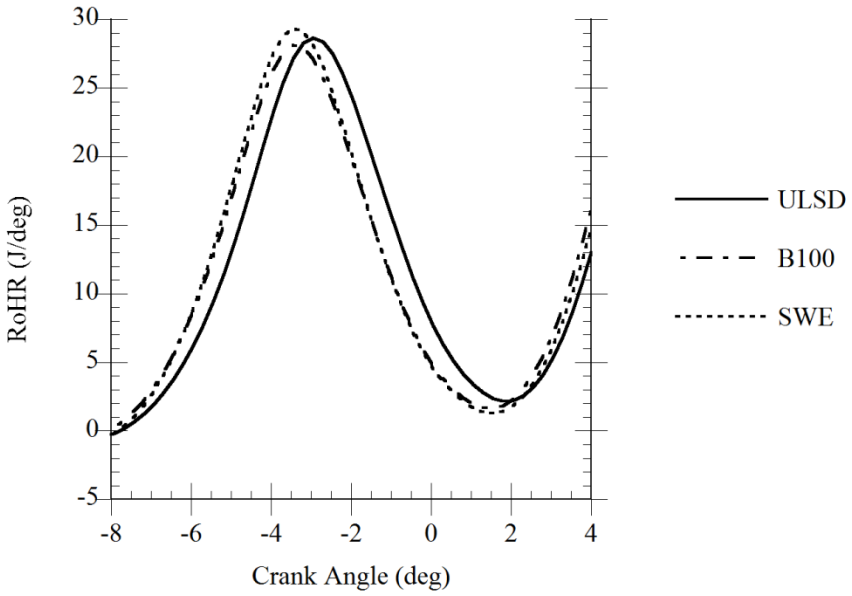

Figure 3.10: RoHR of the pilot injection region of neat fuels used in the study for conventional combustion

With mean combustion properties nearly identical, differences in engine performance are clearly related to fuel chemistry and not necessarily the fluid properties of the fuels. For example, some report NO_X emissions for biodiesel to increase compared with petroleum diesel citing its lower bulk modulus (Szybist et al., 2003). Mechanical unit injection systems cause fuel to be injected earlier for the same commanded timing depending on the compressibility of the fuel. This advanced timing allows combustion to occur closer to TDC thus raising peak cylinder temperatures. NO_X emissions, related mostly to local peak temperatures in the cylinder due to the extended Zeldovich Mechanism (Turns, 1996), subsequently increase. However, if combustion phasing is maintained constant and peak RoHR is the same due to load-compensated fueling rates, NO_X emissions are the same for all the fuels to the accuracy of the measurements as shown in Figure 3.11.

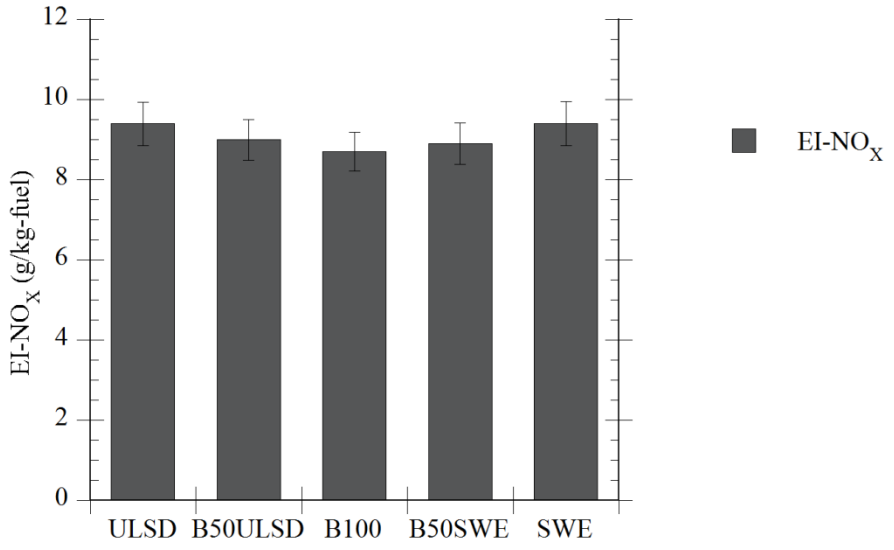

Figure 3.11: EI-NO_X fuel comparison for conventional combustion

Physical fuel properties like viscosity and surface tension can also lead to differences in spray breakup and vaporization from diesel injection systems. These differences cause an alteration in ignition and combustion phasing for a given injection timing. This in turn can change emissions and combustion efficiency thus altering the fuel consumption of an engine for a given load. If combustion phasing is maintained constant, differences caused by injection differences can be minimized and direct fuel chemistry effects can be seen. For example, BSFC is clearly different for the fuels tested in the study though brake fuel conversion efficiency is identical as given in Figure 3.12. Differences in LHV between biodiesel and the other fuels are effectively isolated from other fuel properties.

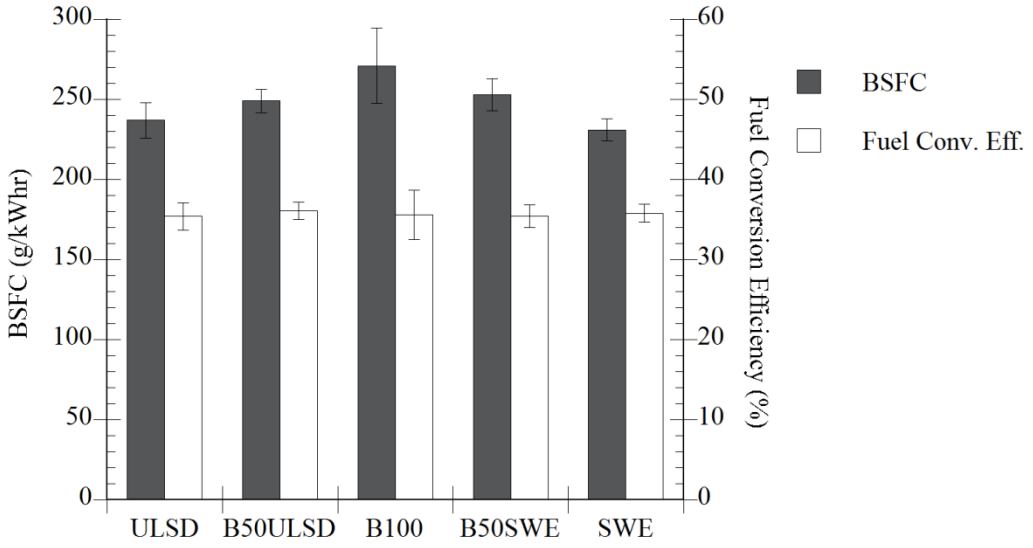

Figure 3.12: BSFC and fuel conversion efficiency for conventional combustion

3.2.3 LLTC Condition

The LLTC operating point has much different combustion properties than the conventional mode as illustrated in the RoHR and injection timing plot shown in Figure 3.13. As reviewed in Chapter One, one criterion for premixed LTC is that it has a shorter duration of injection than ignition delay. This can be seen for the LLTC condition for both biodiesel and ULSD in the figure. The main heat release is symmetrical, implying mostly premixed combustion. Between fuels, B100 has a larger peak main RoHR although the combustion phasing is the same as ULSD. Although not shown to enhance clarity of the plot, the low-aromatic SWE diesel fuel has the same peak rate of main RoHR as ULSD with both B50 blends falling between B100 and the petroleum fuels.

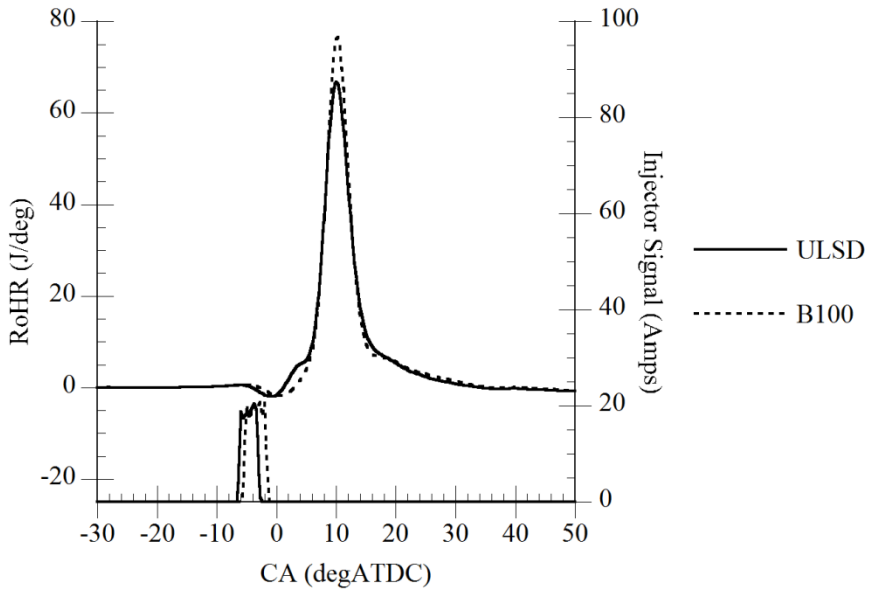

Figure 3.13: RoHR and injection timing for ULSD and B100 for the LLTC condition

One possible explanation for differences in the peak RoHR is that the ignition region is retarded for B100. Therefore, the maximum rate is higher for the same engine load and total heat release.

In diesel ignition, radical species are first formed in a slightly exothermic chemical reaction just prior to the main ignition event. Species like OH are essential precursors for starting the combustion event (Westbrook and Dryer, 1984). This process is easily seen on a RoHR plot for combustion regimes like premixed LTC where ignition delay is very long and can be seen as a small area just before the main heat release. This region is referred to as the low temperature heat release (LTHR) or the cool flame region and can be seen more clearly in Figure 3.14 where a closer view of the ignition region is shown for all fuels tested. LTHR cannot be as easily detected using a plot of RoHR for

conventional combustion due to shorter ignition delay but has been measured using other methods (Higgins et al., 2000).

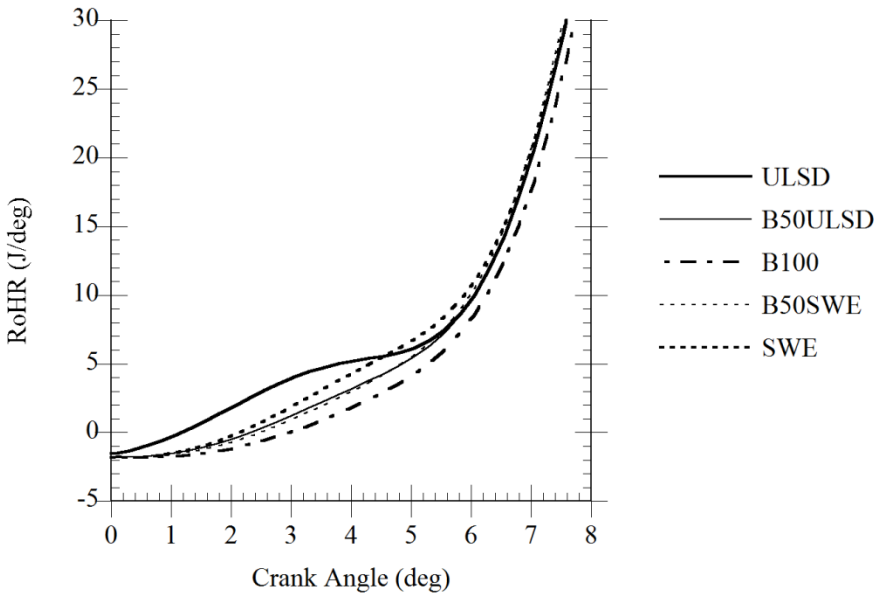

Figure 3.14: Fuels comparison of RoHR in the LTHR region of the RoHR for the LLTC condition

In comparing the ignition region of the neat fuels, ULSD and SWE both have a discernable LTHR process though for B100, it is absorbed into the main heat release process. It has been shown that methyl ester fuels do exhibit LTHR phenomena but proceed by a slightly different kinetic mechanism then for conventional diesel fuel (Szybist et al., 2007). Ignition for petroleum fuels is largely attributed to the breakdown of n-paraffin species. Szybist et al. showed that the aliphatic chain of methyl esters first react similarly to petroleum fuel in the first stages of ignition. The ester group undergoes decarboxylation later in the ignition process forming CO_2 to higher concentrations than for LTHR of n-alkanes.

The ignition differences explained above can be also seen by comparing ignition delay both measured by SOI to SOC and by SOI to CA10, the point of 10% mass fraction burned. A normalized combustion event timeline starting from SOI as the origin is shown in Figure 3.15. This diagram illustrates that although B100 has the median cetane number of the fuels tested; it has the longest ignition delay as measured by SOI to SOC. However, B100 has the median SOI to CA50 duration following the trend in cetane number of the fuels with ULSD as the lowest and SWE being highest as given in Table 2.7. This was also seen in the preliminary study where the duration from SOI to CA50 was a better indicator of cetane number than the ignition delay (Northrop et al., 2009).

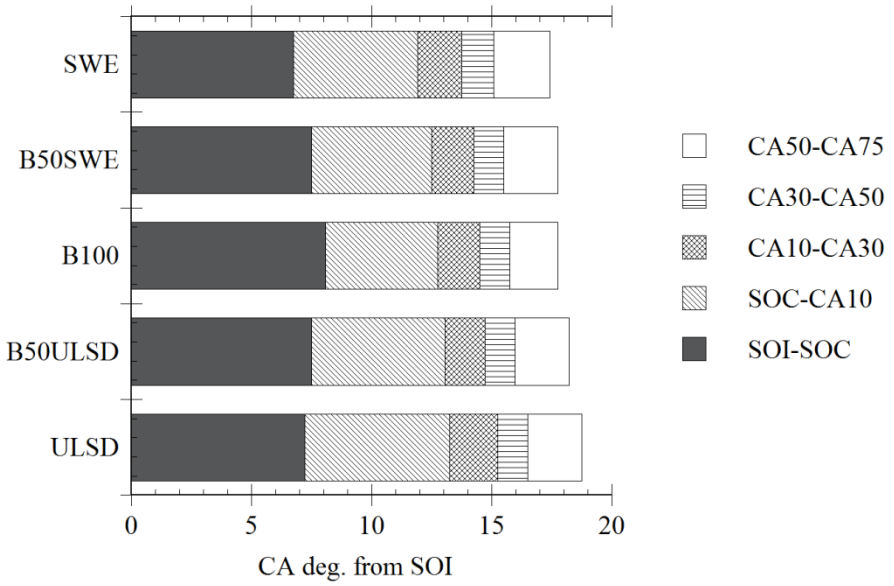

Figure 3.15: Combustion event timeline from SOI for the LLTC condition

For B100 to have longer ignition delay from SOI to SOC but shorter SOI to CA50 it has the shortest duration from SOI to CA10 showing that although very little LTHR is seen in the RoHR plot, the fuel has a very fast burn rate once combustion is initiated. The overall combustion event as measured by SOI to CA75 follows cetane number of the

fuels with ULSD being the longest and SWE the shortest corresponding to their different injection timings set to match CA50.

Even though B100 has a higher peak RoHR, it does not exhibit a distinctively higher peak cylinder pressure for the same combustion phasing and load as shown in Figure 3.16. Corresponding to the constant peak cylinder pressures, mean cylinder temperatures were near constant at approximately 1400 K for all the fuels tested. Slight differences in NO_X emissions, a strong function of temperature, for the LLTC condition tend with cetane number of the fuel rather than the peak cylinder pressure. Since NO_X formation is more a function of local conditions, it is likely that shorter ignition delay for the higher cetane fuels like SWE contributed to less mixing and increased local temperatures.

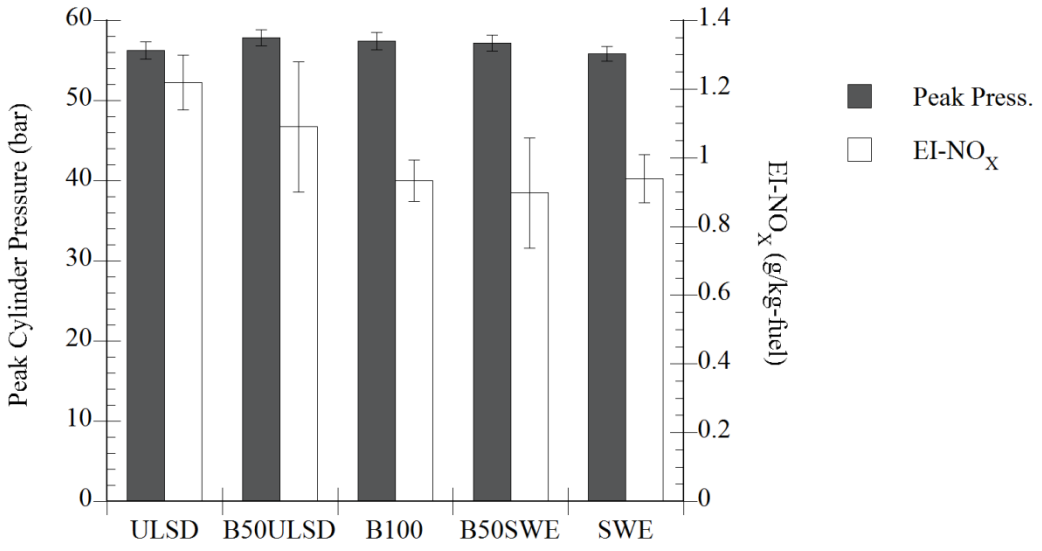

Figure 3.16: Peak cylinder pressure and EI-NO_X for all fuels at the LLTC operating condition

Like for the conventional combustion case, BSFC increases with biodiesel concentration in the fuel for LLTC whereas the brake fuel conversion efficiency remains the same. This plot is not shown for brevity. In summary, the LLTC operating condition maintains similar combustion properties for all the fuels tested even though measurements from the ignition region are inconsistent with what would be expected from the cetane number.

3.2.4 ELTC Condition

Maintaining constant CA50 for the ELTC condition requires larger differences in SOI for the fuels tested as shown in Figure 3.16. The main heat release event for early injection was sharper than for LLTC due to longer ignition delay and more premixed combustion. This is also deduced from the symmetry of the heat release curve shown in Figure 3.17 where very little “tail” exists at the end of the heat release suggesting extremely limited diffusion burning. Peak RoHR are lower in magnitude than for LLTC due to the lower engine load and higher EGR rate.

Between fuels, ULSD has the lowest peak RoHR and SWE the highest with B100 in the middle. The B50 blends fell between the neat fuels and are not shown in the figure for clarity. With larger changes in ignition timing required to maintain constant CA50, the ignition region becomes more abbreviated with increasing cetane number as would be expected. With a shorter LTHR region, more fuel energy is released in the main heat release creating a higher maximum value.

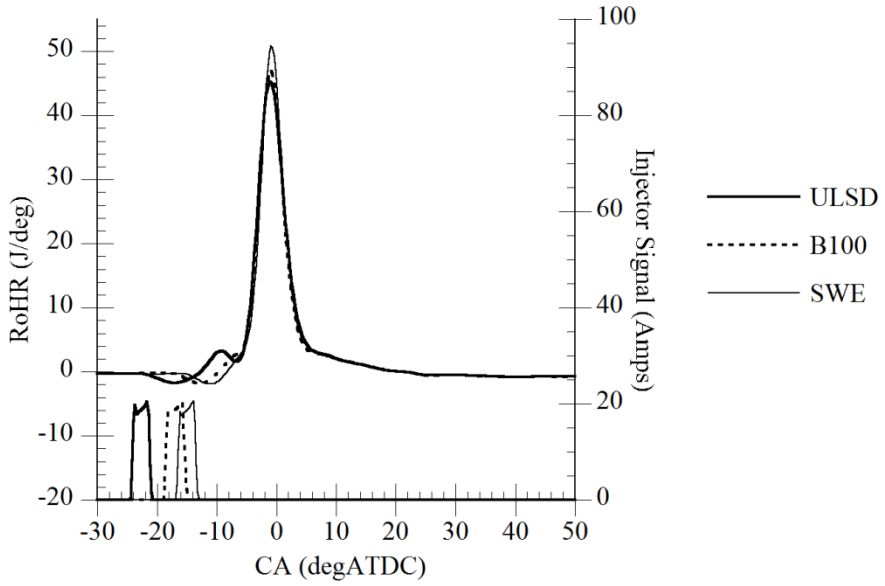

Figure 3.17: RoHR and injection timing of the three neat fuels for the ELTC condition

Looking more closely at the ignition region, the LTHR for ELTC is more pronounced than for LLTC since ignition delay is longer and reaction kinetics slower for the radical forming reactions. Unlike the LLTC case, the ELTC condition shows a distinct LTHR region for B100. In Figure 3.18 where a detail of the ignition region for all the tested fuels is given, the size of the LTHR region varies with the cetane number of the fuels, a trend not seen for LLTC. Similar to the LLTC condition, the LTHR region is delayed for B100 creating a higher peak RoHR for B100 as seen in Figure 3.17.

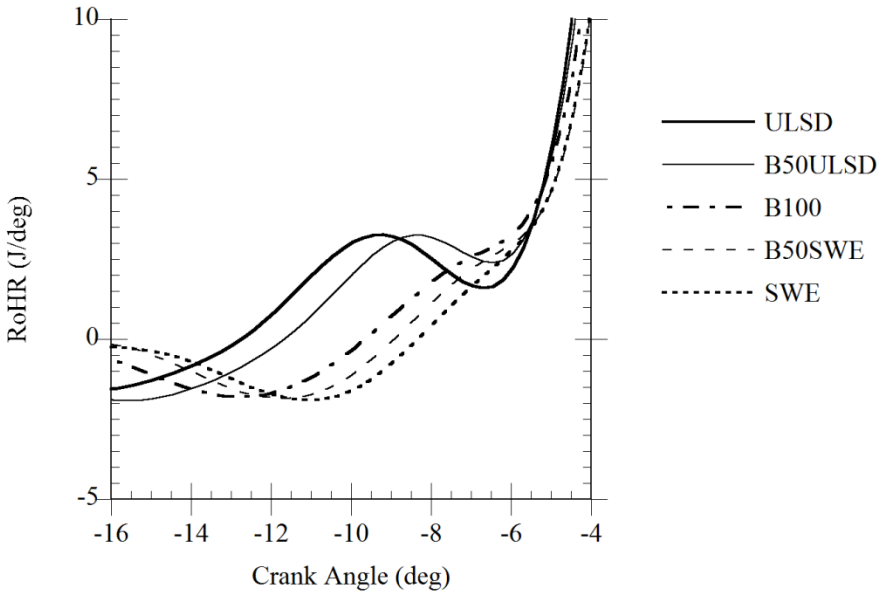

Figure 3.18: LTHR region of the RoHR for the ELTC condition and all tested fuels

The entire combustion process for the tested fuels in ELTC can be seen more clearly in the combustion timeline shown in Figure 3.19. Like for the LLTC condition, a relationship exists between the overall combustion duration and cetane number where SWE has the shortest SOI to CA75 duration and ULSD the longest. Unlike the LLTC case however, the ignition delay for the fuels also follows the cetane number trend with B100 having the median value for SOI to SOC and SOI to CA10.

Differences between fuels in the ignition region are clearer for the ELTC condition than in LLTC because longer ignition delay allows more premixing and vaporization. If all fuel is vaporized for all fuels tested, reactivity plays a more significant role in determining ignition properties. It is possible that the longer than expected SOI to SOC found for biodiesel in LLTC is due to the fuel's lower volatility. This would result in less vaporized fuel at ignition and cause the delay to increase. For ELTC, the amount of fuel

injected is less and more vaporization occurs, allowing biodiesel's higher reactivity to shorten the ignition delay more in accordance with what would be expected from the cetane number trends.

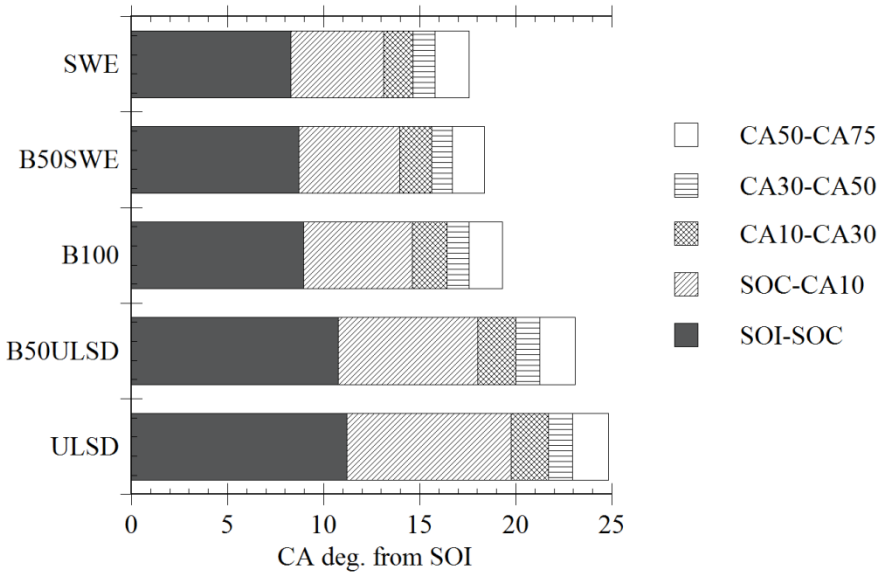

Figure 3.19: Combustion timeline for the ELTC condition

Similar to the LLTC case, ELTC has approximately a constant peak cycle pressure over the range of fuels tested even though the peak RoHR increases with cetane number. Compared with LLTC, the magnitude of peak cylinder pressure is higher; a result of more premixed combustion occurring. NO_X emissions increase for B50SWE and SWE although the uncertainty is higher in the very low range of concentration measured. The higher NO_X for the low aromatic SWE fuel was most likely a result of higher peak RoHR indicating more localized areas of lean and high temperature combustion. The NO_X emissions are higher in ELTC than for LLTC as a result of higher peak cylinder pressure and lower average equivalence ratio.

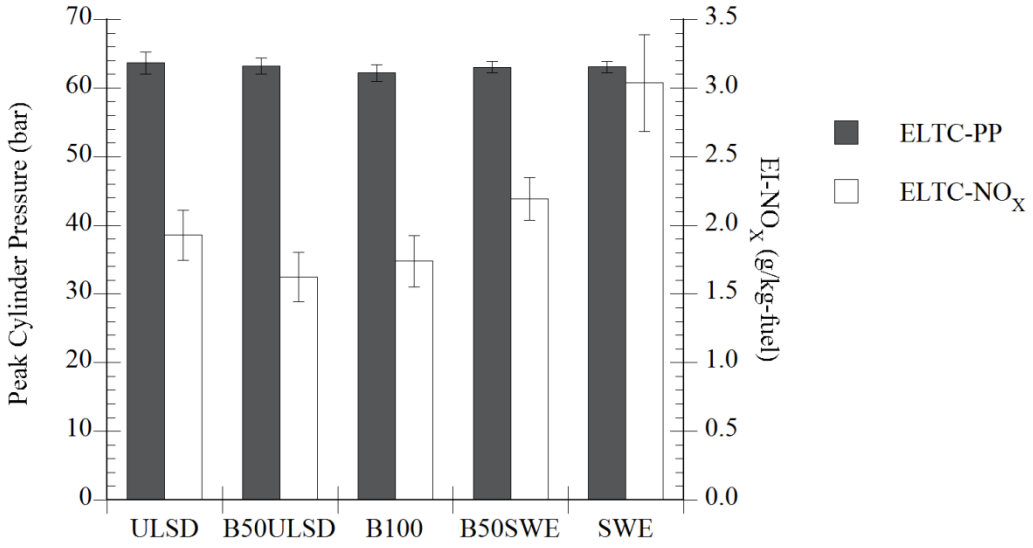

Figure 3.20: Peak cylinder pressure and EI-NO_X for all fuels at the ELTC operating condition

3.2.5 Summary of Operating Conditions

From the above discussion, the ELTC case is a more distinct example of partially premixed combustion than the LLTC case as evidenced by the longer ignition delay and narrower RoHR curves. The conventional case exemplifies a stock engine combustion mode where a pilot and main injection create two distinct heat release rate peaks. Differences in injection timing to maintain constant CA50 were smallest for the conventional case due to the pilot strategy whereas the LLTC condition required some retarding of timing with increasing cetane number. The ELTC case required the largest changes in injection timing to maintain CA50 creating the largest differences in peak RoHR between fuels.

For the three conditions, maintaining constant CA50 for all tested fuels by changing injection timing was an effective way to normalize engine performance with respect to

combustion phasing. Although duration of combustion and ignition properties varied among fuels for each condition, peak cylinder pressures, and therefore mean cylinder temperatures, were essentially constant. As a result, NO_X emissions were largely the same for all fuels at each condition. By fixing combustion phasing using CA50, the complex effects of differing physical fuel properties and cetane number are best minimized when examining the emissions of HC and PM in the following chapters.

CHAPTER FOUR

GASEOUS HYDROCARBON AND CARBON MONOXIDE EMISSIONS

4.1 Background

The primary goal of this chapter is to show how the data taken in this study can be used in concert with work presented in the literature to achieve the first goal set forth in Chapter One. Restated, this is; "To explain why the gaseous HC and CO emissions from biodiesel LTC decrease compared to petroleum diesel fuels by exploring the distribution of light hydrocarbons within the THC measurement."

The work described here extends beyond the identification of VOCs as defined by the US-EPA but encompasses the highest concentration LHC species found from incomplete diesel combustion. First, background information will be reviewed describing previous work in the identification of what partially reacted species are important for premixed diesel combustion and where they are thought to originate. Then, THC, CO and H_2 emissions data taken for the ELTC and LLTC steady state engine operating conditions will be presented and compared with the conventional combustion case. To look deeper into the species contained within the THC, LHCs measured using FT-IR will be presented and the trends between fuels and operating conditions will be analyzed.

4.1.1 Sources of HC and CO in Diesel Combustion

Fuel is never completely consumed in engine combustion processes where it is directly injected into the cylinder. Heywood (1988) describes several sources of HCs in compression ignition engines. The first is from over-mixing to yield equivalence ratios below the lean flammability limit of the fuel not permitting it to completely oxidize within relevant engine time scales. Generally, over-mixing occurs at low loads in conventional combustion and for LTC conditions due to long ignition delays. Under-mixing can also lead to a similar situation where insufficient oxygen exists to consume the fuel completely. These regions generally occur at high loads or in as a result of over-fueling. Small volumes of fuel can also leak from the injector sac volume into the combustion chamber during expansion creating fuel rich pockets which do not burn.

HCs in diesel combustion also occur due to quenching processes. Wall quenching occurs when fuel comes into contact with cool surfaces like the firedeck or top of the piston. Fuel can also be trapped in crevice volumes like those near the piston rings and re-released into the cylinder unreacted during expansion. Bulk gas quenching also exists where slow burning rates in some areas do not allow combustion to complete due to lowering cylinder temperatures during the expansion stroke. Slow rates of burning generally occur during the mixing-controlled portion of conventional combustion but can also exist in premixed modes where considerable EGR is present.

The goal for complete combustion is to emit all fuel carbon as CO_2. Therefore, it is formed in all areas of the combustion chamber where oxidation of fuel is occurring. In the expansion stroke, equilibrium reaction rates are high enough to change the proportion

of CO, CO_2, H_2 and H_2O. CO is left as a result of these equilibrium reactions and is also emitted a product of the incomplete combustion processes mentioned above.

Recent work has explored the primary sources of HCs in partially premixed LTC. Concentrations of all partially reacted species are well known to increase for LTC compared to conventional combustion. In early injection strategies like the ELTC condition studied here, Colban et al. (2007) studied crank angle-resolved THC concentrations using a fast FID analyzer from near the exhaust valve of a similar engine to that used in this study. They found that high HCs in LTC are primarily a result of the mean combustion cycle and are not due to combustion variability from cycle to cycle. Further, the study found that most HCs exit the cylinder later in the exhaust process indicating that they originate from zones along the top of the piston or from the piston bowl. The inference from the work is that the bulk gas plays a significant role in HC generation for early injection strategies.

Some studies have used optical techniques to identify the primary sources of HC emissions from LTC. Lachaux and Musculus (2007) found that the evolution of formaldehyde (H_2CO) closely tracks that of the THC the bulk gas. By using planar laser induced fluorescence they were able to track the zones of formaldehyde during both early and late LTC conditions. At the end of injection, mixtures near the injector tip were too lean for complete combustion. The study contributed to the diagrammatic view of the progression of LTC combustion shown in Figure 1.4.

Bulk gas quenching is also known to be a significant source of partially burned species in LTC. Kashdan et al. (2007, 2008) ran a low load early injection to late

injection timing sweep in both an optical and metal engine and was able to track HC emissions using tracer laser-induced fluorescence. They found that bulk quenching of low temperature over-rich and over-lean zones in the combustion chamber were the most significant sources of HC emissions from LTC. For early injection strategies like the ELTC condition presented in this work, Kashdan et al. found that liquid films forming on the piston top and re-evaporating during the expansion stroke also play a major role in HC emissions although crevice flows from the piston ring area were still not significant for the engine tested. This theory is seen in Figure 3.3 where for timings earlier than approximately 25 °BTDC, THC emissions increase drastically apparently due to more injected fuel missing the piston bowl.

In summary, the longer ignition delay found in LTC enhances mixing but creates zones where mixtures are not within the flammability limits of the fuel. Further, the low temperature of combustion due to high levels of EGR contribute to slow burning in these zones and eventually bulk quenching of the reactions. In early injection strategies such as the ELTC condition reported here, liquid films can also collect at the top of the piston which later evaporate and contribute to higher THC emissions.

4.1.2 Primary Species Emitted from Diesel Combustion

Diesel fuel and biodiesel are composed of a blend of hydrocarbon components with molecular weights ranging from about 100-250 for petroleum diesel and around 300 for biodiesel. During combustion, species of both lower and higher molecular weights than the original fuel are created. Lighter compounds like ethylene (C_2H_4) and formaldehyde are primary species created from fragmentation of longer aliphatic molecules in the fuel.

Species like poly-aromatic hydrocarbons (PAH) created that are the same or heavier than the fuel are created from the lighter molecules by polymerization and dehydrogenation reactions. Some fuel also directly escapes the combustion process without reacting originating from over lean areas from the sac volume, liquid pools on surfaces, crevice flows and bulk quenching processes as described in the previous section. Figure 4.1 shows a schematic of fuel-derived emissions from diesel engines as a rough function of their molecular weight. THC as measured by the FID analyzer in this study is assumed to incorporate all gaseous hydrocarbon species including most of those in the higher molecular weight range.

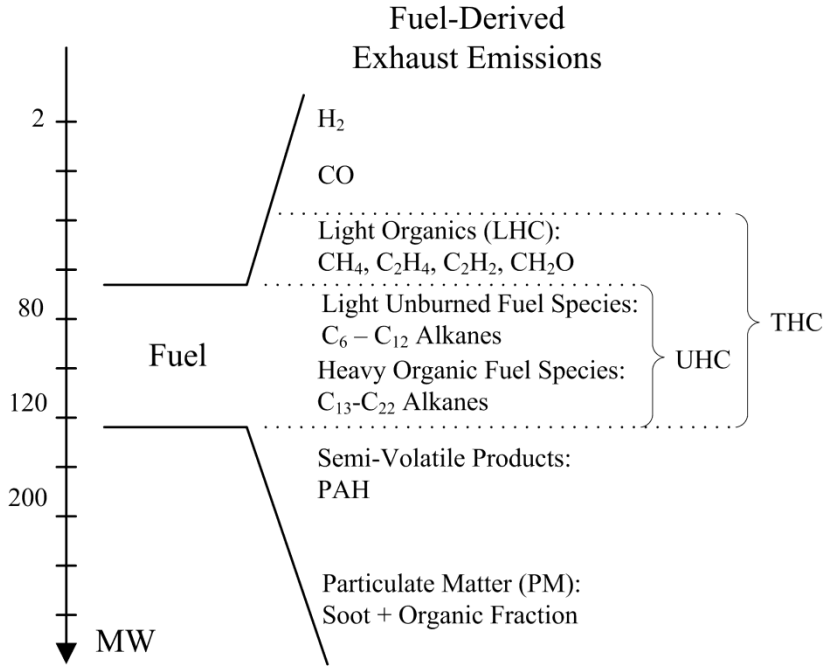

Figure 4.1: Diagram of fuel-derived exhaust emissions from diesel combustion

4.1.2.1 Premixed LTC of Petroleum Diesel

Some previous work has been done in examining the hydrocarbon species formed from premixed LTC. Cook et al. (2008) in a modeling study predicted that lean and rich zones produce different types of partially reacted products. In an early-injection strategy, they showed that nearly all methane emissions originated from rich zones of combustion whereas lean zones accounted for the majority of CO and unburned fuel. Ethylene is also predicted to be a major product and originates from either lean zones or areas where mixtures are cold, allowing fuel to decompose but not completely burn. In their findings they estimate that with better mixing or colder combustion temperatures the proportion of ethylene to methane would increase.

Sluder et al. (2004) speciated diluted exhaust products from an engine late injection LTC condition. In their study, they found that by increasing EGR to enter the LTC combustion regime, carbonyl species like the aldehydes, formaldehyde and acetaldehyde increased approximately proportionally with THC corresponding well to the work of Lachaux and Musculus (2007). Methane and ethylene were not mentioned in their work although Koci et al. (2009) in a comprehensive study of sources of HC and CO in LTC found that methane, ethylene and acetylene (C_2H_2) were the primary light species found over a range of injection timings and EGR. In that study, CO emissions were found to track well with trends in light ($<C_6$) HCs indicating that they originate in the same regions. Speciation work done by Han et al. (2009) from a diesel engine operating in late injection LTC confirm that methane, ethylene and acetylene make up the majority of light HCs for premixed modes of combustion.

The light hydrocarbon fraction of THC varies according to study. Ethylene concentrations can vary from about 2.5% (Lewis et al., 2005) to near 18% (Han et al. 2009) by volume in different modes of LTC. CH_4 varies more widely from approximately 1.8% (Han et al. 2009) approaching 25% (Koci et al, 2009). Based on the theory of Cook et al. (2008), this indicates that lean and rich zones can appear to differing magnitudes in the LTC regime depending on engine geometry, injection timing, EGR and other factors. Aldehydes can also make up a significant fraction of the THC. Lewis et al. found formaldehyde and acetaldehyde to be the primary aldehyde species produced by LTC. In their study, they found the two species to have similar concentrations and to make up around 2.5% of the THC over a range of injection timing and fuel cetane number.

Heavy gaseous hydrocarbons like those from the fuel increase for LTC corresponding well to the ethylene and formaldehyde found in over-lean portions of the combustion chamber. For early injection timings where liquid layers form on the piston or in crevice volumes, the unburned fuel portion of the THC increases significantly indicating that it escapes combustion completely (Koci et al, 2009).

Heavy species produced from lower molecular weight hydrocarbons like PAH have also found to increase for LTC combustion. Naphthalene is most prevalent PAH compound by about a factor of 10 over the remaining compounds in LTC (Merritt et al., 2006). This distribution is the approximately the same for conventional combustion and is a result of carryover from PAH in the fuel along with that formed during combustion (Rhead et al. 2003). PAH compounds can range from naphthalene with a molecular weight of 128 up to those with multiple rings and molecular weights of more than 350 (Dobbins et al., 2006). Heavier PAH compounds are generally not captured by the FID at

190°C but account for a miniscule portion of the THC measured. Merritt et al. (2006) showed that for an early injection LTC condition that THC was on the order of 80 g/hr whereas the total PAH found from both gas and particulate phase was not more than 2 x 10^{-4} g/hr for the same condition. Even with the low concentrations PAH emissions, especially those with higher molecular weight merit the intense investigation by researchers since they have extremely high mutagenic capability in humans (IARC, 1983). PAHs are not measured in this study since it is primarily the bulk HCs contained in the gas and particulate phase that are of interest.

Other HC species emitted from diesel combustion that do not originate from the fuel include those from the lubricating oil which come into contact with the combustion gases along the cylinder walls mainly during expansion (Heywood, 1988). Just as species from the oil can be emitted from the engine, fuel components can make their way into the oil through dilution processes as will be discussed in Chapter Five.

4.1.2.2 Conventional Combustion with Biodiesel

Previous work has compared HC emissions for biodiesel versus petroleum diesel using conventional combustion strategies. In general, it is found that THC and CO emissions decrease with increasing concentrations of biodiesel in the fuel as was mentioned in Chapter One. For example, Payri et al. (2009) found that THC decreased by 64% and CO by 50% on an EI basis for B100 versus diesel fuel for a conventional combustion condition very similar to that tested in this work. In general, light HCs less than C_7 were extremely small as a fraction of total THC. Some semi-volatile, partially burned species were detected but were less significant for B100 than for diesel fuel.

Ballesteros et al. (2008) also found a near 50% reduction in THC emissions excluding CH_4 for biodiesel for an engine operating over a European driving cycle. In their results, most fuel species reduced with increasing biodiesel except for aldehyde species which increased.

Aldehyde emissions for biodiesel in conventional combustion have been reported to go up as compared to petroleum diesel as in the case of Ballesteros et al., remain unchanged (Lea-Langton et al., 2009) or go down (Peng et al., 2008). Peng et al (2008) reported the decrease in overall aldehydes for B20 from a petroleum diesel fuel in a light-duty diesel engine over a US drive cycle on a brake specific basis. In their study, they found that formaldehyde and acetaldehyde accounted for about 75% of the total aldehydes in the diluted exhaust. Differing trends in aldehyde emissions depend strongly on operating condition as was found in McGill et al. (2003) where a low load condition had higher aldehyde emissions for petroleum and similar aldehydes for biodiesel at higher engine loads. Since aldehyde emissions, like ethylene are strongly linked to lean combustion, they are also dependent on the amount of mixing occurring in the cylinder. Ignitability differences in the fuels at the same injection timing could account for large differences in aldehyde emissions found in previous work. By keeping combustion phasing constant between fuels, this study allows comparison of aldehyde and other gaseous hydrocarbon emissions independent of when combustion occurs.

4.2 Experimental Results and Discussion

4.2.1 Combustion Efficiency

As has been mentioned in previous chapters, combustion efficiency (η_c) is a measure of the ratio of energy contained in the exhaust to that contained in the fuel. Put another way, it measures how effectively a fuel is converted into complete combustion products. It is an important metric for obtaining an overview of how complete the combustion process is. In the experimental study η_c is calculated from the bulk gas emissions recorded by the emissions analyzer bench using Equation 2.7. It is related to the overall fuel conversion efficiency (η_f) by Equation 4.1.

$$\eta_{th} = \eta_c \cdot \eta_f \tag{4.1}$$

In Equation 4.1, η_{th} is the thermal efficiency and represents the first law thermodynamic efficiency of the engine cycle. Figure 4.2 shows η_c for all the fuels tested and for the three operating conditions tested. Conventional combustion has the highest η_c of the three conditions at over 99% which indicates almost complete conversion of the fuel. For the LLTC condition, η_c decreases and is lower still for ELTC.

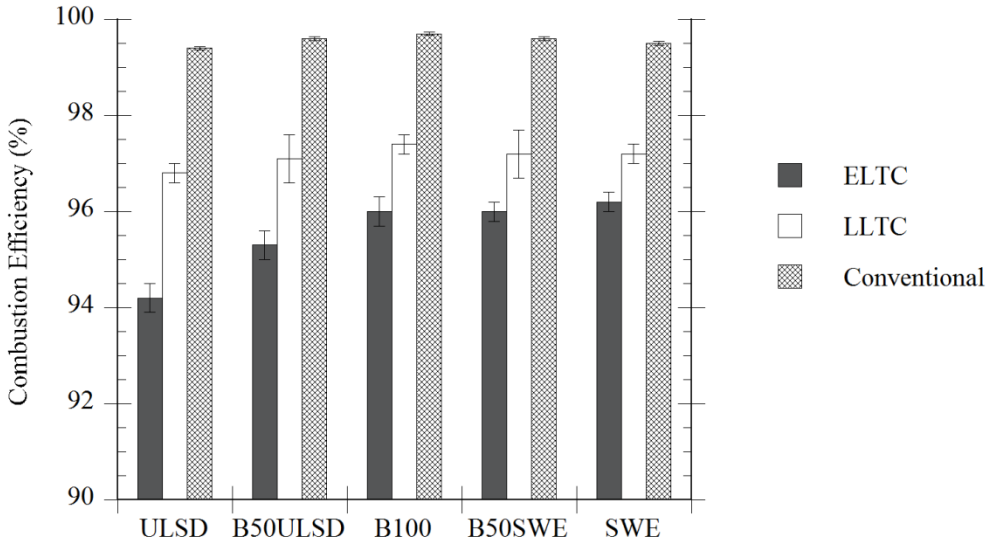

Figure 4.2: Combustion efficiency for the three conditions and all fuels

In comparing η_c for biodiesel versus the two diesel fuels, conventional combustion shows no differences in fuel conversion. For LLTC, ULSD has slightly lower η_c though with little statistical significance. ELTC however exhibits this trend more clearly with a 2% difference in η_c over B100, B50SWE and SWE. The increasing η_c follows an inverse relationship to ignition delay time for ELTC both measured by SOI-SOC and by SOI-CA50 as shown in Table 4.1. The correlation becomes stronger for ignition delay measured as SOI-CA10 as calculated by the Microsoft Exel *Correl* function which automatically determined the correlation coefficient between two arrays of data. Fuel ignition properties appear to have a dominant effect on η_c since both ULSD and SWE are petroleum fuels of similar distillation but with differing cetane number.

Table 4.1: Correlation between η_c and ignition delay for ELTC conditions

	ULSD	B50ULSD	B100	B50SWE	SWE	Correl.
η_c	94.2%	95.3%	96.0%	96.0%	96.2%	
SOI-SOC (ms)	1.25	1.19	0.99	0.97	0.92	**-93.8%**
SOI-CA10 (ms)	2.19	2.00	1.62	1.58	1.46	**-96.6%**

Although combustion phasing is maintained constant between fuels, mixing times allowed before combustion occur play a major role in how much over-leaning occurs in the cylinder prior to and during combustion. As the duration before ignition increases, more mixing is allowed thus increasing zones where lean conditions may exist. Another possible reason for lower η_c for ULSD in ELTC is that the SOI was advanced closer to the point where a portion of the fuel spray may miss the piston bowl allowing liquid to collect on the top of the piston.

4.2.2 Carbon Monoxide and THC Emissions

Emissions of CO and THC are among the most common data measured from diesel engines since they are limited by governmental regulations. Beyond certification of engines, these two measurements are useful for understanding the combustion process. Figure 4.3 shows the THC emissions for the fuels and conditions run in this study. Emissions of THC are very low as expected for the conventional combustion condition, higher LLTC and the highest for ELTC. Very high THC emissions are expected for ELTC since ignition delays are much higher allowing more time for mixing to occur in the cylinder.

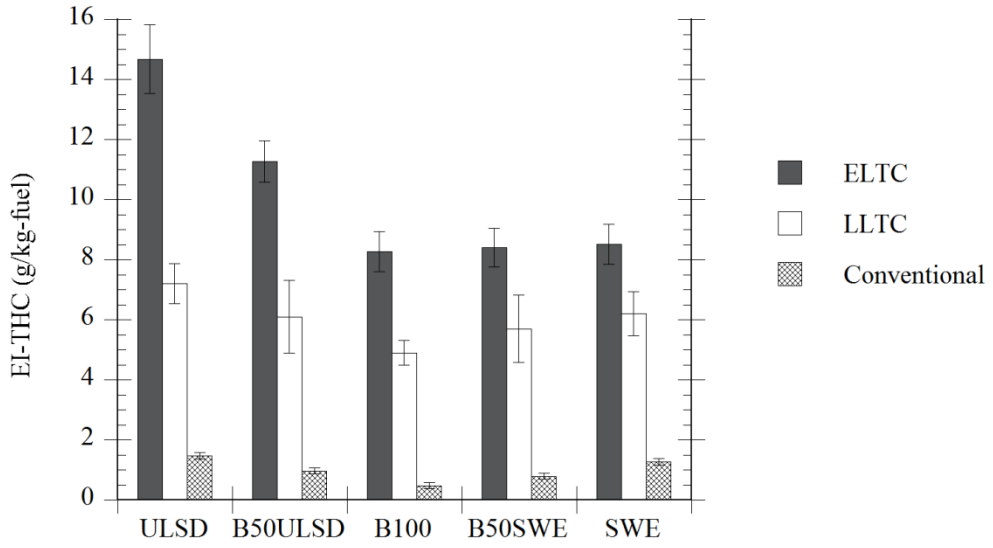

Figure 4.3: EI-THC emissions for all fuels and operating conditions

SWE has lower THC emissions than ULSD for ELTC and less so for LLTC. Reasons for this include shorter ignition delay for SWE leading to less over-leaning prior to combustion. The disproportionally higher THC for ULSD and B50ULSD could be also due to higher quantities of liquid pooling on the piston top as previously mentioned.

Evidence for the theory of more unburned fuel from liquid quenching for ULSD and B50ULSD can be inferred from the EI-CO data shown in Figure 4.4. Here, the ELTC CO is more commensurate between LLTC and ELTC for ULSD and SWE. Restated, both LLTC and ELTC show lower CO for SWE than ULSD but in approximately equal proportions. Since CO is a product of partial combustion and has little to do with liquid wall quenching processes, it is a logical conclusion that wall quenching is a larger component of the higher THC emissions for ULSD in ELTC.

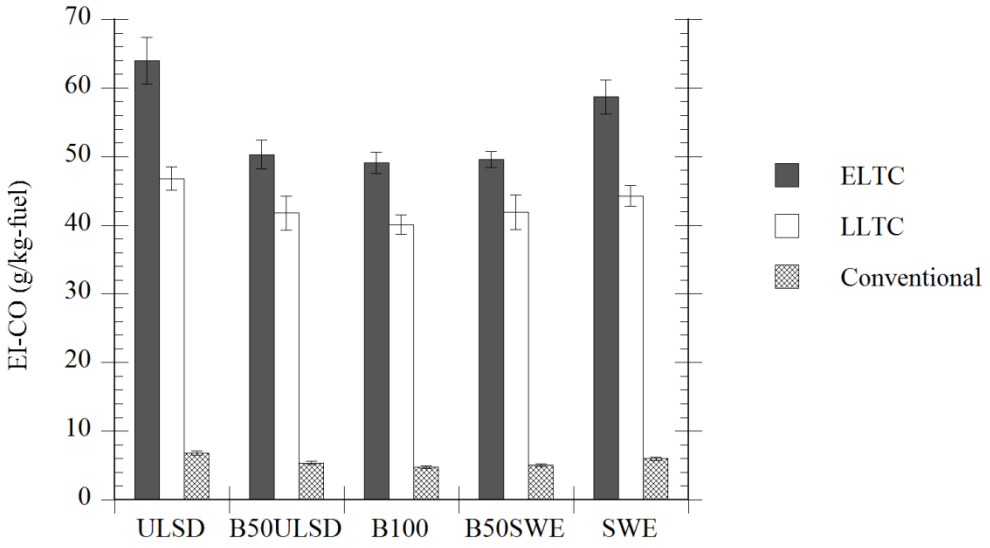

Figure 4.4: EI-CO emissions for all fuels and operating conditions

Both THC and CO emissions are lowest per mass of fuel for B100 for all three conditions. This trend is independent of cetane number since B100 had the median ignition delay time. Part of the cause for the dip in EI-THC and EI-CO for B100 and the B50 blends is that biodiesel contains less carbon per mass of fuel than ULSD or SWE as given in Table 4.2 due to fuel-borne oxygen. Therefore, as a function of the mass of fuel used, the amount of carbon emitted as CO or HC will be lower. If the emissions of CO were plotted on a brake specific basis, differences would be less clear between fuels since the biodiesel cases had a higher fuel flow rate to maintain the same brake power output.

Table 4.2: Carbon weight percent of fuels used in the experimental study

	ULSD	B50ULSD	B100	B50SWE	SWE
Wt. % Carbon	86.55	81.71	77.27	81.22	85.72

Other reasons for lower CO and THC for biodiesel and B50 blends include possible measurement error since some loss of unburned biodiesel in the heated sample line and filter at 190 °C could be expected due to adsorption as shown in Chang et al. (1998). In that study they found that if a FID is used to measure total hydrocarbons for neat biodiesel at light load, the THC measurement could be under predicted by as much as 28.7% for biodiesel compared with petroleum diesel. Even compensating for this estimation, they still found biodiesel to lower THC emissions compared to the baseline diesel fuel. Likewise, in considering the percent reductions in EI-THC and EI-CO for all the fuels tested in this study shown in Table 4.3, this amount of error still does not account for the entire reduction in THC for B100. However, if up to 30% of the THC is missing from the FID measurement for the B100 case, the differences in reduction of EI-CO and EI-THC are much closer which lends support to this explanation if the sources of CO and HCs in combustion are largely the same.

Table 4.3: Percent reductions in EI-THC and EI-CO from ULSD for the three operating conditions

	ULSD	B50ULSD	B100	B50SWE	SWE
ELTC					
% Red. EI-THC	0.00	23.14	**43.66**	38.60	42.04
% Red. EI-CO	0.00	21.36	**23.38**	22.59	8.31
LLTC					
% Red. EI-THC	0.00	15.16	**32.11**	21.22	14.47
% Red. EI-CO	0.00	10.59	**14.31**	10.43	5.24
Conventional					
% Red. EI-THC	0.00	34.28	**67.22**	46.01	13.49
% Red. EI-CO	0.00	21.22	**29.85**	26.06	12.45

Another possible reason for lower CO and THC for biodiesel over petroleum diesel is the high oxygen content in biodiesel allowing for more complete combustion in fuel-rich areas of the combustion chamber. This reasoning has been given by others (Rakopolous et al., 2004) though has as yet been not completely explored. Optical diagnostics or more detailed flame studies would be necessary to understand whether the oxygen content lowers the formation of partially reacted species. One argument supporting the theory is other work proving that oxygenated fuels reduce carbonaceous soot (Gonalez et al., 2001) in diesel combustion processes. Since soot is formed from precursor HCs found in rich areas of combustion, any reduction in soot formation may indicate reductions in CO and THC made in these regions as well. Some work has shown that PAH species, the major precursor to soot, are lower for biodiesel (Karavalakis et al., 2009) compared to diesel fuel. This finding may however be due to a lack of PAH species in biodiesel that are normally found in diesel.

Diatomic hydrogen is a byproduct of partial oxidation reactions in rich areas of combustion. After being created it is generally considered to be emitted in some proportion to CO based on a pseudo-water gas shift equilibrium constant (Stivender, 1971). However, it has been shown to be lower than predicted for combustion with lean average equivalence ratios (Northrop et al., 2009) due to oxidation by residual oxygen during expansion. Figure 4.5 shows that H_2 emissions are very low for the operating conditions run in this study.

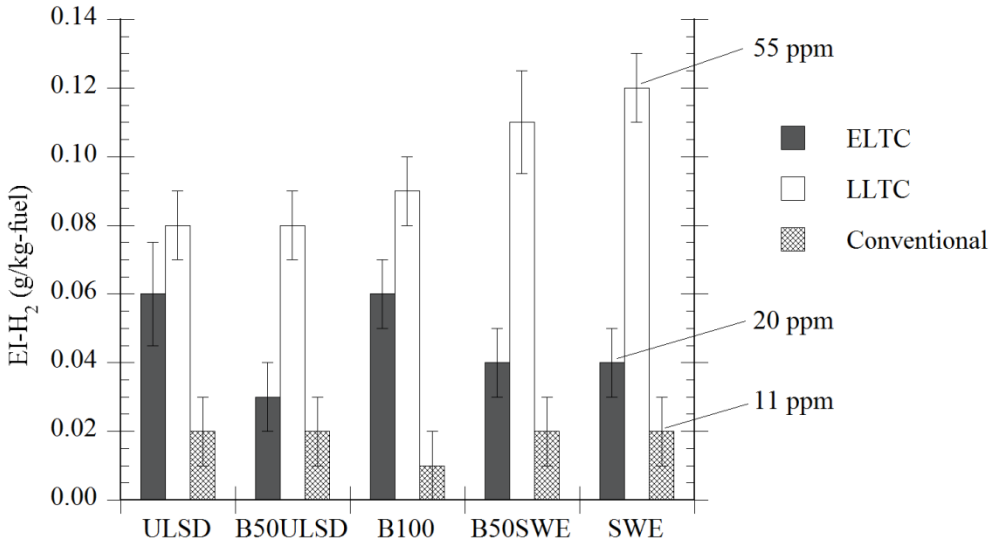

Figure 4.5: EI-H_2 emissions for all fuels and conditions

Although ELTC has considerably higher CO emissions than LLTC, it also has a lower equivalence ratio lending credence to the oxidation theory. H_2 is lowest for conventional combustion since other partial combustion products are also low. Little difference in H_2 emissions is seen for biodiesel compared to the diesel. For LLTC however, the increase in H_2 trends with increasing fuel cetane number indicating that fuel reactivity may play a role.

4.2.3 Primary Light HC Emissions

It is useful to further characterize the THC emissions into species to assist in understanding where they originate for the different fuels and modes of combustion used in the study. For example, partially reacted species like LHC indicate the presence of over-lean and over-rich areas of combustion. Unburned hydrocarbon (UHC) emissions may indicate whether crevice flows or quenching processes are occurring where fuel escapes combustion process unscathed.

From the results of LHC species using the FT-IR, no statistical differences can be discerned in emissions of acetylene, methane, propylene, 1,3 butadiene, formaldehyde or acetaldehyde over the fuel sweep for a given operating condition. The mean values for each of these species for the three conditions are given in Figure 4.6. Error bars reported are the mean uncertainties from the emissions of each species over the five fuels. It is also worthwhile to reiterate from Chapter Two that the EI emissions of individual HC are shown on a C_1 basis. The one LHC species that does show significant deviation as a function of fuel for a given operating condition is ethylene. These results are shown in Figure 4.7.

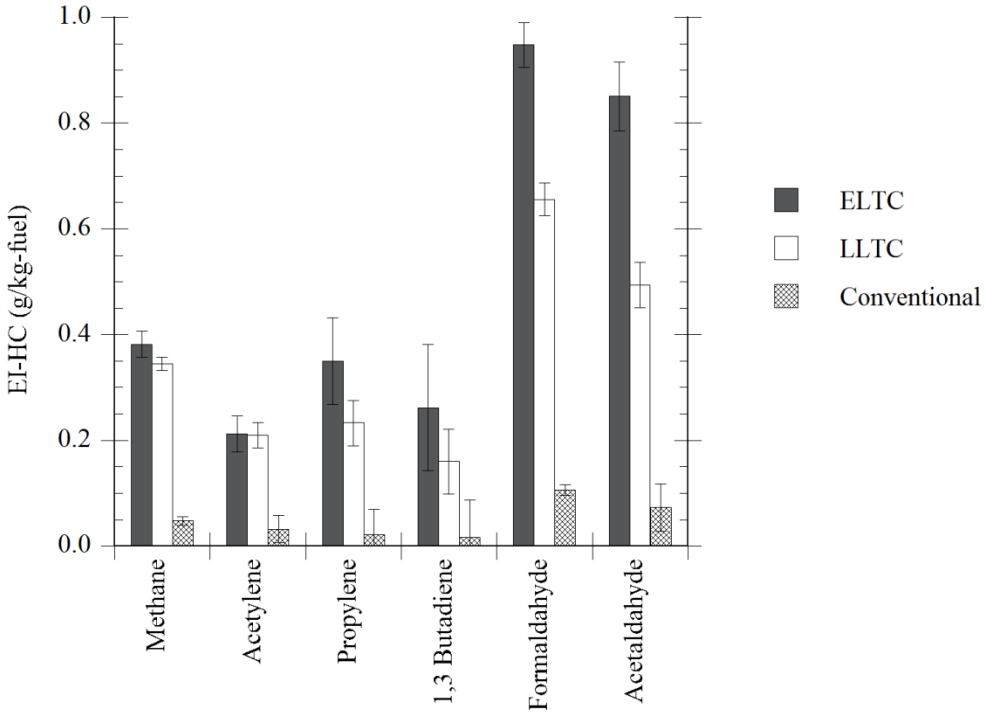

Figure 4.6: Speciated LHC components remaining constant over the fuel sweep for the three operating conditions

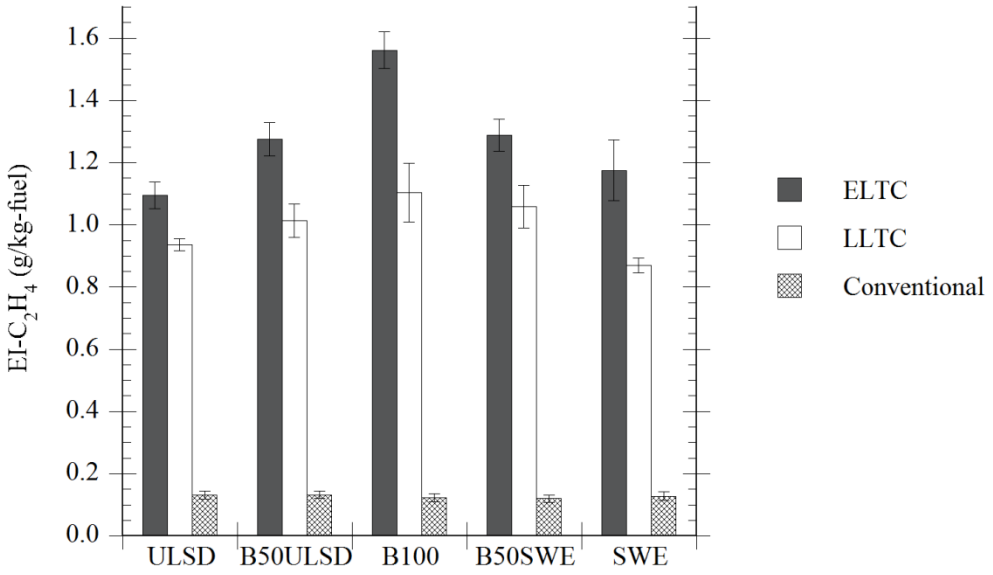

Figure 4.7: Ethylene emissions for all fuels and operating conditions

For all operating conditions, ethylene and formaldehyde were found in the highest concentration for all fuels although the amount of ethylene over other LHC increased with LLTC and more so for ELTC. Methane is almost three times lower than ethylene for the three conditions indicating limited over-rich zones per the findings of Cook et al (2008) and also expected with low soot formation typical of premixed combustion. These results are also comparable with other published work in speciation of HC from LTC (Han et al, 2009). Acetylene, also an indicator of over rich combustion and a known precursor of soot along with PAH (Wang and Frenklach, 1997) is found to be slightly lower than methane on a C_1 basis.

Between fuels, the concentration of biodiesel in the fuel has little correlation to the production of the two primary aldehydes from combustion for either conventional or LTC. Differences in aldehyde emissions reported in the literature for biodiesel versus petroleum diesel as discussed in Section 4.1.2.2 may have been a result of changing

combustion phasing or regime as a result of switching to biodiesel, an effect taken into account in this study in maintaining constant CA50 for a given condition as explained in Chapter Three.

Although ethylene is the same among fuels for conventional combustion, it increases with higher biodiesel concentration for ELTC and LLTC. This tendency for biodiesel to make more ethylene and similar quantities of other LHC components in LTC combustion modes has not been shown in the literature to date. It is an opposite trend to that found for THC where biodiesel had the lowest emissions from Figure 4.3. For the ELTC condition, higher ethylene exacerbates the LHC emissions as shown in Figure 4.8 where the LHC emissions measured using the FT-IR are plotted for the three operating conditions.

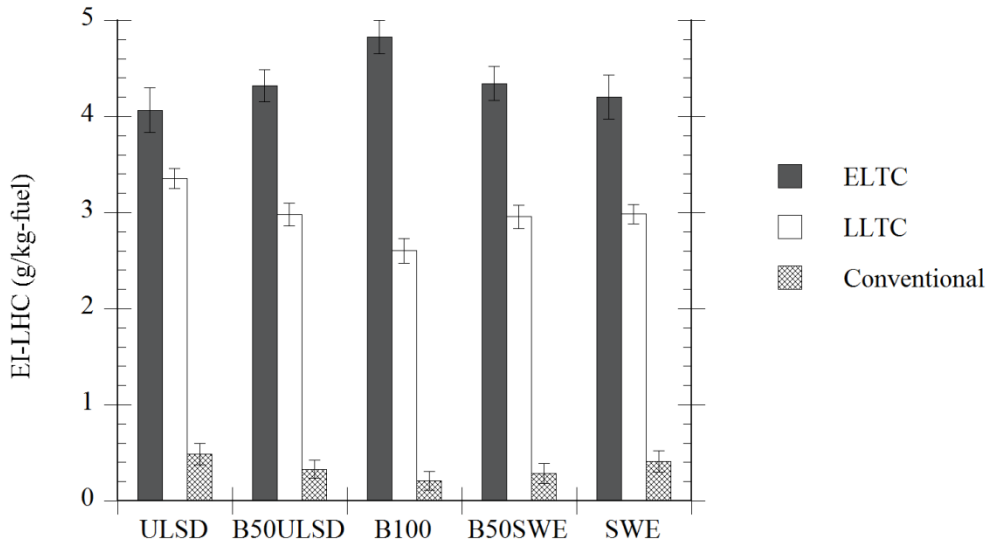

Figure 4.8: EI-LHC emissions for all fuels and operating conditions

For ELTC, using B100 increases the LHC emissions by almost 25%. In general, like for THC, fuel composition appears to have a dominant effect on LHC concentration over ignition delay. From the literature reviewed thus far, it is expected that ethylene emissions are strongly linked to the mixing time prior to combustion. Although the mass emissions of light HCs only increases with biodiesel content for ELTC, the proportion of LHC in the THC shows the same trend for all three operating conditions as shown in Figure 4.9. The light organic fraction (LOF) of the THC is calculated using the combined results from the FT-IR and the FID and is shown by Equation 4.1. As a corollary the THC is assumed to consist of the sum of the LHC and the UHC.

$$LOF_{HC} = \frac{LHC}{THC} \tag{4.1}$$

And

$$THC = LHC+UHC \tag{4.2}$$

In Equation 4.2, it is assumed that partially burned higher molecular weight HCs like light PAH or lubricating oil are in negligible concentrations compared to unburned fuel in the in the gas-phase exhaust and sampling lines at 190°C.

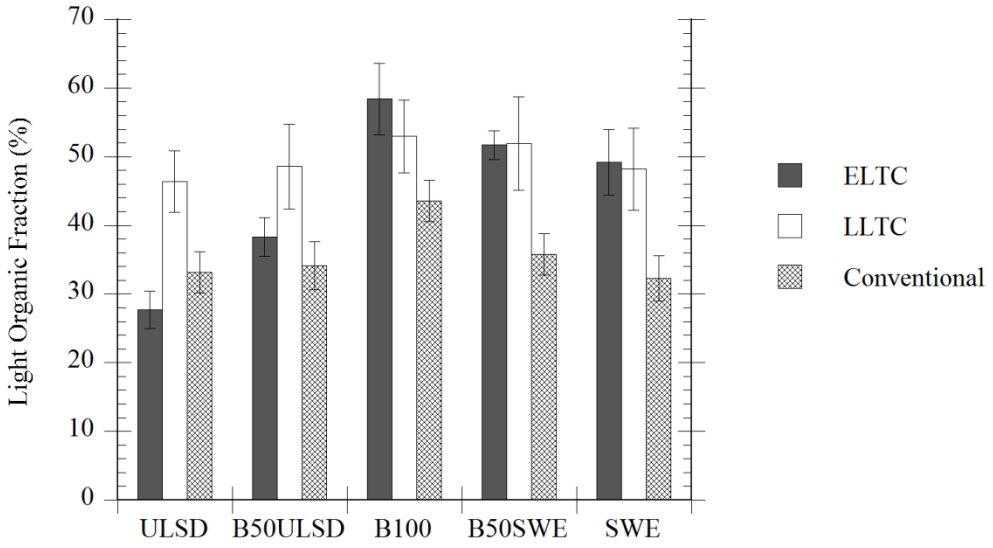

Figure 4.9: Light organic fraction (LOF) of the THC emissions for all fuels and operating conditions

For ELTC, trends in LOF are similar to THC where an asymmetrical distribution about the B100 condition is evident. Since LHC does not increase in proportion to THC for ULSD and B50ULSD, it is likely that fuel escapes combustion due to wall quenching in these cases due to advanced injection timing. These two conditions notwithstanding, LTC combustion has a higher LOF than conventional combustion which corresponds well to more over mixed areas of combustion and the lack of a defined diffusion burn portion of combustion.

Higher LOF in concert with lower THC emissions for increasing biodiesel as illustrated in Figure 4.9 indicates that UHC is lower for biodiesel LTC due to more complete combustion of the fuel or due to unmeasured fuel lost in the sample lines as explained in Section 4.2.2. Further, the dependency of LHC emissions with increasing biodiesel content in the fuel as shown in Figure 4.8 indicates that combustion chemistry also plays a significant role especially in the formation of additional ethylene.

4.2.4 Further Examination of LHC from ELTC Condition

As previously mentioned, the formation of ethylene and other LHC species has a strong dependence on the level of premixing before combustion occurs. This allows for more over-lean areas of combustion where partially burned products are created. Therefore, a dependence of ethylene emissions on ignition delay should appear over a range of injection timing. ELTC is the most extreme case of the three conditions run in the study in terms of premixing since it is expected that most of the fuel that eventually burns is completely vaporized before combustion. Furthermore, larger differences in ethylene emissions between B100 and ULSD are found for this operating condition as shown in Figure 4.7. Overall magnitudes of LHC emissions are also higher for ELTC reducing uncertainties in the measurements.

An additional experiment was undertaken to explore LHC emissions over a range of injection timing for the ELTC condition. Fuels tested included ULSD and B100. And injection timing was swept from 40 °BTDC to 17.5 °BTDC. Engine load was held constant at 200 kPa and the engine throttle was maintained wide open as in the ELTC condition reported thus far. The LOF results are plotted versus ignition delay in Figure 4.10. Ignition delay is reported as the duration from SOI to CA10 per the better correlation with combustion efficiency due to differences in ignition between B100 and ULSD as discussed in Section 4.2.1.

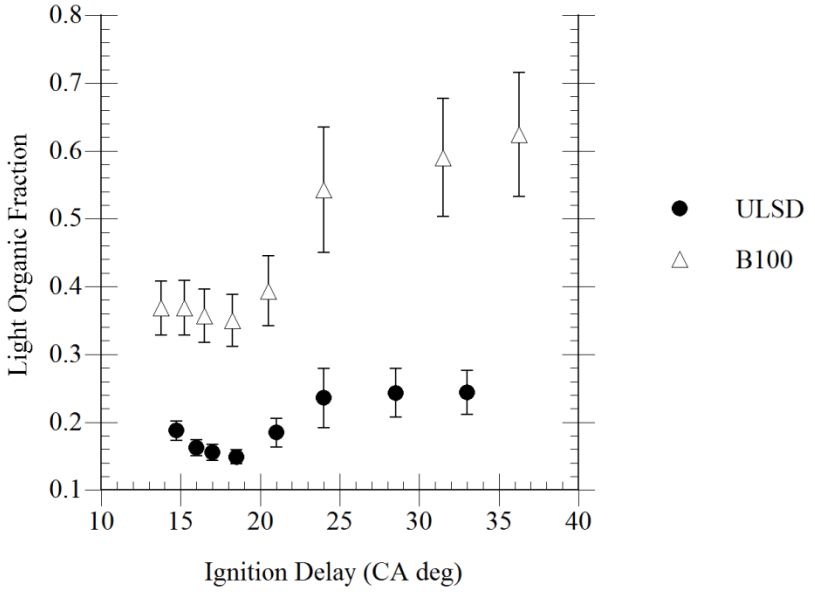

Figure 4.10: Light organic fraction (LOF) of the THC emissions as a function of ignition delay for the ELTC condition with ULSD and B100 fuels

For a given ignition delay, LOF remains higher for B100 than for ULSD over the timing range just as was shown for the single steady state ELTC condition in Figure 4.9 implying that biodiesel emits a higher proportion of partially combusted as LHC. LOF increases as a function of increasing ignition delay since more time is available for mixing. The inflection point in Figure 4.10 at approximately 20 CA° is most likely due to the wall quenching phenomena found in the ELTC timing sweep reported in Chapter Three.

As is shown in Figure 4.7, ethylene has the highest concentration among LHC for the ELTC condition and tends to increase with increasing biodiesel concentration in the fuel. It is also found to be higher for B100 than for ULSD over the timing sweep as shown in Figure 4.11 where the emissions of ethylene is plotted as a function of overall LHC emissions.

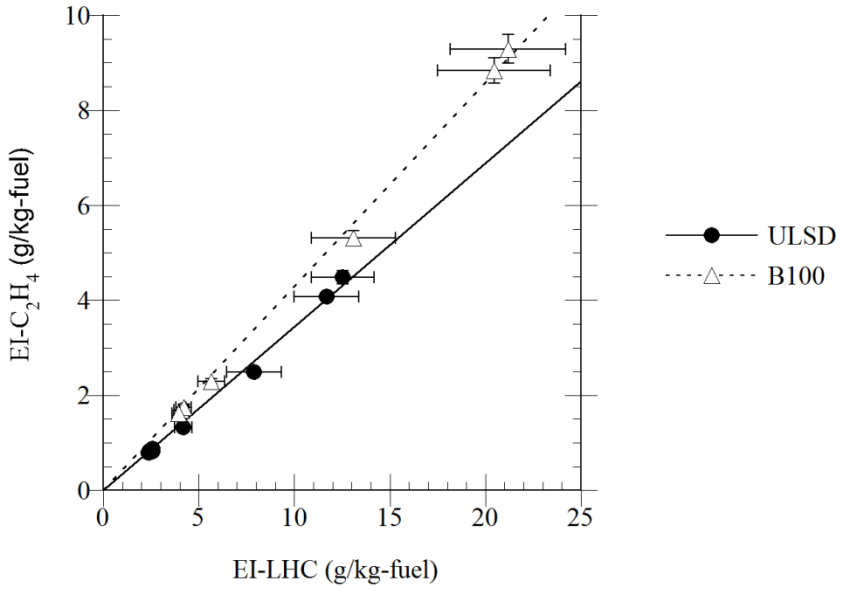

Figure 4.11: EI-Ethylene versus EI-LHC for the ELTC condition with ULSD and B100 fuels over the injection timing sweep

The figure shows that ethylene varies approximately linearly with LHC for B100 and ULSD but at different slopes. At low LHC emissions levels, ethylene fraction is nearly the same for the two fuels but as LHC increases for increasing ignition delay, B100 diverges and shows consistently higher ethylene fraction. This indicates that not only does B100 have higher LHC emissions than ULSD due to higher ethylene concentrations but that ethylene is also higher as a fraction of the total LHC.

Fuel chemistry plays a major role both in what species are formed and in what quantity they are produced at different stages of the combustion process. Kinetic modeling studies typically attempt to capture the characteristics of how fuels oxidize using simpler surrogate species. For petroleum diesel fuel like ULSD, n-heptane is a common surrogate and detailed mechanisms have been proposed for both low temperature ignition reactions and high temperature oxidation (Curran et al., 2002). For

biodiesel, the same group has proposed methyl decanoate as a suitable surrogate over a large range of temperatures (Herbinet et al., 2008) and others have proposed the use of methyl butanoate, a smaller ester, when low temperature reactions are less important (Gaïl, et al., 2008). The use of smaller molecules in the simulation of how larger HC species in the actual fuels react is a compromise between accuracy in predicting accurate trends and saving computational time.

Although in-depth analysis and modeling is beyond the scope of this study, published comparisons of kinetics mechanisms with experimental data has some implication for the results shown in this chapter. For example, ethylene is well known to be a primary intermediate species emitted as a result of partial combustion of aliphatic hydrocarbons (Westbrook and Dryer, 1984). In methyl ester combustion at higher temperature, initial uni-molecular decomposition of C-O and C-C bonds typically results in decomposition of the fuel either by removing the methyl group at either end of the molecule or by removal of the ester from the aliphatic chain altogether (Herbinet et al., 2008). In this case, combustion of the remaining molecule is similar to the oxidation of straight-chain hydrocarbons. However, comparisons of methyl deconoate and methyl butonate kinetic models to jet-stirred reactor experiments of larger methyl esters have shown that ethylene concentration is under-predicted (Gaïl, et al., 2008) especially at temperatures less than 1000 K. Based on this and the results found in this study, ethylene appears to be created to greater concentrations for methyl esters compared with pure aliphatic fuels like petroleum diesel. Future work is advised to further examine the kinetics of biodiesel combustion to explain the differences in LHC emissions seen in this study.

4.3 Summary of Findings

In summary, this chapter was successful in determining the primary species that contribute to the THC measurement for LTC and conventional combustion. The combustion efficiency, a global measure of fuel conversion, closely correlated to ignition delay for all fuels and operating conditions. However, THC and CO are found to decrease for increasing biodiesel concentration in the fuel. Reductions in CO and HC for biodiesel-containing fuels on a g/kg-fuel basis are lower partially due to lower carbon content in the fuel. Lower THC emissions also may arise through adsorption of biodiesel in the sample system, effectively lowering the measured UHC concentration. Although errors like this account for some of the differences seen in the study, the percent reduction in THC is still higher than what would be expected from experimental errors based on previous work. This indicates that differences in combustion between biodiesel and petroleum fuels exist.

For the ELTC condition, the lower cetane number fuels, ULSD and B50ULSD, had the lowest combustion efficiency indicating that some wall quenching was occurring due to their early injection timing. This conclusion is also substantiated by the light organic fraction (LOF) results indicating that the UHC concentration for these cases is disproportionately higher than for SWE in ELTC although ULSD and SWE had the same LOF for LLTC and conventional combustion.

Between fuels, emissions of the primary LHC species acetylene, methane, propylene, 1,3 butadiene, formaldehyde or acetaldehyde were the same to the uncertainty of the measurements for the three operating conditions. For all cases, methane is about three

times lower than ethylene or formaldehyde indicating that more over-lean areas of combustion exist compared to rich zones in LTC. Aldehyde emissions are not found to increase for biodiesel as has been reported in the literature when combustion phasing is held constant for a given operating condition.

Although most LHC species are not found to differ between fuels, the emissions of ethylene are higher for biodiesel-containing fuels, significant enough to increase the overall LHC emissions for the ELTC condition. The LOF of the total THC measurement is also higher for biodiesel for all operating conditions indicating that the measured UHC emissions are lower.

Over a timing range, the LOF is found to increase with increasing ignition delay for the ELTC condition. B100 has a consistently higher LOF than ULSD over the sweep confirming the findings from the steady state experiments. Ethylene varied linearly with LHC emissions for ELTC over the timing range. For B100, the slope of the line was greater than for ULSD indicating that ethylene is produced in greater quantities for biodiesel. Kinetic models from the literature consistently under-predict experimental ethylene emissions from low temperature combustion of biodiesel surrogates setting the stage for future work to explore these findings.

CHAPTER FIVE

PARTICULATE EMISSIONS

5.1 Background

In this chapter, previous presented results along with PM measurements will be used to investigate the second goal outlined in Chapter One; "To prove the hypothesis that the organic fraction of the PM mass is greater for biodiesel in premixed LTC and to determine the primary species that contributes to this increase."

Analytical tools such as a smoke meter, OCEC measurement, particle size distribution from DMS, partial flow dilution tunnel, gravimetric analysis and speciation of PM-based organics are used in the study. First, established literature will be reviewed concerning the formation of diesel particulate for premixed combustion modes and comparing the effects of biodiesel on PM emissions. Carbonaceous soot will then be explored for the three experimental conditions and range of fuels. The PM will be examined for premixed LTC and conventional combustion and characterization of the primary organic species found will be presented. Condensation as the mechanism for deposition of organic species onto the PM will also be discussed and a prediction of trends in PM for LTC will be presented.

5.1.1 Particulate Formation in Diesel Combustion

The subject of PM formation in diesel engines has been well researched and comprehensive reviews can be found in many excellent published resources (Eastwood, 2008, Kittleson, 1998). The purpose of this section is to review the pertinent sources and composition of PM as background for the upcoming sections.

There are four major sources of PM from engines; fuel, lubricating oil, ambient air and material wear. Of these, only fuel and oil create PM in significant quantities. These four sources generate PM which can be further categorized into five distinct compositional fractions; carbonaceous, organic, sulfate, nitrate and ash. Ambient air and engine material breakdown generally contribute to the ash fraction which is not of interest in the work presented here. Both fuel and lubricating oil also contribute to the ash fraction depending on the quantity of additives contained therein.

The sulfate fraction mostly originates from sulfur compounds in the fuel breaking down during combustion and later contributing to PM in the form of sulfuric acid (H_2SO_4). In past decades, high concentrations of sulfur were thought to be the major contributor to PM emissions from fuel (Wall and Hoekman, 1983). Most modern fuels contain less than 15 ppm sulfur and biodiesel contains virtually none. Therefore, the sulfate fraction is assumed negligible compared with the other components in the PM for the purposes of this study.

The nitrate fraction comes from the reaction of nitric dioxide (NO_2) and water in the exhaust creating nitric acid (HNO_3). Since NO_X emissions are very low in premixed combustion and differences in NO_X emissions between fuels for a given combustion

mode are small as shown in Chapter Three, the nitrate fraction is assumed insignificant in the comparison of PM for different fuels in this work.

The carbonaceous and organic fractions are of most interest in the discussion of PM from premixed combustion modes with varying fuels. The fuel and lubricating oil are the primary sources of these fractions. These make up the elemental carbon (EC) portion which, in this work is considered synonymous to the terms "carbonaceous" and "soot". EC is sometimes distinct from black carbon (BC) since other carbon containing compounds besides soot can have "blackness" or light absorption when using optical measurement techniques like a smoke meter.

The EC fraction of PM originates mostly from the fuel used in the engine. As mentioned in Chapter One, soot is generally formed in the diffusion, or mixing-controlled duration of diesel combustion in fuel rich zones. Here with a deficiency of oxygen and at high temperatures, fuel undergoes pyrolysis where it is first broken down into molecules of lower molecular weight via dehydrogenation and bond rupture. Then as temperatures decrease, these light compounds combine by polymerization creating soot species with molecular weights larger than the original fuel molecules.

It is thought that two types of precursor molecules lead to the inception of soot in diesel combustion, unsaturated hydrocarbons and PAH species (Wang and Frenklach, 1997). The primary unsaturated HC that is considered important in soot formation is acetylene. PAH species are both formed during combustion and originate directly from the fuel. Mono-ring aromatics contained in the fuel can also lead to direct polymerization to PAH (Martinot et al., 2001) though some studies shown that these species decompose

by ring rupture and reform to create pyro-synthesized aromatics leading to PAH (Haynes and Wagner, 1981). Such long aromatic chains eventually combine to form molecules of ever increasing molecular weight and become soot particles in a process termed nucleation. Many models have been proposed for formation of soot nuclei from such precursors (Kennedy, 1997) and will not be discussed here in detail.

Oxidation of soot occurs simultaneously with formation of particulates in the combustion chamber and continues well into the exhaust manifold. This effect mitigates the formation of PM throughout all phases of the process, from combustion through the exhaust system to when the effluent interacts with the environment over longer time scales. A comprehensive review on soot oxidation is given by Stanmore et al. (2001) and will not be further discussed here.

The organic fraction of particulate generally forms after the combustion process or after dilution of the exhaust by gas to particle conversion mechanisms. Both fuel and lubricating oil contribute significantly to the organic fraction. Fuel can contribute either directly or indirectly to PM as in Figure 5.1 where the fuel-derived emissions shown in Figure 4.1 are shown to contribute to the gas and particulate phases after dilution. Unburned fuel that escapes combustion from over-mixing in LTC modes for example, can enter the particulate phase directly. Fuel-derived species like PAH and other heavy hydrocarbons originating from rich zones of combustion that do not have time to pyrolize completely to form soot can later convert to the particulate phase. These species are indirect contributions to the PM emissions from fuel. Lubricating oil usually directly contributes to soot as it becomes exposed to the exhaust products of combustion along the cylinder wall during the expansion stroke. Since it is assumed that lubrication oil

properties do not change significantly between different fuels used in the engine, this fraction is not examined in detail for the work presented here.

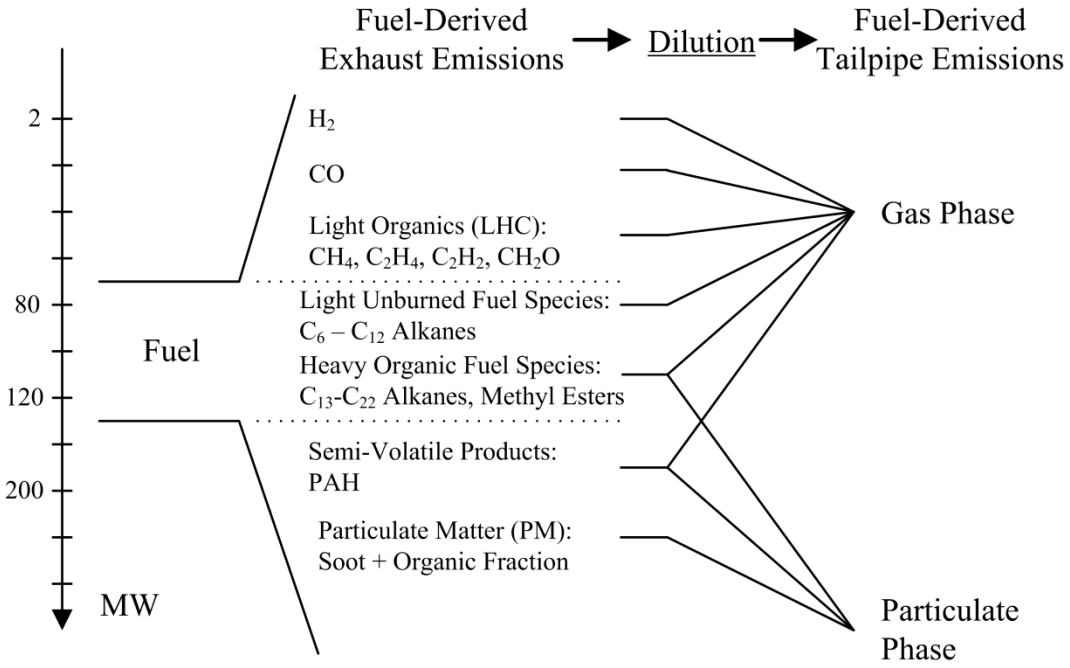

Figure 5.1: Contribution of fuel-derived species to gas and particulate phase emissions after dilution

Organic species can enter the particulate phase by many routes. They can either homogeneously nucleate to form particles by themselves or as is most often the case, they collect on the soot particles already contained in the exhaust gas. Primary methods of gas to particle conversion include adsorption and condensation. These mechanisms generally occur late in the exhaust process and in the exhausting plume as ambient air dilutes and rapidly cools the stream. Generally, higher molecular weight petrogenic compounds from the fuel and pyrogenic species, those created during combustion, are in the highest concentration on the PM. Light hydrocarbon species like those described in the Chapter Four do not generally contribute to PM emissions to a significant extent.

5.1.2 PM Emissions from Premixed LTC

As stated in Chapter One, in-cylinder reduction of soot is one of the key motivations for the use of LTC strategies in diesel engines. Low combustion temperatures combined with a lack of diffusion burning creates an environment where soot precursors, though present in high concentrations, do not polymerize to create larger molecules as readily. Soot does form however which implies that mixtures in LTC are only partially homogeneous. From the work of Musculus et al (2009), it is apparent that high temperature rich zones are present in LTC combustion in recirculation zones created by the vaporized fuel plume coming in contact with the piston bowl. In these zones, precursor species have been detected (Genzale et al., 2008) which lead to the creation of soot.

There is little literature to date concerning the overall PM mass emissions for LTC combustion. Sluder et al. (2004) investigated PM emissions for a similar engine to that used in this study operating in a late injection mode analogous to the LLTC condition. At 55% EGR, the brake specific emissions of insoluble carbonaceous species were 0.2 g/hp-hr whereas the rate of PM was near 1.0 g/hp-hr giving an organic fraction of near 80%. The reasoning for such a high percentage of organic species on the PM was assumed to arise from the high levels of HC in the exhaust for the LTC operating condition. Speciation of the extracted samples found that the majority of the organics on the PM were fuel molecules and other partially oxidized species from the fuel.

5.1.3 Effects of Biodiesel on PM Emissions

The use of biodiesel or other oxygenated fuels in diesel engines is generally assumed to be an effective way to mitigate soot emissions (Eastwood, 2008, pp. 256). It has been well documented that by operating diesel engines with oxygenated additives soot is reduced in proportion to the quantity of oxygen in the fuel (González et al., 2001). In fact, if 30-40% of the fuel is oxygen, soot has been shown to be eliminated completely (Miyamoto et al., 1998).

Although PM mass has been mostly shown to decrease for conventional diesel combustion, the organic fraction of particulates is well known to be higher for biodiesel than for petroleum diesel fuels especially at part load conditions (Lapuerta et al.; 2007, Last et al.; 1995, Bagley, 1998; Chang and Van Gerpen, 1998). This implies that the decrease in soot formation due to the increase in oxygenated compounds is compensated for by higher organic fraction on the PM. At light loads, engines are known to generate higher HC emissions leading to increasing gas to particle conversion of higher molecular weight species onto the soot. Biodiesel, having higher molecular weight than species in petroleum diesel fuel and with lower volatility is assumed to aid in the higher level of organic species on the emitted PM.

As mentioned in the previous section, oxidation of organic material is a continual mitigating factor in the reduction of PM throughout the exhaust process. Biodiesel PM has shown to exhibit higher oxidation rates than PM from petroleum diesel fuels which may contribute to its lower PM mass emissions. Boehman et al. (2005) studied the oxidation rates of biodiesel blends and the same authors in Song et al. (2006) looked at

pure soy-based biodiesel. They found that along with higher oxidation rates, the microstructure of soot from biodiesel combustion contained more hollow cavities and graphene ribbon structures evidently caused by the oxidative processes occurring during its formation.

Particle size distribution for biodiesel in comparison to petroleum diesel has mixed results in past studies. Some research reports larger number of smaller particles resulting from biodiesel combustion (Krahl et al., Purcell et al., 1996) but others find that biodiesel creates less small particles (Aakko et al). Mean particle sizes generally are found to decrease along with total number of particles as shown in Jung et al. (2006) but others show that biodiesel lowers mean particle size but increases the number of particles (Tsolakis, 2006). Such disparities result from differences in engine operating condition, sample dilution and analytical equipment used such that comparisons between literature studies must be carefully made. In general, it is seen that for part load conditions or for engines operating with higher EGR rates, mean particle sizes increase for biodiesel use as in the preliminary study (Northrop et al., 2009). In another study, Theinnoi et al. (2008) found that at part load with 20% EGR, PM from conventional combustion of biodiesel contained considerably less nuclei mode and more accumulation mode particles than for a condition with 0% EGR.

The combination of LTC and biodiesel has been shown to have a compounding effect in the reduction of soot formation. In an optical engine study, Fang et al. (2009) found lower soot luminosity during combustion of biodiesel versus petroleum diesel in early and late LTC modes. However, the measurement of PM following a dilution process for this combination has not been reported as of the writing of this dissertation. It is the

intention of the following sections to fill this gap in knowledge and to examine the effects of biodiesel on PM emissions in the LLTC and ELTC conditions.

5.2 Experimental Results and Discussion

5.2.1 Soot Emissions

Soot, as was stated previously, refers to the carbonaceous portion of PM formed by pyrolysis of fuel into precursor molecules before forming large carbon chains with low organic content. In this work, soot emissions are measured in two distinct ways: by using the OCEC technique to selectively oxidize only the elemental carbon from a quartz filter; and by measuring the FSN using a smoke meter. From the FSN reading the soot mass is calculated using the Christian (1993) correlation given in Equation 2.9 and then converted to an EI basis using Equation 2.10. For the conventional combustion operating condition, Figure 5.2 shows that the two measurement techniques are well correlated over the range of fuels tested.

Soot emissions for biodiesel compared with both SWE and ULSD show expected trends based on the established literature for conventional diesel combustion. Soot magnitudes are lower than generally reported however, with FSN between 0.4 and 1.3, since the condition presented here utilizes a large pilot injection and a good portion of the heat release is premixed. As mentioned in a previous section, the oxygenated nature of biodiesel reduces carbonaceous matter formation by allowing local oxidation in fuel-rich zones concurrent with soot formation.

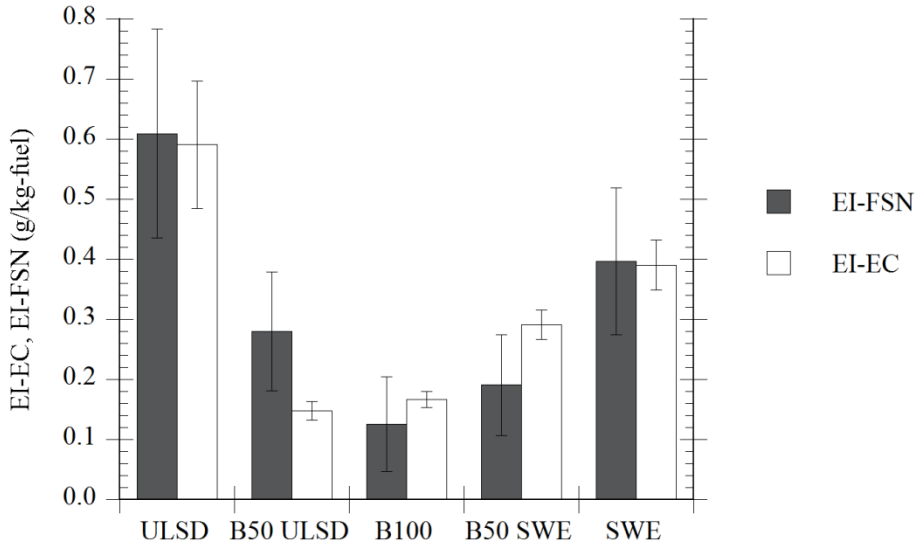

Figure 5.2: EI-FSN and EI-EC emissions for the conventional operating condition

For LLTC the soot emissions are reduced by a factor of ten for ULSD as illustrated in Figure 5.3 but the trends from the conventional combustion case remain the same. These results are expected based on previous work in using a similar LLTC combustion mode (Jacobs et al., 2005). Error bars are not shown for EI-FSN since they exceed the y-axis scale in the figure due to high systemic error of the smoke meter in the low detection range. However, even with the high instrument errors, the accuracy of the EI-FSN measurement is assumed to be high since the data correlates well to the EC measurement.

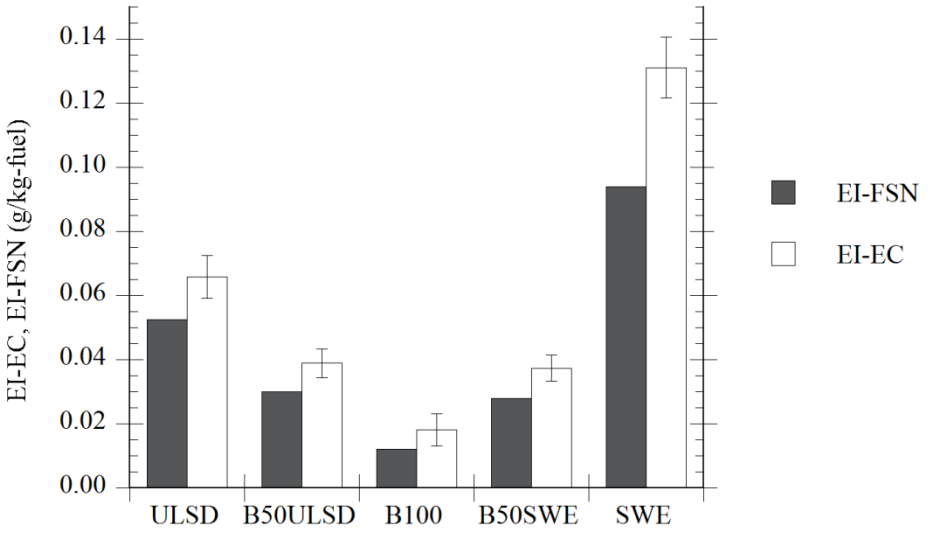

Figure 5.3: EI-FSN and EI-EC emissions for the LLTC operating condition

As was found in the preliminary study (Northrop et al, 2009), SWE has higher soot emissions than ULSD. The primary reason for the increase include the shorter ignition delay for SWE preventing over-rich zones to mix with air prior to the commencement of combustion. As biodiesel is mixed with either petroleum diesel however, soot emissions are drastically reduced proving that the simultaneous oxidation of soot from the oxygen containing fuel present in conventional combustion is also present in LTC.

For the lower load ELTC condition, soot emissions are reduced further. At this point the FSN readings are near zero and the error bars for this measurement are again not shown in Figure 5.4. Surprizingly, the FSN and EC data correlate extremely well even at this low emissions level.

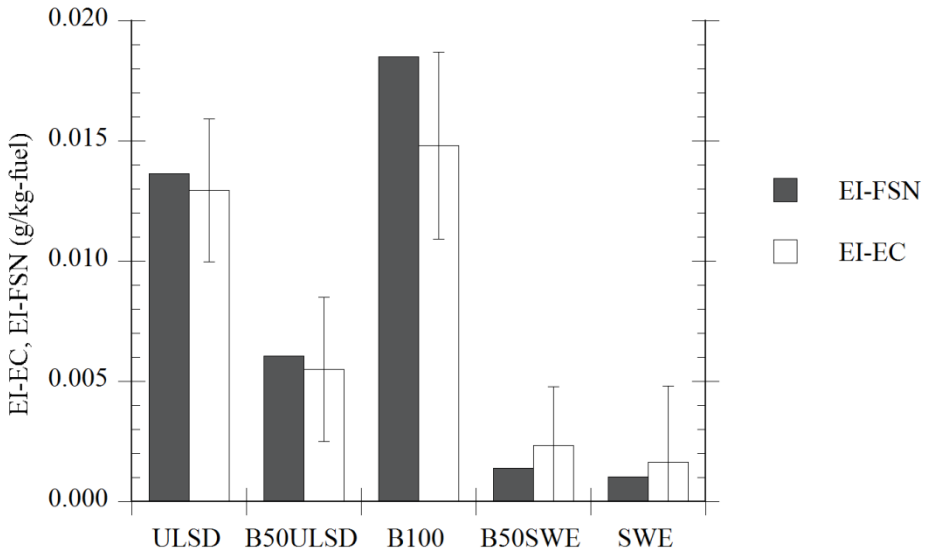

Figure 5.4: EI-FSN and EI-EC emissions for the ELTC operating condition

Differences in soot emissions from the ELTC mode are difficult to discern given the extremely low values found given the large 95% confidence interval of error. However, it appears that SWE has the lowest soot emissions and B100 the highest, an opposite finding to that from the LLTC mode.

The high correlation between soot mass emissions measured by OC/EC techniques and by using the Christian correlation from FSN readings is a promising finding since the optical smoke meter is an inexpensive and well established instrument for measuring soot from engines. Table 5.1 shows the relationship between all values measured for the three conditions using the correlation coefficient calculated by the *Correl* function in Microsoft Excel described in Section 4.2.1. By showing that, even for FSN magnitudes lower than the recommended range of operation of the instrument, EI-FSN corresponds to the more accurate EI-EC measurement; carbonaceous species can be reported in low soot regimes with considerably more confidence.

Table 5.1: Correlation between EI-FSN and EI-EC for the three operating conditions

	FSN-EC Correlation
Conventional	**89.4%**
LLTC	**99.7%**
ELTC	**99.3%**

5.2.2 Particulate Emissions

5.2.2.1 Gravimetric Analysis

The overall PM emitted by the engine includes both soot and all other particulate phase elements found in the exhaust gas for a given dilution and temperature condition. As is explained in Chapter Two, the dilution ratio in this work is 10:1 with ambient air and the filter collection temperature is 47°C. The conditions during PM collection are important in interpreting the results as will be explained later in this chapter.

The results of the gravimetric analysis of PM in comparison to the soot emissions based on the EC measurement for the conventional combustion case are given in Figure 5.5. The trends in PM match that for soot quite closely with B100 having the lowest PM and SWE the highest. In general, the literature trends for PM emissions in conventional diesel combustion are confirmed.

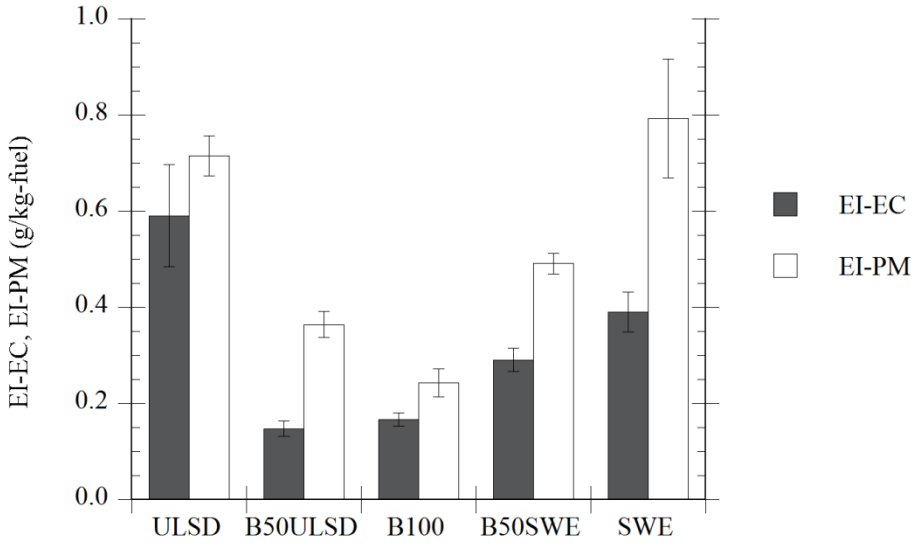

Figure 5.5: EI-EC compared to EI-PM as measured by gravimetric analysis for the conventional operating condition

In LLTC the situation is completely different. Figure 5.6 shows quite clearly that trend in PM emissions is opposite to that of soot for this operating condition. With more biodiesel in the fuel, PM increases dramatically such that it is over an order of magnitude higher than the soot emissions for B100. This trend indicates that the organic fraction of the PM with increasing biodiesel in the fuel has a dominant effect on the overall emissions proving the hypothesis set forth in the beginning of this chapter.

The trends are similar for the ELTC condition with even more drastic differences in soot and PM for increasing biodiesel in the fuel as shown in Figure 5.7. PM is over two orders of magnitude higher than EC for B100 indicating that at the dilution conditions used in the study, a “white smoke” condition may be present (Eastwood, 2008) where visible traces of the organics may be present from the exhaust of a vehicle running at this operating condition. The neat petroleum diesel fuels, ULSD and SWE, also had much

higher PM mass than soot indicating high organic content though not as high the biodiesel containing fuels.

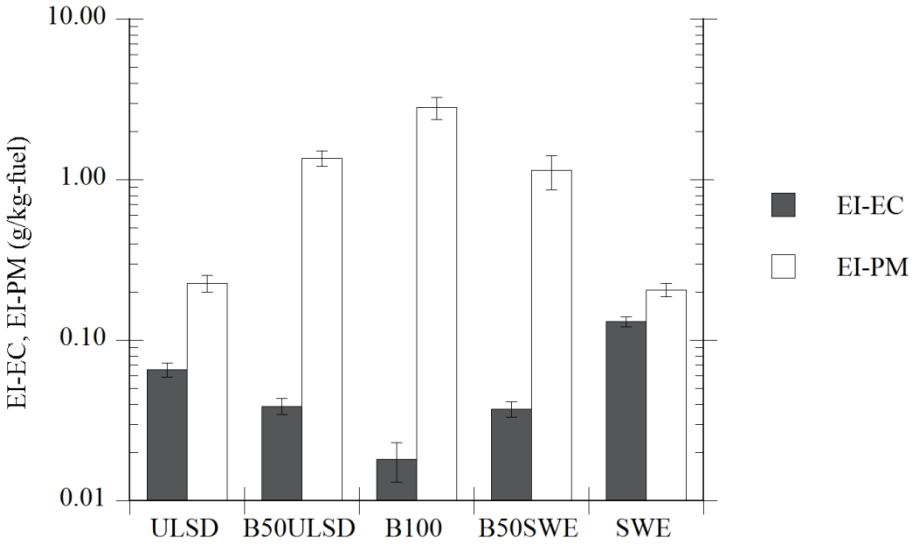

Figure 5.6: EI-EC compared to EI-PM as measured by gravimetric analysis for LLTC operating condition

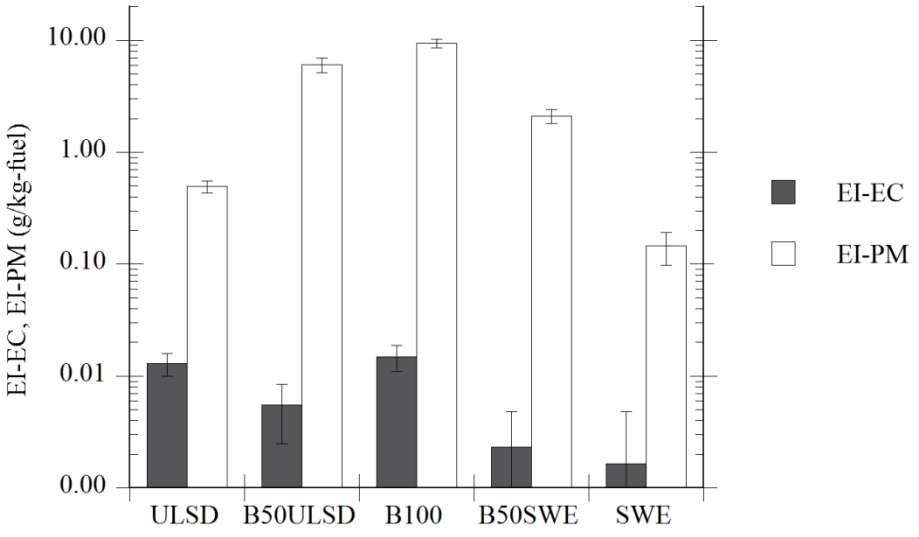

Figure 5.7: EI-EC compared to EI-PM as measured by gravimetric analysis for ELTC operating condition

The total organic fraction of the PM (TOF) which represents the total amount of organic matter on the PM including partially reacted HCs, fuel HCs and lubricating oil HCs can be calculated using the results of the gravimetric PM analysis and the EC measurement using Equation 5.1. The TOF is calculated from the results shown in the previous figures and is compiled in Table 5.2.

$$TOF = \frac{EI_{PM} - EI_{EC}}{EI_{PM}} \quad (5.1)$$

Table 5.2: TOF as calculated by Equation 5.1 for all fuels and operating conditions

	ULSD	B50ULSD	B100	B50SWE	SWE
Conventional	20.4%	59.5%	31.5%	40.8%	50.8%
LLTC	71.0%	97.1%	99.4%	96.7%	41.2%
ELTC	97.4%	99.9%	99.8%	99.9%	98.8%

For both LTC conditions and for any biodiesel containing fuels, the TOF exceeded 96%. The remainder of this chapter will be devoted to the study of why such disparity between soot and organic-containing PM exists for biodiesel operating in LTC modes of combustion.

5.2.2.2 Particle Size Distribution

Particle size distribution gives more detailed information about what types of particles cause differences in mass emissions of PM between fuels and engine operating conditions. In this study, the dilution ratio of the DMS instrument was maintained at 5:1. Therefore mass calculated from the distribution based on correlations like that given by

Symonds, et al. (2007) cannot be expected to give the same results as those found in the gravimetric analysis using a dilution ration of 10:1 and are not presented here.

Figure 5.8 shows the distribution of particles for the conventional combustion case. The total area encompassed by the distribution was smallest for B100 and largest for SWE and ULSD corresponding to trends in PM mass. The B50 fuels fit within the magnitude of the neat fuels much like the PM mass shown in Figure 5.5.

A bimodal distribution exists for all fuels. The smaller peak in particle diameter from 10-50 nm is generally termed the nuclei range where single particles are thought to predominate. The peak occurring in the range of 50-200 nm is considered the agglomeration range where nuclei mode particles have combined and gas to particle processes have increased their size. For the conventional case, the nuclei mode particle distribution is approximately the same for all fuels though the neat petroleum diesel fuels have a larger magnitude of agglomerated PM.

For the LLTC condition, starker differences in particle size distribution exist between fuels as seen in Figure 5.9. All fuels showed a larger number of nuclei mode particles with ULSD exhibiting the largest magnitude peak in this range.

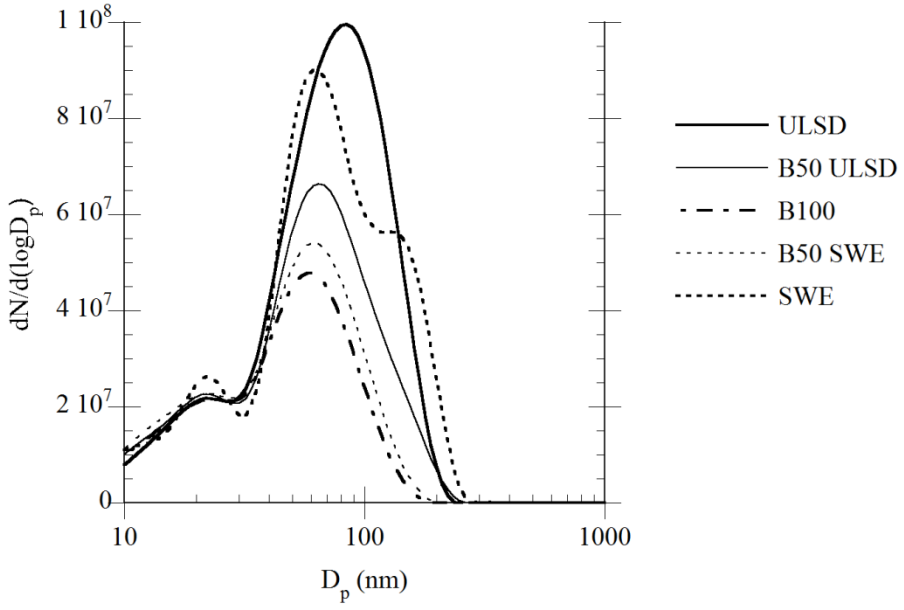

Figure 5.8: Particle size distribution for the conventional operating condition

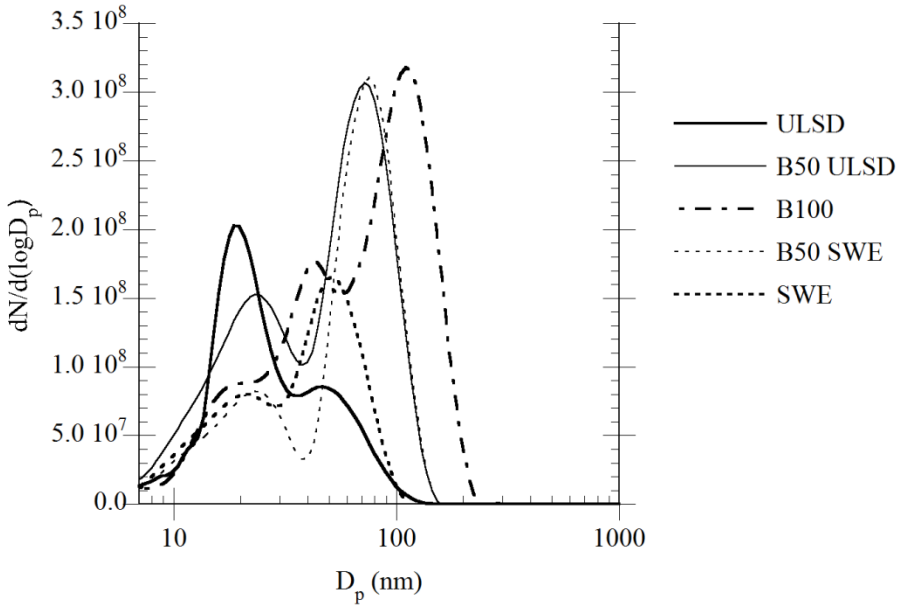

Figure 5.9: Particle size distribution for the LLTC operating condition

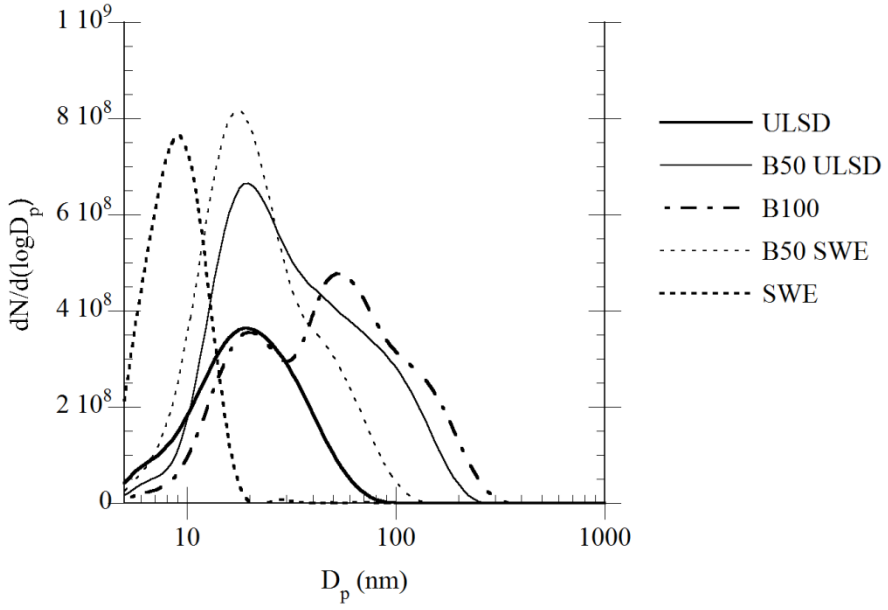

Figure 5.10: Particle size distribution for the ELTC operating condition

Particle size distribution shifts towards larger particles with higher concentrations of biodiesel in LLTC as was found in the preliminary study. For the ELTC condition, a similar phenomenon is apparent. For this operating condition, the distribution shifts to higher diameter than for LLTC indicating more agglomeration of particles. This result for both LTC conditions and biodiesel is consistent with the PM mass trends shown in Figures 5.6 and 5.7 since the overall mass of a distribution is dominated by larger particles.

In further examining the trends, the curves shown in Figures 5.8 through 5.10 were integrated to solve for total number of particles for each case and are shown in Figure 5.11. Here, ELTC has the most particles and conventional the least. The trends in total particle number are the same as PM mass where for conventional combustion it decreases for increasing biodiesel whereas in LTC the total particles increase to a maximum for B100.

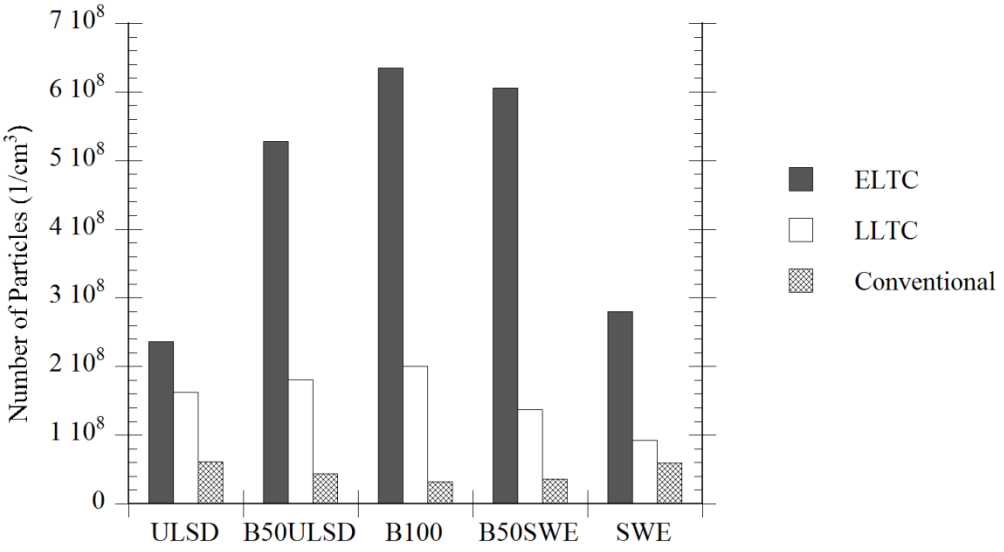

Figure 5.11: Number of particles per cubic centimeter for all fuels and operating conditions

Beyond the particle number analysis presented, mean particle size is also a key parameter in identifying differences between fuels and operating conditions. Figure 5.12 shows clearly that the mean particle diameter decreases with increasing biodiesel composition for conventional combustion but the opposite is true for the LTC modes. This result clearly indicates that higher amounts of organic content found for biodiesel is based on agglomeration of particles.

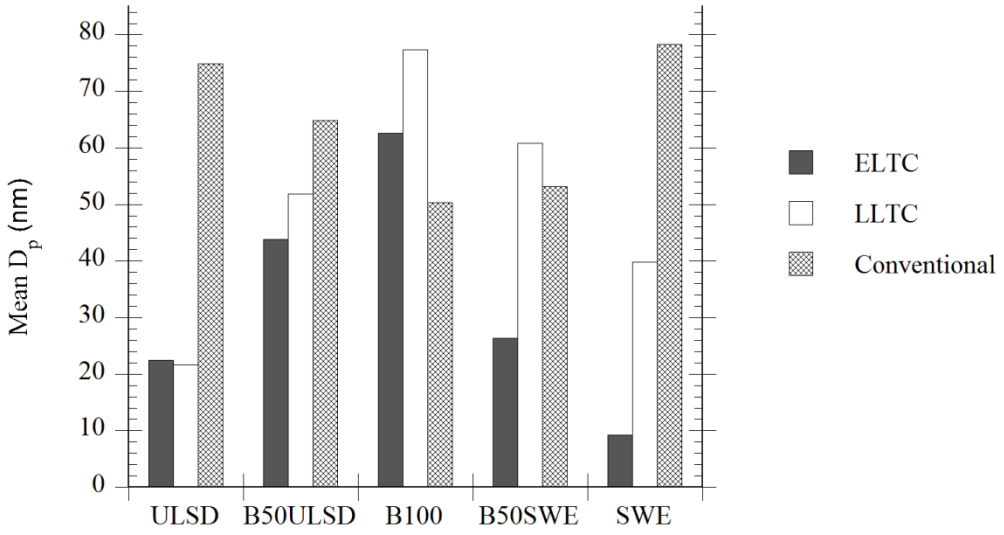

Figure 5.12: Mean D_p for all fuels and operating conditions

5.2.2.3 Bulk Composition of Organic Fraction

To confirm the primary culprit in the dramatic increase in PM mass for biodiesel in LTC, extracted organics were analyzed using GC-FID. Using the method described in Chapter Two, the neat fuels used in the study were first tested to identify species to be found later in the extracted PM. Figure 5.13(a) shows the raw signal for ULSD from the GC analysis.

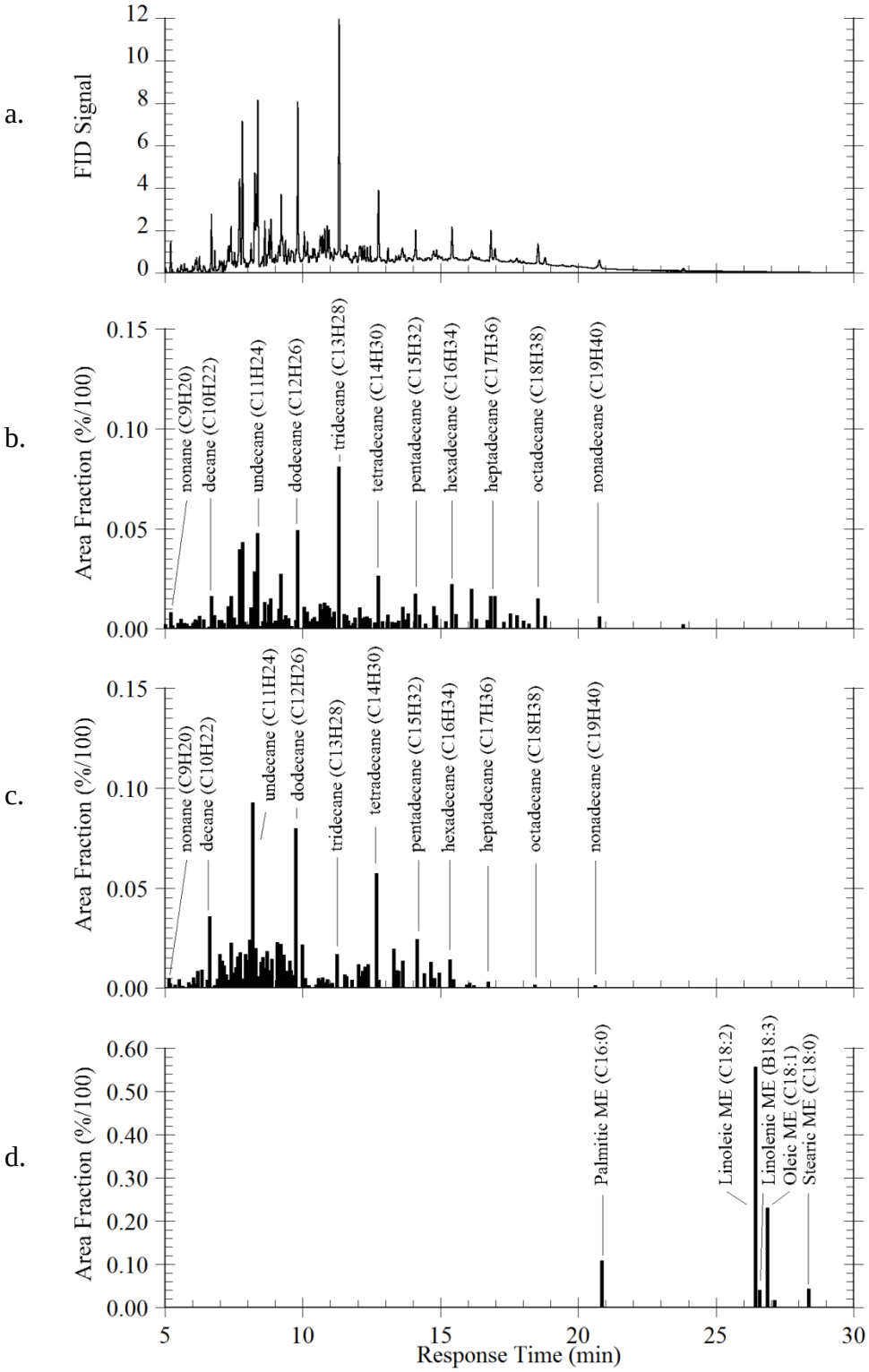

Figure 5.13: (a) Raw GC-FID signal for ULSD; Area fraction versus retention time for: (b) ULSD; (c) SWE; and (d) B100 fuels

To more easily see the areas of the resultant peaks as a function of detector response time, area plots are shown in Figure 5.13(b)-(d) for the three neat fuels tested. For ULSD and SWE n-alkanes were identified as unburned fuel markers. ULSD contained 31% n-alkanes and SWE had 33% n-alkane content. For biodiesel, the five methyl primary methyl esters were detected using the GC method as shown in figure 5.13(d). The values matched well with those found from the fatty acid profile done by Midwest Laboratories presented in Chapter Two.

Table 5.3: Comparison between biodiesel fatty acid profile from outside analysis and GC-FID method

Fatty Acid	Midwest Labs	GC-FID (Area Frac.)
Linoleic (C18:2)	52.3%	52.7%
Oleic (C18:1)	22.4%	23.6%
Palmitic (C16:0)	11.2%	11.1%
Alpha Linolenic (C18:3)	8.3%	4.2%
Stearic (C18:0)	4.5%	4.4%
Arachidic (C20:0)	0.3%	N.D.

Four primary fractions of hydrocarbons are identified in the extracted PM samples; known biodiesel species, known n-alkanes, unidentified light species eluting below nonadecane ($C_{19}H_{40}$) and unidentified heavy hydrocarbons which includes the lubricating oil fraction. The known n-alkanes are assumed to be representative of unburned petroleum diesel fuel. Figure 5.14 shows the quantitative results for the mass of extracted hydrocarbons from the conventional combustion operating condition. Here n-alkanes from SWE and ULSD are found in low quantities but biodiesel is found in relatively higher concentrations for the B100 and B50 cases. Unidentified light HCs remained

essentially constant for all fuels and the heavy HCs did not follow any discernable trend ranging from 10 µg to 55 µg.

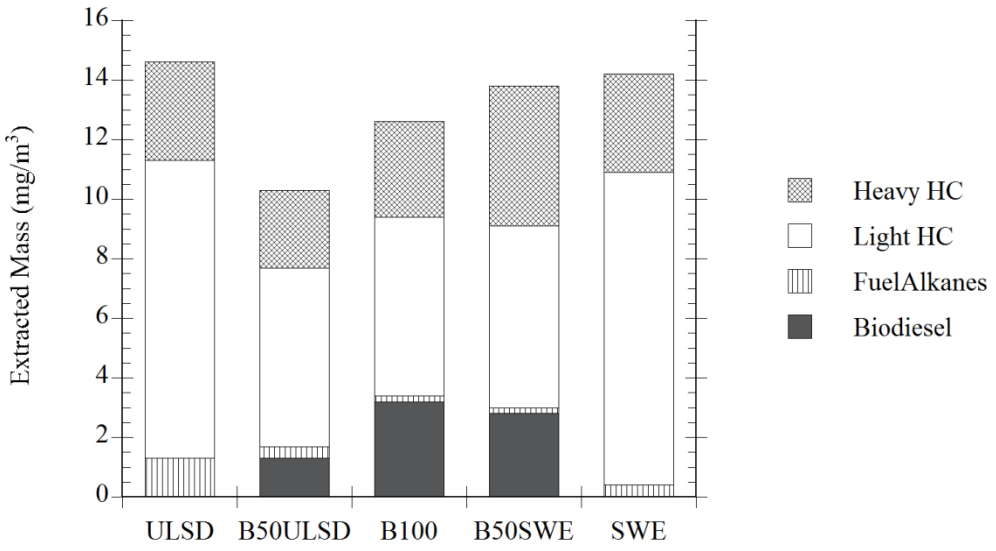

Figure 5.14: Masses of four categories of extracted organics for the conventional combustion operating condition

For the LLTC condition, methyl esters from unburned biodiesel were overwhelmingly the dominant HC fraction detected in the extracted PM samples as seen in Figure 5.15. Other fractions appeared nearly constant for all fuels. ELTC show the same trends but with much higher fraction of biodiesel in the extracted PM as shown in Figure 5.16. It is conclusive from this data that unburned biodiesel is the primary component responsible for the increase in PM mass for biodiesel in LTC combustion.

Taken with the findings of Chapter Four, the results from the speciated extracted PM paint a more complete picture of the total unburned hydrocarbon emissions of both LTC modes. THC is lower in the undiluted exhaust but the LHC fraction is higher indicating lower concentrations of unburned fuel. However, when subjected to quenching and

dilution as would occur if the gas were mixed in the atmosphere, the unburned fuel present in the biodiesel cases converts readily to the particle phase. In Section 5.3, condensation is presented as the most likely mechanism for this to occur.

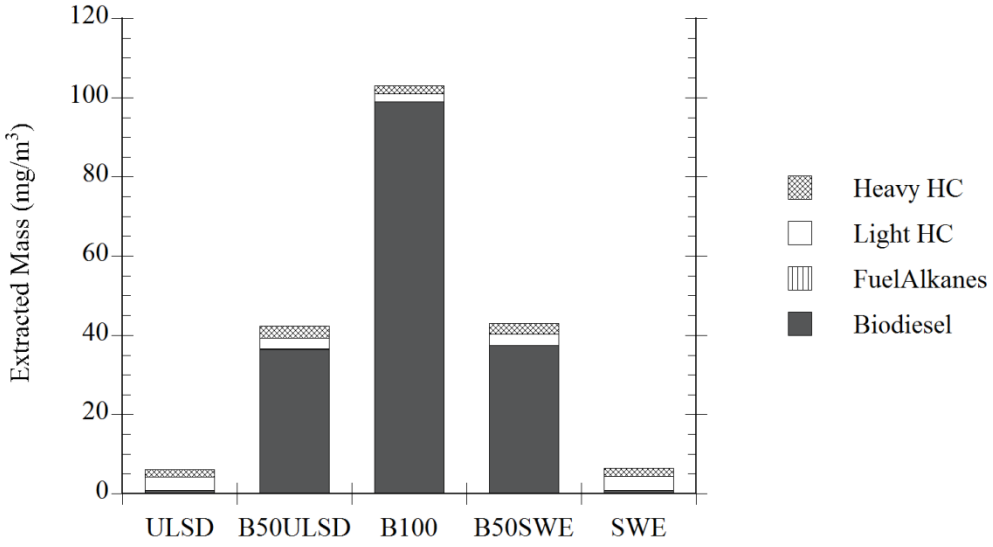

Figure 5.15: Masses of four categories of extracted organics for the LLTC operating condition

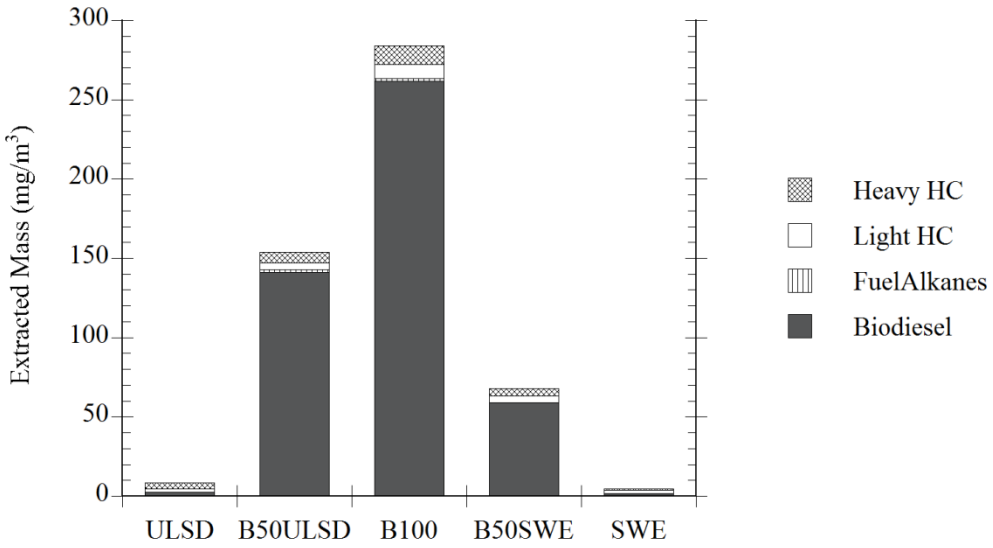

Figure 5.16: Masses of four categories of extracted organics for the ELTC operating condition

5.2.2.4 Fuel Switching Error

In Figures 5.15 and 5.16, a small amount of biodiesel is shown in the extracted PM from both neat ULSD and SWE. This indicates an error in the testing procedure where residual methyl esters from a previous biodiesel run are somehow introduced. A separate experiment was run in which the engine operates on biodiesel for 30 minutes, the fuel switching procedure described in Chapter Two was done followed by the engine warm-up procedure. A sample was then taken from the fuel system and analyzed using the GC-FID method. Results from the analysis are shown in Figure 5.17.

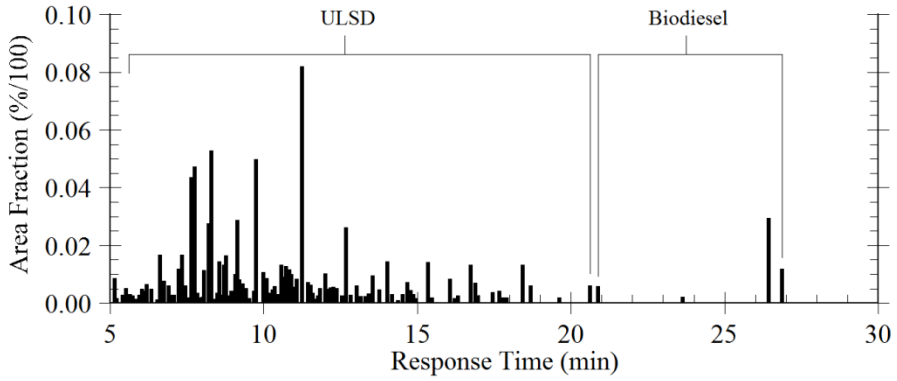

Figure 5.17: Area fraction versus response time for ULSD fuel sampled after switching procedure

Based on the area fraction, the ULSD fuel contained 4.7% biodiesel after the switching procedure. Therefore, in all the data presented in this study, neat petroleum fuels contain up to 5% of biodiesel and vice versa. Results from ULSD and SWE cases showing identifiable biodiesel components in the PM extract shows that even at very low concentrations in the exhaust, methyl esters convert to the particle phase very easily.

5.2.2.5 Oil Dilution with Biodiesel

Another source of error in the testing is unburned biodiesel coming into contact with lubricating oil and mixing along the cylinder walls before returning to the oil system. Biodiesel is known to mode readily dilute engine oil by this method than petroleum based fuels (Knothe, 2005). This is a primary concern for engine durability.

Engine oil was not changed during the duration of the data taken in this study; a duration of approximately 200 hours of engine operation. GC analysis of new and used oil was done using the methods described previously and the results are shown in Figure 5.18.

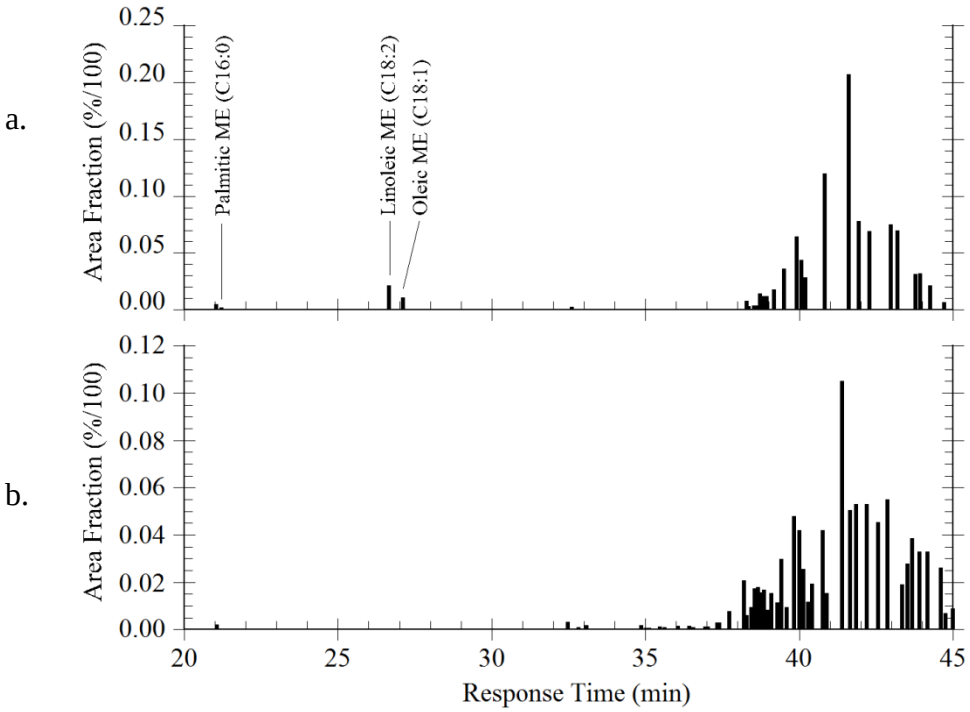

Figure 5.18: Area fraction versus response time for: (a) Used lubricating oil and; (b) Fresh lubricating oil

In the test, the same quantity of oil was analyzed for both samples. Figure 5.18(a) shows 3.1% methyl esters in the oil by area fraction, roughly equating to its mass fraction. This finding is consistent with that of Thornton et al. (2009) where oil was diluted by 4 to 10% after implementation of a post-injection strategy which allows more fuel to come into contact with engine oil on the cylinder walls during expansion.

5.3 Condensation Mechanism for Increased Organic Fraction of PM

From the experimental results, significant gas to particle conversion occurs as a result of biodiesel in the exhaust after dilution in LTC modes. As previously mentioned, adsorption and condensation are the primary mechanisms by which this occurs. In a comprehensive study of PM sampling, Plee and MacDonald (1980) explored the effects of dilution ratio and collection temperature on PM mass and composition. Then, by comparing experimental data to simple models, they found that adsorption was the primary mechanism responsible for conversion of semi-volatile organics to the particle phase. Confirming this finding, Clerc and Johnson (1982) developed a more complex model for predicting the rate of adsorption onto PM prior to a dilution process. Adsorption is a process wherein organic species traveling in the exhaust come into contact with the micro-porous surface of soot molecules and attach based on intermolecular forces. Once on the surface, they become part of the particle, thus transitioning from the gas phase to the particle phase.

Adsorption, while generally thought to be the predominant mechanism for conventional diesel modes with less than 50 ppm THC in the raw exhaust, is not considered the primary mechanism for the increases seen in this study. A first reason is

that although the number of particles more than doubles for ELTC as shown in Figure 5.10 from ULSD to B100, the number of sites for adsorption may be assumed to be linearly related to this increase and does not explain the more than one order of magnitude increase in PM mass. Secondly, the methyl esters found in biodiesel have lower volatility than any species found in ULSD or SWE. This factor is not accounted for with the adsorption model since it is largely independent of vapor pressure. Also, with adsorption, the soot particle sites cannot be assumed to have such a higher preference for biodiesel over petroleum diesel components leading to such large differences in soot mass for the same combustion condition. Lastly, although Plee and MacDonald found that adsorption best fit the trends in dilution ratio and temperature for their combustion condition, they indicated that with increasing concentrations of semi-volatile species, like in LTC, the condensation mechanism plays a more important role.

Condensation, the second mechanism for gas to particle conversion is a logical explanation for the increase in PM mass found in this study. The increasing concentration of low volatility methyl esters for LTC along with increasing mean particle size for biodiesel implies that these species are preferentially condensing over petroleum diesel. Confirming this idea, Durán et al. (2006) found that the adsorption mechanism was inadequate for completely explaining organic content on PM when biodiesel is used in conventional diesel combustion even with relatively lower THC concentrations.

Condensation and evaporation are important processes in the atmosphere. Cloud formation proceeds by heterogeneous condensation of water on salt particles in the troposphere and models for growth of such particles are well known (Hinds, 1999). Organic species in the atmosphere also contribute to atmospheric aerosols over time. A

model is presented in the following section to examine the role of condensation of biodiesel and petroleum diesel components in the growth of engine PM during a dilution process.

5.3.1 Calculations and Assumptions

A model is presented which follows the condensational growth model given by Jacobson and Kittleson et al. (2005). The rate of liquid concentration growth of a species on the surface of a particle is a function of the saturated vapor concentration, and the concentration of each species in the gas phase.

$$\frac{dC_{i,liq}}{dt} = k_{i,diff}\left(C_{i,vap} - \frac{C_{i,liq}}{\sum_i C_{i,liq}} S^* C_{i,sat}\right) \quad (5.2)$$

Where:

$C_{i,liq}$: Concentration of species i in the liquid phase (mol/m3)
$k_{i,diff}$: Rate of diffusion of species i to the surface (1/s)
C_{ivap}: Concentration of species i in the vapor phase (mol/m3)
k_{des}: Rate coefficient for desorption
S^*_i: Kelvin ratio

The Kelvin ratio (S*) is a unitless coefficient that expresses the difference in thermodynamic liquid/vapor equilibrium between a curved surface and a flat surface and is always greater than unity. The Kelvin ratio for a given species is given by Equation 5.3.

$$S_i^* = \exp\left(\frac{4\sigma_i MW_i}{\rho_i RTd^*}\right) \tag{5.3}$$

Where:

σ_i:	Surface tension of species i
ρi:	Density of species i
MW_i:	Molecular weight of species i
R:	Ideal gas constant
d*:	Kelvin diameter
T:	Temperature

For a system that has reached steady state, the worst case scenario for condensation of species onto a surface the equation reduces to the following. Equation 5.4 is also an expression of Raoult's law which allows for the interaction of other species in determining thermodynamic equilibrium of a two phase system.

$$C_{i,vap} = \frac{C_{i,liq}}{\sum_i C_{i,liq}} S_i^* C_{i,sat} \tag{5.4}$$

The system of non-linear equations (5.4) is solved together with a species mass balance for a given number of species using the *fsolve* function in Matlab. For the model, the four primary methyl esters in proportion to the fractions in Table 5.3 are used for biodiesel and C_8-C_{19} n-alkanes in proportion to that found in Han et al. (2009) are used to approximate petroleum diesel fuel. Other semi-volatiles like olefins contained in the diesel fuel are not considered. This is a conservative assumption since for a given carbon number, paraffins have the highest boiling point. The saturated vapor pressure for each species is calculated using the Antoine equation with coefficients for methyl esters given by Yuan et al. (2005). Other physical properties of methyl esters are taken from Yuan et al. (2003). The Antoine coefficients for n-alkanes are from Yaws' Handbook (2003).

For a given condition, UHC concentration is divided by the dilution ratio and is assumed to be in proportion to the fuel used. For example, a B50 condition has 50% by volume biodiesel and 50% of the n-alkane mixture in the UHC. For the model, the Kelvin diameter (d*) is assumed to be 50 µm, temperature (T) is the filter collection temperature of 45°C and the dilution ratio is assumed to be 10:1 as in the experimental study.

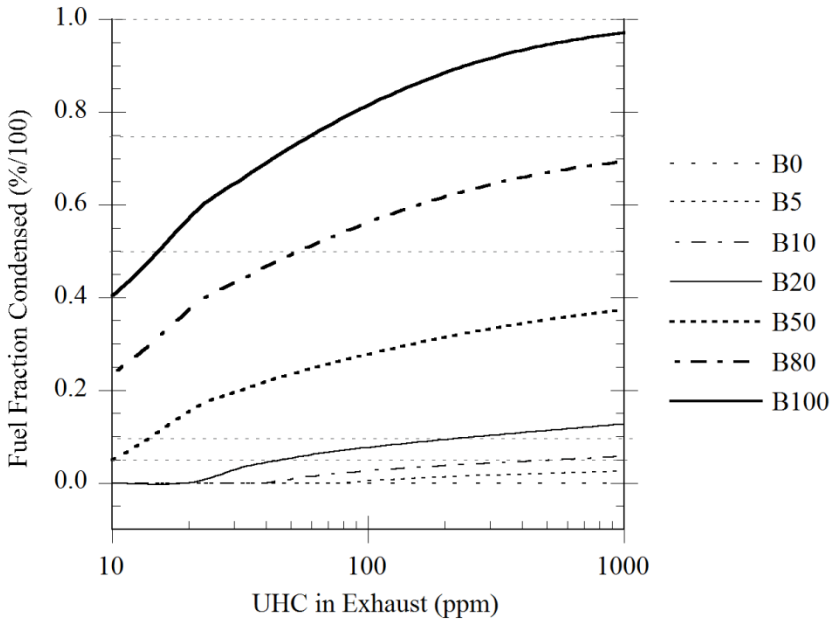

Figure 5.19: Fuel fraction condensed from model prediction for varying amounts of biodiesel mixed with petroleum diesel surrogate

Figure 5.19 shows the results of the model for a range of UHC from 10 to 1000 ppm on a log scale and different concentrations of biodiesel. The fraction of fuel condensed for B0 at the conditions shown is approximately zero up to 1000 ppm of total UHC. For B100 however, almost all of the biodiesel comprising the UHC condenses out of the exhaust. This is a promising result as it predicts that methyl esters preferentially condense over n-alkanes from petroleum diesel fuels found in exhaust to the proportion of biodiesel in the fuel.

5.3.2 Experimental Validation

To validate the model based with the experimental data taken in this study the mass of fuel condensed for a given UHC concentration in the undiluted exhaust is compared to the data taken. For the experimental data, the UHC concentration is given by Equation 4.2 and the condensed mass is estimated by subtracting the EC mass concentration from the overall PM concentration for a given condition as in Equation 5.1. The B50SWE and B50ULSD cases were combined into one B50 data set and the SWE and ULSD cases were combined into the B0 data. All data from the three operating conditions were combined creating a spectrum of UHC data over a range from 30 to 700 ppm. Figure 5.20 shows that the condensation model predicts the experimental data quite well confirming that this mechanism is the likely cause of biodiesel converting to the particle phase for LTC.

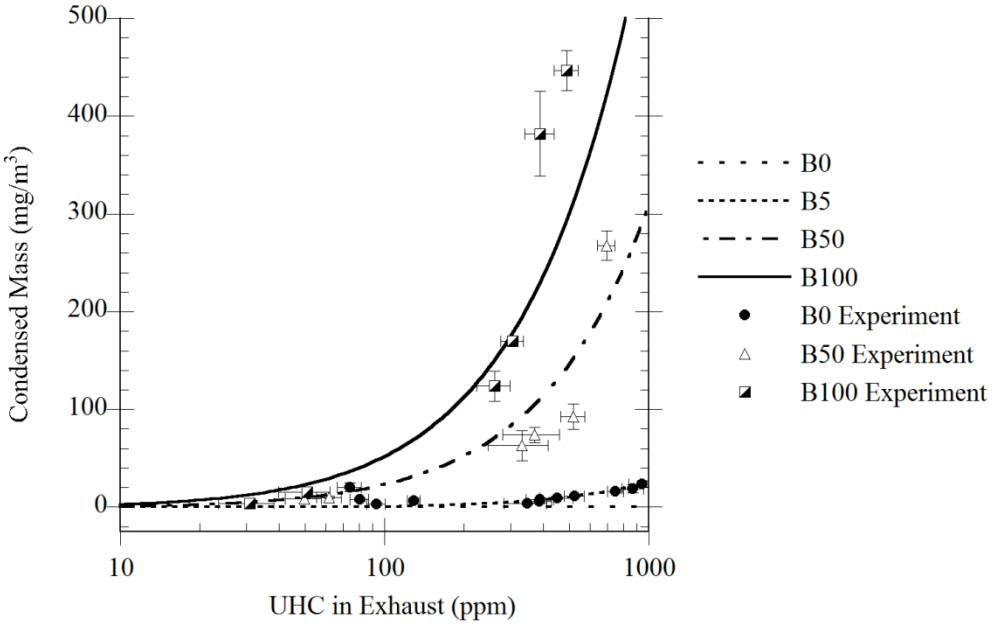

Figure 5.20: Condensed mass on PM versus UHC in undiluted exhaust for model prediction and experimental data

For all the data points, the uncertainty of the PM mass is based on twice the standard deviation of the three filter masses taken per condition. With such small sample sizes, the possibility for larger experimental error is likely. Following the student's t-distribution, the measured 95% confidence interval error would be multiplied by 3.182 (Figliola and Beasley, pp.122) in which case the model may predict the condensed mass to even higher precision.

As mentioned in section 5.2.2.4, the neat petroleum diesel cases had close to 5% biodiesel in the fuel as methyl esters were found in both in the PM and in the fuel after the switching procedure. The model predicts this as well since the B0 experimental data more closely approximates the B5 model results as opposed to the B0 model results as a function of UHC concentration.

Contrary to some literature findings (Chang et al., 1998), the model predicts that no condensation of biodiesel onto PM occurs in the undiluted raw exhaust sample lines at 190°C without air dilution. It is then expected to higher confidence that all the biodiesel is still in the gas phase in the heated sample line and DOC inlet.

5.4 Summary of Findings

With regards to the stated goal of this chapter, PM mass emissions are confirmed to be more than an order of magnitude higher for B100 than for ULSD for the LLTC and ELTC operating conditions following a controlled dilution process. The primary contributors to this increase are high concentrations of unburned biodiesel from over-lean areas from combustion heterogeneously condensing onto the carbon particles in the

exhaust. This gas to particle conversion process also skews the particle size distribution towards larger particles and increases the mean particle diameter.

The PM emission for conventional combustion decreases with increasing biodiesel confirming trends found in the literature. Soot decreases for all operating conditions with increasing biodiesel content in the fuel as a result of concurrent oxidation processes during soot formation in rich areas of the combustion chamber. The soot mass emissions as measured by the OC/EC measurement match well with the calculation of soot mass based on the smoke meter readings using a well established correlation even in the low range of FSN measurement.

From speciation of extracted PM from the engine operating conditions in this study, the primary contributors to increased PM emissions for biodiesel LTC are unburned methyl ester species. Also from the speciation results, methyl ester components diluted the lubricating oil to 3.1% during the course of the study consistent with published studies. The experimental fuel switching procedure used in the study was found to inadequately purge all biodiesel from the system and therefore many of the neat petroleum diesel cases contained approximately 4.7% biodiesel by mass.

Condensation is the primary mechanism by which biodiesel in the gas phase converts to the particle phase following dilution. A model based on Raoult's Law was developed to predict the amount of condensed unburned fuel on the PM given the dilution ratio, filter collection temperature and concentration of individual fuel species in the raw exhaust. The model accurately predicted the amount of unburned fuel species found on the PM in the experimental study.

CHAPTER SIX

DIESEL OXIDATION CATALYST PERFORMANCE

6.1 Background

Findings from the previous chapter indicate that unburned biodiesel from the exhaust of an engine operating in LTC plays a significant role in increasing particulate emissions due to condensation. Since this process occurs upon a reduction in temperature due to exhaust dilution, if the concentration of UHC in the gas phase can be lowered prior to exiting the atmosphere, the observed increase in PM could be averted. This chapter uses the material presented thus far and additional measurements from the exit of a diesel oxidation catalyst (DOC) to meet the third goal set forth in Chapter One; "To identify whether a DOC can oxidize organic species in the exhaust that contribute to increased PM mass emitted from a vehicle tailpipe using biodiesel in the LTC mode."

First, the overall conversions of THC, LHC, UHC, CO, and H_2 through the DOC with a constant inlet temperature and space velocity are determined. The tests were performed by taking samples from the raw exhaust of the engine operating in the LLTC condition before and after the DOC for ULSD, B100 and SWE fuels. PM mass was also taken after the DOC following the same dilution process as performed previously. Finally the organic species from the PM were extracted and speciated using the GC-FID method to determine how much biodiesel remained on the particles following the DOC.

6.1.1 General Characteristics of DOCs

Aftertreatment catalysts for diesel engines hold the promise to largely purge HC, CO, NO_X and PM from the exhaust stream before they enter the environment. Originally designed for use in diesel engines for the reduction of organic species from PM (Otto et al., 1980), the DOC has become an essential tool for meeting emissions targets worldwide (Walker, 2004). Reviews like that by Zelenka et al. (1990) surveyed the use of oxidation catalysts to that point in time and found them a suitable solution for the reduction of SOF, THC and CO from light and heavy-duty diesel engines.

One obstacle for the early adaptation of DOC was high amounts of sulfur in the fuel that poisoned the active catalytic materials. Fortunately, the introduction of ultra-low sulfur diesel (ULSD) with sulfur contents less than 15ppm in recent years has made the use of DOCs more feasible. Biodiesel contains virtually no sulfur; also an advantage for catalyst longevity.

DOCs are usually configured as ceramic monoliths due to a desire for high durability and low pressure drop. The active metal typically used is platinum though palladium is also commonly added to aid in stabilizing the catalyst against thermal aging and sintering (Morlang et al., 2005). Aluminum oxide (alumina) supports have been commonly used in DOCs. Zeolite-containing supports have also been implemented for adsorbing HC species at lower engine exhaust temperatures where the catalytic material is not active (Kamijo et al. 2000). Cerium oxide (ceria) is also often used as a component in support material for its oxygen storage capacity during rich excitations of the engine and for its ability to oxidize SOF on PM (Farrauto, 1996).

6.1.2 DOC for LTC Modes

Even though PM emissions are much lower in partially premixed LTC modes, the DOC is essential for reducing the higher CO and HC emissions generated. Bohac et al. (2006) looked at the conversion of CO and HC from an engine operating in the LTC mode over a platinum-based catalyst. They found that the conversion efficiency for CO was near 100% while for hydrocarbons it was near 80%. Methane, being a major component among partially reacted species in premixed combustion did not react at the temperatures found in the DOC for LTC and accounted for a large portion of the hydrocarbons passing, unreacted, through the catalyst.

Issues related to the use of DOCs in LTC modes arise related to the poisoning effects of engine exhaust species on the catalyst. Knafl et al. (2007) in a combined engine and bench reactor study found that catalyst light-off temperature increased for LTC exhaust due to high concentrations of CO. Complicating the effect is low load operation where LTC operating strategies are typically implemented. Here, exhaust temperatures can be as low as 200°C, close or below the light-off temperature of most catalysts. Northrop et al. (2007) also examined the self-inhibiting effects of unsaturated hydrocarbon species on a platinum-based DOC catalyst. They found reduced hydrocarbon conversion efficiency when more of such species were present in the exhaust like the case of a rich LTC mode as described above.

Han et al. (2008) performed a more detailed study of the HC species converted by the DOC from a late LTC mode similar to the LLTC mode in this work. They found that alkenes and alkynes were almost completely converted whereas non-methane alkanes like

ethane and propane had a conversion efficiency of only 80%. Higher carbon number HCs like those from unburned fuel had conversions that fell from 85% for C_8 to lower than 50% for C_{18}.

6.1.3 DOC Performance with Biodiesel-Fueled Engines

Although biodiesel combustion generally creates lower exhaust manifold concentrations of THC and CO than petroleum fuels, conversion of these pollutants through a DOC is still necessary to meet emissions standards. In general, conversions of THC and CO are comparable between biodiesel blends and neat diesel fuel (Peterson et al., 2009, Theinnoi et al., 2008). Purcell et al. (1996) performed a study where a heavy duty diesel engine was operated over a transient test cycle on commercially available diesel fuel, B50 made with soy-based biodiesel and B100. The results of the average gaseous conversion of THC, CO and formaldehyde are shown in Table 6.1. THC conversion for all three fuels remained constant at near 60% and CO conversion was nearly constant at 80% but H_2CO conversion significantly reduced for B100.

Table 6.1: Average conversion of THC, CO and H_2CO through a DOC calculated from the data presented in Purcell et al. (1996) for diesel, B50 and B100

	Diesel	B50	B100
THC Conversion	60%	64%	61%
CO Conversion	77%	80%	76%
H_2CO Conversion	42%	50%	20%

For conventional biodiesel combustion, DOCs have been implemented to reduce higher organic content contributing to PM emissions compared with petroleum fuels. For

example, Sharp et al. (2000) tested the effectiveness of a DOC to reduce the total PM emissions on a 5.9L medium-duty engine over an FTP cycle. They found that HC conversion efficiency of the catalyst was reduced but the CO conversion remained the same when comparing 100% biodiesel (B100) to a reference diesel. However, total PM and SOF conversion efficiency improved. Others have confirmed this finding (Stein, 1996) showing that the organic content leading to the same or higher PM emissions for biodiesel in conventional combustion are reduced through a DOC since the soot emissions are lower than for petroleum diesel. There are some dissenting findings however. Baik and Han (2005) found that conversion of PM through a DOC at 200°C decreased from 37% to 26% for a heavy duty engine operating at part load for B20 compared with ULSD. Peterson et al (2009) also found that the conversion of PM for four different modes of combustion was lower for a B20 blend than for ULSD.

Even though PM mass is generally reported to be reduced through a DOC it has been shown ultrafine particles of diameter less than 100 nm are not reduced irrespective of fuel used (Frank et al. 2007). However, the DOC is effective at reducing larger agglomeration mode particles. Theinnoi et al. (2008) showed that a DOC reduced overall particle number for biodiesel by 5% by reducing the larger particles in a particle size distribution. They also found that the DOC reduced PM mass by more than 30% indicating oxidation of organics residing on the particle surface were oxidized.

DOC conversion of high concentrations of unburned biodiesel like that found in the exhaust from LTC has not to this date been reported. This chapter presents experimental data to show whether a production-style DOC is effective in reducing UHC from the

LLTC condition such that PM emissions do not increase later due to gas to particle conversion processes once the exhaust mixes with the ambient air.

6.2 Experimental Results and Discussion

6.2.1 DOC Conversion of HC and CO

This experimental study tested the effectiveness of the DOC for the LLTC engine operating condition and the three neat fuels; ULSD, B100 and SWE. The test engine was held to the same constant parameters as shown in Table 3.1 for LLTC. In the test setup, gaseous species measured from before and after a DOC at a constant inlet temperature. The catalyst conditions including 95% confidence interval are shown in Table 6.2.

Table 6.2: GHSV and temperatures for steady state conditions used for conversion tests with three neat fuels

	ULSD	B100	SWE
GHSV (hr^{-1})	**82,700** ± 4,300	**85,200** ± 5,400	**82,700** ± 4,600
Inlet Temperature (°C)	**239.5** ± 2.3	**239.6** ± 2.3	**240.2** ± 2.5
Monolith Temperature (°C)	**270.7** ± 3.2	**269.0** ± 2.6	**268.8** ± 2.6
Outlet Temperature (°C)	**246.7** ± 4.0	**248.4** ± 3.3	**244.4** ± 3.4

Gas hourly space velocity (GHSV) is defined as the volumetric flow rate of exhaust gas though the catalyst at standard conditions divided by the total volume of the catalyst monolith. GHSV, DOC inlet temperature, monolith temperature, and outlet temperature are the same for all three fuels tested to the precision of the measurements. More accurate comparisons of fuel-effects on catalyst conversion can be made when such parameters are held constant.

DOC conversion of CO and THC is shown for the three fuels in Figure 6.1. Here, conversion is defined as the change in volumetric concentration of species through the catalyst. The figure shows that conversions of THC and CO are the same to the error of the measurements for the three fuels. This result is consistent with findings from the literature referenced above.

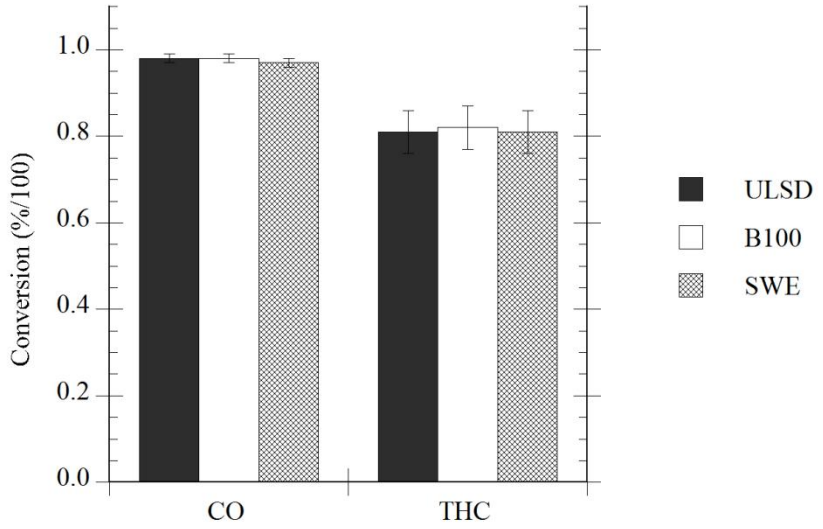

Figure 6.1: Conversion of CO and THC through the DOC for the LLTC operating condition

More subtle differences between the fuels can be seen in Figure 6.2 where the conversion of individual HCs as measured by the FTIR along with H_2 is shown. Here, the only statistical differences in conversion occur for methane and formaldehyde. Consistent with the finding from Purcell et al. (1996) formaldehyde conversion is lower for the biodiesel case. Strangely, methane conversion increases for the B100 case. Usually methane is not converted by any extent through DOCs based on the established literature (Han et al., 2008, Northrop et al. 2009).

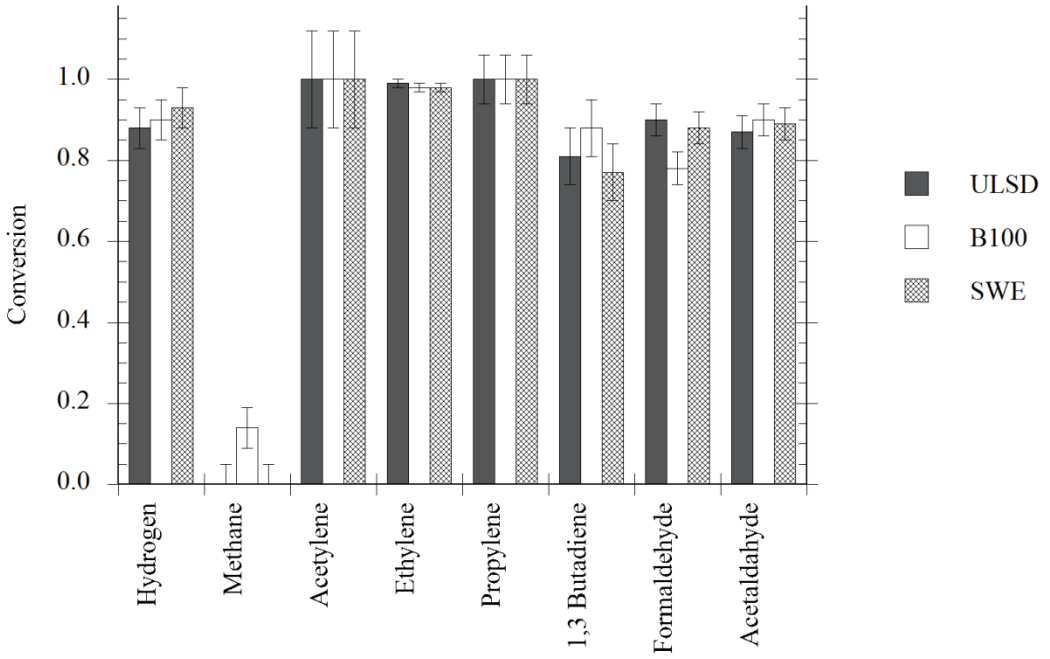

Figure 6.2: Conversion of individual LHC compounds and H_2 through the DOC for the LLTC operating condition

Low temperature oxidation of biodiesel proceeds in a slightly different pathway than petroleum diesel fuels. Some literature indicates that formaldehyde is created through additional pathways for methyl esters not found in the oxidation of aliphatic compounds (Huynh and Violi, 2007, Herbinet et al., 2008). This may contribute to additional formaldehyde being formed simultaneously to its oxidation thus reducing the net conversion as shown in Figure 6.2. Reasons for methane conversion for biodiesel as shown in the figure are unknown. Future work is recommended to examine the oxidation of biodiesel through a DOC to better understand the mechanisms by which it is converted.

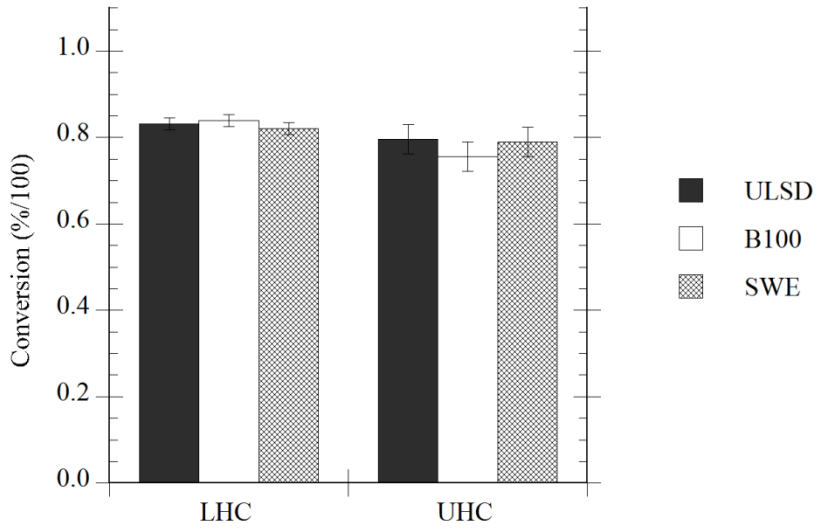

Figure 6.3: Conversion of LHC and UHC through DOC for the LLTC operating condition

Though some minor differences are seen in the conversion of CH_4 and H_2CO through the DOC, no significant net change in LHC conversion is found. Calculating LHC and UHC based on Equation 4.1, Figure 6.3 shows no statistical differences in conversion through the DOC.

6.2.2 DOC Conversion of PM

For the LLTC condition, the DOC is effective at significantly reducing PM emissions. Figure 6.4 shows the comparison of PM mass measured before the DOC from Chapter Five compared to that measured after the DOC. The post-DOC PM emissions are of similar magnitude for the three fuels whereas the pre-DOC PM emissions are ten times higher for B100 compared the other two fuels. The DOC converts almost all of the PM for the B100 case indicating that the methyl ester species shown earlier to be responsible for PM growth are eliminated to a significant extent.

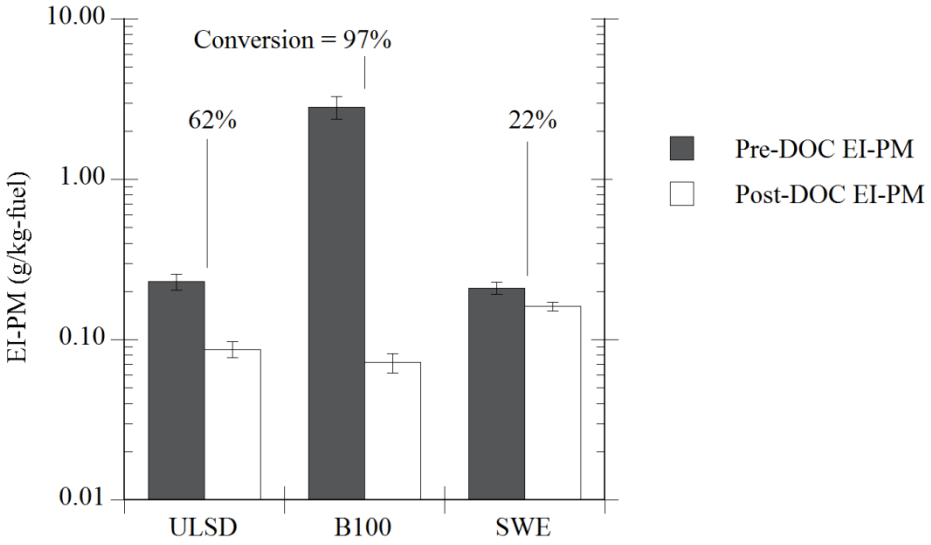

Figure 6.4: EI-PM taken pre-DOC from Chapter Five compared with post-DOC with conversion of PM indicated for the LLTC condition

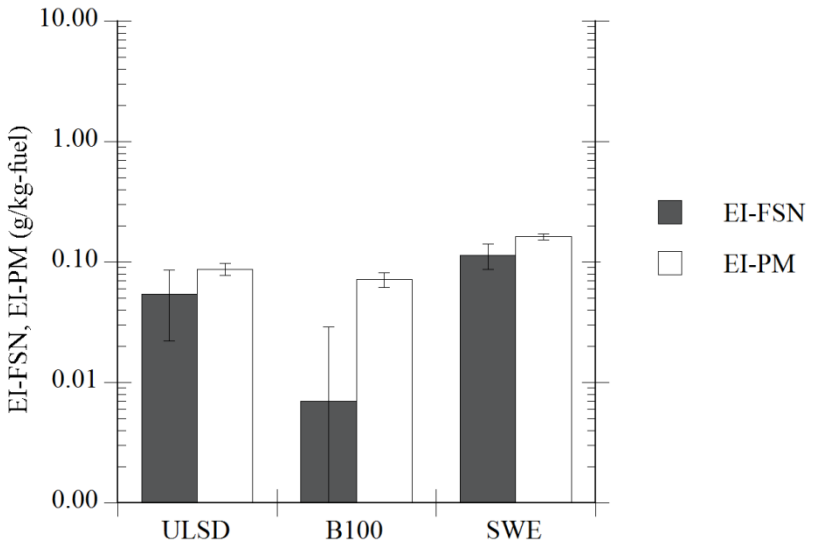

Figure 6.5: EI-FSN and EI-PM for the LLTC condition after the DOC

Using the same log scale for the y-axis as in the previous figure, Figure 6.5 shows the comparison of PM mass emissions and soot mass from after the DOC. Here, as was

shown in Chapter Five, the soot emissions are lower significantly for B100. However, the PM emissions are nearly the same for all three fuels tested. This larger difference between PM and soot mass for B100 indicates that the organic fraction of the PM is still large for this case. Table 6.3 shows the TOF calculated based on the results shown in Figure 6.5 using Equation 5.1 compared with the results from Figure 5.6. Here it is seen that the post-DOC TOF for B100 is still over 90% proving that organics species on the PM are still more significant for biodiesel compared with the petroleum diesel cases. Further TOF is only reduced slightly from the pre-DOC condition. It is therefore likely that unconverted UHC after the DOC converted to the particle phase at a higher rate for B100.

Table 6.3: Total organic fraction for the pre-DOC LLTC condition from Chapter Five compared with post-DOC TOF calculated from the data shown in Figure 6.5

	ULSD	B100	SWE
Pre-DOC	71.0%	99.4%	41.2%
Post-DOC	37.5%	90.6%	29.4%
Reduction in TOF	**47.1%**	**8.9%**	**28.6%**

In further examination of the organic species remaining on the PM for the three cases, Figure 6.6 gives the proportions based on Soxhlet extraction and GC-FID analysis. Biodiesel still remains on the PM, increasing the total extracted mass of organics for the B100 case. This is consistent with the findings of Figure 6.5 and Table 6.3 where the TOF for B100 equalizes the overall PM mass with respect to the other two fuels. Based on this result and the 80% conversion of UHC as shown in Figure 6.3, the increase in TOF for biodiesel is assumed to be the result of unreacted gaseous methyl esters escaping

the DOC and condensing onto the soot as they proceed through the dilution process. As shown in Chapter Five, components from petroleum diesel do not convert to the particle phase as readily upon dilution. Therefore, those UHC components left unreacted through the DOC for the ULSD and SWE cases do not significantly contribute to their PM mass emissions.

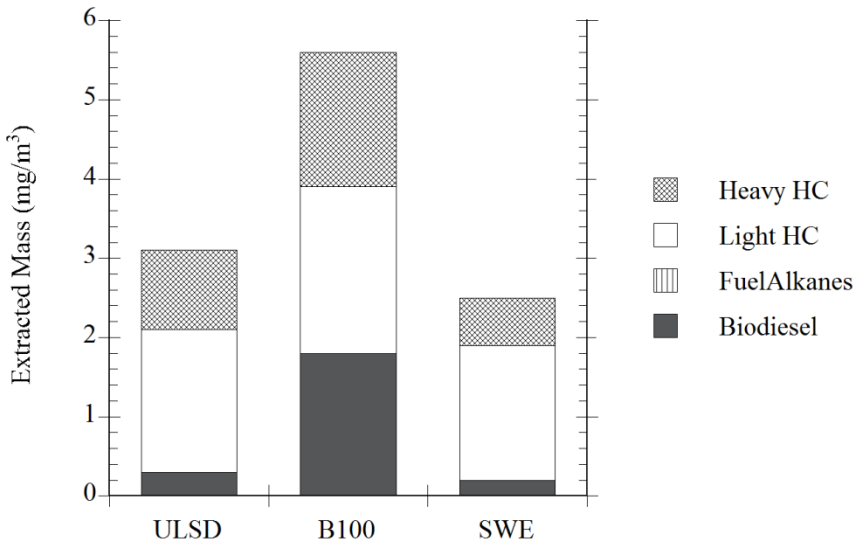

Figure 6.6: Extracted mass of species from the PM for the LLTC operating condition taken after the DOC

The fuel switching error mentioned in Section 5.2.2.4 also plays a role in the data presented here as biodiesel again contributes to the PM for the neat petroleum diesel cases. Alkanes from the diesel fuel are not detected in any samples indicating that the DOC oxidizes these species to a low enough concentration such that they do not contribute to PM emissions. Heavy HCs are largely the same as is expected since these are more difficult to oxidize by the DOC and most likely reside on the PM in the raw exhaust prior to the dilution process.

6.3 Summary of Findings

Based on the above findings, overall conversion of THC, LHC, UHC and CO are the same for ULSD, B100 and SWE in LTC through a DOC operating at a constant inlet temperature and space velocity. Conversion of gaseous methane increases for B100 and formaldehyde conversion decreases, countering each other within the net LHC conversion.

In addressing the goal of this chapter, it is apparent that a DOC can eliminate enough unburned biodiesel from an LTC condition with B100 to significantly reduce PM emissions down to the level of ULSD and SWE at the same engine operating condition. However, since the soot emissions are lower for biodiesel LTC than for the petroleum diesel fuels, the organic content is higher. This organic fraction contains significant unreacted biodiesel which condenses onto the PM after exhaust dilution. Therefore, from the perspective of engine out PM emissions, unburned biodiesel from LTC is a factor that deserves additional study. It is likely that for conditions where UHC is higher like for ELTC or a fuel rich LTC mode as described by Jacobs et al. (2005), PM mass could still be higher for biodiesel than for petroleum diesel fuels after a DOC.

CHAPTER SEVEN

SUMMARY, CONCLUSIONS AND FUTURE RECOMMENDATIONS

7.1 Summary of Research

Emissions reductions from engines can be accomplished by in-cylinder means, by utilizing alternative fuels or by implementing aftertreatment devices. Partially premixed LTC in diesel engines is an effective method for the simultaneous reduction of soot and NO_X emissions. By utilizing high EGR rates, ignition delay is extended and combustion temperatures are reduced thus avoiding creation of regions where these pollutants are created. Disadvantages of LTC operation include higher THC and CO emissions than for conventional diesel combustion. The use of biodiesel in engines has not only advantages based on its partial renewability and the ability to make it from local sources but it also been shown to reduce emissions from diesel engines. Soot, THC and CO emissions have all been reported to be lower for engines operating on biodiesel and blends compared to petroleum diesel. Aftertreatment catalysts are commonly used to convert pollutant emissions from engines before they escape into the atmosphere. The use of a DOC for LTC operation is necessary to oxidize the higher levels of THC and CO emissions created.

In this work, an experimental study was undertaken to explore the use of biodiesel in LTC modes of operation with the use of a DOC catalyst. Data are presented from a

comprehensive study of gaseous HC and PM emissions from a test engine operating in three steady state modes: conventional combustion; late-injection LTC (LLTC); and early-injection LTC (ELTC). Soy-based biodiesel, two neat petroleum diesel fuels and 50% by volume blends of biodiesel and the diesel fuels were tested in the study. The two petroleum fuels were chosen to bound the cetane number of B100 thereby isolating the effects of ignition differences and physical fuel properties on emissions.

Partially premixed LTC operating conditions were chosen based on typical usage scenarios in practical engine applications. ELTC utilizes injection earlier than 15 °BTDC to maximize premixing before combustion begins and is generally used at low loads since peak cylinder pressure generally occur near TDC. Injecting fuel nearer to TDC and retarding combustion allows LLTC conditions to be run at higher loads and speeds. This mode still has limitations in load when injection duration begins to exceed the ignition delay, causing diffusion burn to occur. A conventional combustion mode using a pilot and main injection strategy was also tested to verify established findings for biodiesel use in engines from the literature and to use as a point of comparison for the LTC cases.

Published results from a preliminary study on biodiesel LTC were used as a starting point for establishing three research goals for this dissertation. The first was to explain why the gaseous HC and CO emissions from biodiesel LTC decrease compared to petroleum diesel fuels by exploring the distribution of light hydrocarbons within the THC measurement. The second was to prove the hypothesis that the organic fraction of the PM mass is greater for biodiesel in premixed LTC and to determine the primary species that contribute to this increase. Finally, the use of DOC was explored to oxidize organic

species in the exhaust that lead to increased PM mass emitted from a vehicle tailpipe using biodiesel in the LTC mode.

In achieving the goals of the study, the three operating conditions were first developed on the test engine using the ULSD reference fuel. Data from injection timing and EGR sweeps were analyzed to optimize the conditions based on performance and emissions criteria. The three steady state conditions were then run for all test fuels and emissions data were taken repeated times at each point to ensure accurate results. Between fuels for a given operating condition, speed, load and EGR were maintained constant. Injection duration was altered to maintain a given load, compensating for lower heating value differences between fuels. The CA50 for each fuel was maintained constant by changing the injection timing, allowing for compensation for changes in emissions due to combustion phasing.

Emissions data were collected from numerous instruments for each steady state data point taken. A five gas analyzer bench was used to take basic gaseous emissions and an FT-IR was used to measure individual light HC species. A smoke meter was used to measure soot emissions and data was compared to separate OCEC measurements. A DMS was used to measure particle size distribution and a partial flow dilution tunnel was used to collect filter samples for gravimetric analysis. Organic species were removed from the PM filters collected from the dilution tunnel using Soxhlet extraction and were analyzed using GC-FID. The GC-FID method used in the study was developed to specifically quantify methyl ester species found in biodiesel and n-alkanes found in petroleum diesel fuels.

As part of the study, a model was developed to explain the results for organic material found on the PM. It used a Raoult's Law correlation to estimate the amount of condensation occurring in a gas stream of given temperature, dilution ratio and undiluted hydrocarbon concentration. Outputs of the model included the amount of biodiesel and n-alkanes from the undiluted exhaust that condensed onto particulates following a controlled dilution process like that achieved in the experimental study.

The ability of a standard DOC to reduce emissions from the engine was also studied for the LLTC condition and for the three neat fuels. Gaseous emissions from the analyzer bench and FT-IR from before and after the catalyst combined with PM data were used to examine the effectiveness of the DOC. Gravimetric and speciation analyses were performed to determine whether the species of interest were oxidized to sufficient levels such that excess PM did not appear for the biodiesel case.

7.2 Conclusions

The primary conclusion derived from the work described in this dissertation is that for partially premixed LTC of biodiesel, excessive gas-phase unburned methyl esters in the in raw exhaust condense onto a relatively smaller mass of soot after dilution with atmospheric air. This condensation process resulted in over an order of magnitude increase in PM emissions for B100 in the LLTC condition as compared to petroleum-derived fuels. For the ELTC condition, PM emissions were almost 100 times higher than the diesel fuels tested. The high molecular weight methyl ester components contained in biodiesel have lower vapor pressure and reach a near 95% conversion into the particle

phase with concentrations of 1000 ppm of UHC in the undiluted exhaust for a 10:1 dilution ratio and 47°C collection temperature.

Biodiesel components also condensed onto the particulates in the conventional combustion mode though since THC was more than 10 times lower than for the LTC modes, the difference in PM emissions between fuels was small. The total organic fraction of the PM did increase however since soot emissions were significantly lower for B100 as has been reported in the literature.

From the GC-FID analysis it was found that the switching procedure for changing fuel in the experimental study resulted in residual biodiesel remaining in the fuel system for subsequent tests. For most of the neat ULSD and SWE cases tested in the study, up to 5% by mass biodiesel was contained in the fuel. The small quantity of methyl esters in the UHC from the neat ULSD and SWE cases also condensed on the PM for those cases. The condensation model also predicted that the measured condensed mass for those cases matched better to the B5 estimation, further validating this result.

Biodiesel also diluted the lubricating oil to approximately 3.1% by mass during the course of the experimental testing. This was verified by speciation of the used oil compared to fresh oil using the developed GC-FID method.

Although significant differences in PM emissions in the diluted exhaust exist between biodiesel and petroleum diesel fuels in LTC, undiluted emissions differences are more subtle. For example, combustion efficiency was found to be better correlated to ignition delay than fuel composition directly.

Some findings from the study were expected based on the established literature. Soot emissions are lower for biodiesel in LTC and in conventional combustion due to simultaneous oxidation during combustion from fuel-borne oxygen molecules. In the study, soot mass emissions as calculated from FSN measurements and a well-used calculation compared to those from the more accurate OCEC method had correlation coefficients of greater than 97% for the three operating conditions.

Another expected finding is that THC and CO emissions decrease with increasing biodiesel in the fuel for both biodiesel and petroleum diesel. The reduction in emissions was the same for both B50 blends and the same for the neat petroleum diesel fuels except in the ELTC case. Here, wall quenching of fuel due to early injection timings for ULSD and B50ULSD was responsible for higher THC emissions than for SWE and B50SWE. Reductions in EI emissions for THC and CO for biodiesel are partially related to the lower mass fraction of carbon in the fuel.

Emissions of LHC species are largely the same for all fuels run for a given engine operating condition with the exception of ethylene. This species is a primary intermediate species in the oxidation of higher hydrocarbons. For the LTC modes run in the study, it increased with increasing amounts of biodiesel in the fuel significantly enough to increase overall LHC emissions for the ELTC condition. Overall, the fraction of LHC species, or LOF, increased with increasing biodiesel in the fuel indicating that the UHC emissions were lower. Over a timing sweep for ELTC, LHC emissions depended on the amount of over-mixing in the cylinder as measured by ignition delay but the LOF for biodiesel was consistently higher. Furthermore, ethylene was emitted as a function of LHC according to a linear relationship but with biodiesel having a higher slope. This

indicates that ethylene not only increases the LHC emissions for biodiesel combustion in ELTC modes but that it accounts for a higher proportion of the LHC as well. Based on these findings, it can be assumed that biodiesel is more reactive during combustion, generating higher amounts of partially-reacted species, particularly ethylene. Though detailed kinetics analysis was beyond the scope of this work, it is left to future researchers to investigate these trends further.

Although it was found that the use of biodiesel in LTC increases PM emissions significantly following dilution of the raw exhaust, the results of this work indicate that 80% of the UHC in the exhaust can be oxidized by a standard DOC with an inlet temperature of 240°C and GHSV of 85,000 hr^{-1}. The same conversion was found for ULSD and SWE and the CO conversion for all cases was near 100%. Unfortunately, the remaining unburned biodiesel left unconverted by the DOC still contributes significantly to the PM following dilution. In this study, it was found that although the soot emissions were much lower for the B100 case, the PM emissions were the same compared to that from the ULSD and SWE fuels. Methyl esters from biodiesel were found to be the primary species contributing to the higher total organic fraction (>90%) on the PM for biodiesel LLTC following a DOC.

Although DOC conversion of THC was largely the same for the fuels tested, two interesting trends emerged when the conversion of individual LHC species was examined. Methane, generally found to be left unconverted through a DOC catalyst when petroleum diesel is used had a conversion of 15% for the biodiesel case. Further, formaldehyde conversion decreased for the biodiesel LLTC condition as compared to ULSD and SWE. Literature suggests additional pathways to formaldehyde creation as a

result of methyl ester oxidation at low temperature indicating that it could be produced as well as oxidized through the catalyst, thus reducing its net conversion.

7.3 Implications of Research Findings

The findings presented in this dissertation have some important implications for practical engines. Biodiesel replaces petroleum diesel in the existing fleet of diesel-powered vehicles in a number of countries and its use is projected to grow in coming years. Some of these vehicles implement LTC strategies as part of their stock engine calibrations. For all diesel engines, idle and low load conditions operate with a high level of premixed combustion and emit relatively high THC emissions, similar to LTC, compared with high load operation. If neat biodiesel or blends are used in these engines, unburned methyl ester components exiting the vehicle are susceptible to condensation following dilution with the atmosphere, increasing the mass of PM emitted to above regulated emissions standards.

Although most vehicles are equipped with aftertreatment devices, even small concentrations of methyl esters passing unreacted through a DOC increase the organic fraction of the PM for biodiesel. At high UHC levels, this could negate the decrease the mass reductions of soot generally found with biodiesel operation or even increase the overall PM emissions compared with operation with petroleum diesel fuel. To accommodate the use of low volatility fuels like biodiesel, DOC catalysts may need to be larger, have higher activity or be operated at higher temperature to prevent excessive PM to be emitted.

Condensation of methyl esters could occur in other locations in an engine system where exhaust is cooled. For example, in most engines utilizing an EGR cooler, exhaust can be cooled to 80°C or lower if the engine is cold starting or if a separate cooling loop is used. In these cases, it is most likely that biodiesel in the recycled exhaust will condense on the cold surfaces of the cooler and cause considerable fouling or even blockage of some heat exchange channels.

Another area of diesel engines where exhaust is cooled is downstream in the tailpipe and in aftertreatment devices located far from the exhaust manifold. In cold ambient conditions, a DPF located downstream could be near atmospheric temperature when the engine is starting. If a biodiesel blend is used in the engine, unburned methyl esters are likely to condense on the DPF, possibly blocking the porous channels. This could cause excessive pressure drop requiring more frequent regeneration or worse, permanently reduce the effectiveness of the device.

A practical implication of the findings to laboratory applications is that FSN and the Christian Correlation (Christian et al., 1993) can be used to good accuracy for estimating the mass of soot even at the low end of the smoke instrument's measurement range. Since a smoke meter is a commonly used instrument in testing of diesel engines, this result improves the level of confidence in reporting soot mass emissions data.

7.4 Suggestions for Future Work

Often in research, answering a question leads to many more questions asked. Based on the work presented in this dissertation, some recommendations for future work can be made. First, more comprehensive data on PM emissions from diesel engines operating on

biodiesel should be collected at diverse operating conditions to more completely understand PM formation following dilution. A follow-on study could use design of experiments (DOE) methods to create a test plan with the goal of developing a correlation for the amount of biodiesel converting to the particulate phase.

In the recommended study, variables should include UHC in the undiluted exhaust, percent of biodiesel in the fuel, dilution ratio and PM filter collection temperature. More accurate measurement of gaseous fuel species in the undiluted exhaust should be made by increasing the sample line temperature to 250°C per the recommendation of Chang et al. (1998) both for the FID and the FT-IR to eliminate the possibility of condensation or adsorption of methyl esters before detection. A spectral calibration for methyl ester components and the actual petroleum diesel used in the study should be implemented for the FT-IR to more accurately measure the UHC composition during the study.

The model developed in this work should be improved to take into account adsorption, the other primary gas to particle conversion mechanism besides condensation. Together with the experimental data taken from the recommended study, a physics-based correlation could be realized to estimate the increase in PM mass as a function of percent biodiesel in the fuel, dilution ratio and temperature, and FSN. In the past, empirical correlations have been developed to estimate the increase in PM mass due to THC mass in the exhaust (Greeves and Wang, 1981). Modifications to those have been recently proposed to estimate the biodiesel contribution to the PM using neural network-based models fed with experimental data (Duran et al., 2006). These models, however accurate for the engines and fuels tested, are not based on physical mechanisms and therefore fall short of accurately predicting PM increase for a wide range of conditions.

Additional future work that can be recommended following the findings of this dissertation is to look more closely at the conversion of biodiesel though a DOC catalyst. Since the remaining methyl ester components from the engine exhaust have been shown to convert readily to PM, it would be interesting to more thoroughly quantify their conversion over an oxidation catalyst. Variables in the study should include catalyst inlet temperature, GHSV and biodiesel concentration. Other interesting trends alluded to in Chapter Six could also be explored including the increase in methane conversion through a DOC when biodiesel is present and the decrease in formaldehyde conversion.

Other studies that should be undertaken as a result of this work are to examine in more detail the effects of biodiesel condensation on EGR coolers and DPF reactors. Finally, the findings of this dissertation will hopefully inspire additional thought on research topics related to biodiesel combustion in engines.

REFERENCES

Agarwal, A. K. (2006). Biofuels (alcohols and biodiesel) applications as fuels for internal combustion engines. *Progress in Energy Science and Combustion , 33* (3), 233-271.

Akasaka, Y., Suzuki, T., & Sakurai, Y. (1997). Exhaust emissions of a DI diesel engine fueled with blends of biodiesel and low sulfur diesel fuel. *Society of Automotive Engineers* , Technical Paper 972998.

Akihama, K., Takatori, Y., Inagaki, K., Sasaki, S., & Dean, A. (2001). Mechanism of the smokeless rich diesel combustion by reducing temperature. *Society of Automotive Engineers* , Technical Paper 2001-01-0655.

Alam, M., Song, J., Zello, J., & Boehman, A. (2006). Spray and combustion visualization of a direct-injection diesel engine operated with oxygenated fuel blends. *Int. J. Engine Research , 7* (6), 503-521.

Bagley, S. T., Gratz, L. D., Johnson, J. H., & McDonald, J. F. (1998). Effects of an oxidation catalytic converter and a biodiesel fuel on the chemical, mutagenic, and particle size characteristics of emissions from a diesel engine. *Environ. Sci. Technol. , 32*, 1183-1191.

Baik, D. S., & Han, Y. C. (2005). The effect of biodiesel and ultra low sulfur diesel fuels on emissions in 11,000 cc heavy duty engine. *J. Mech. Sci. Tech. , 19* (3), 870-876.

Ballesteros, R., Hernandez, J. J., Lyons, L. L., Cabanas, B., & Tapia, A. (2008). Speciation of the semi-volatile hydrocarbon engine emissions from sunflower biodiesel. *Fuel , 87*, 1835-1843.

Birch, M. E., & Cary, R. A. (1996). Elemental carbon-based method for monitoring occupational exposures to particulate diesel exhaust. *Aerosol Science and Technology , 25* (3), 221-240.

Boehman, A. L., Song, J., & Alam, M. (2005). Impact of biodiesel blending on diesel soot and the regeneration of particulate filters. *Energy and Fuels , 19*, 1857-1864.

Bohac, S. V., Han, M., Jacobs, T. J., Lopez, A. J., Assanis, D. N., & Szymkowicz, P. G. (2006). Speciated hydrocarbon emissions from an automotive diesel engine and DOC utilizing conventional and PCI combustion. *Society of Automotive Engineers* , Technical Paper 2006-01-0201.

Bosch Automotive Handbook (5th Edition ed.). (2000). Robert Bosch GmBH.

Bozbas, K. (2008). Biodiesel as an alternative motor fuel: production and policies in the European Union. *Renewable and Sustainable Energy Reviews , 12*, 542-552.

Chang, D. Y., & Van Gerpen, J. H. (1998). Determination of particulate and unburned hydrocarbon emissions from diesel engines fueled with biodiesel. *Society of Automotive Engineers* , Technical Paper 982527.

Chauvanne, C. G. (1938). Belgian Patent 422,877 Aug. 31 1937. *Chem. Abs. , 32*, 4313.

Cheng, A. S., Upatnieks, A., & Mueller, C. J. (2007). Investigation of fuel effects on dilute, mixing controlled combustion in an optical direct-injection diesel engine. *Energy and Fuels , 21*, 1989-2002.

Cheng, A. S., Upatnieks, A., & Mueller, C. J. (2006). Investigation of the impact of biodiesel fuelling on NOx emissions using an optical direct injection diesel engine. *Int. J. Engine Research , 7*, 297-318.

Choi, C. Y., & Reitz, R. D. (1999). An experimental study in the effects of oxygenated fuel blends and multiple injection strategies on DI diesel engine emissions. *Fuel , 78*, 1303-1317.

Christian, V. R., Knopf, F., Jaschek, A., & Schneider, W. (1993). Eine neue messmethodik der Bosch-Zahl mit erhoehter empfindlichkeit. *Motortechnische Zeitschrift , 54* (1), 16-22.

Clerc, J. C., & Johnson, J. H. (1982). A computer heat transfer and hydrocarbon adsorption model for predicting diesel particulate emissions in dilution tunnels. *Society of Automotive Engineers* , Technical Paper 821218.

Colban, W. F., Miles, P., & Oh, S. (2007). On the cyclic variability and sources of unburned hydrocarbon emission in low temperature diesel combustion systems. *Society of Automotive Engineers* , Technical Paper 2007-01-1837.

Cook, D. J., Pitsch, H., & Nentwig, G. (2008). Numerical investigation of unburnt hydrocarbon emissions in a homogeneous-charge late-injection diesel-fueled engine. *Society of Automotive Engineers* , Technical Paper 2008-01-1666.

Correa, S. M., & Arbilla, G. (2006). Aromatic hydrocarbons emissions in diesel and biodiesel exhaust. *Atm. Environment* , 6821-6826.

Cummins, L. C. (1989). *Internal Fire.* Society of Automotive Engineers.

Curran, H. P., Gaffuri, P., Pitz, W. J., & Westbrook, C. K. (2002). A comprehensive modeling study of n-heptane oxidation. *Combustion and Flame , 129*, 253-280.

D'Alleva, B. A., & Lovell, W. G. (1936). Relation of exhaust gas composition to air-fuel ratio. *SAE Journal* , 90-97.

de Lucas, A., Duran, A., Carmona, M., & Lapuerta, M. (1999). Characterization of soluble organic fraction in DPM: optimization of the extraction method. *Society of Automotive Engineers* , Technical Paper 1999-01-3532.

Dec, J. A. (1997). A conceptual model of D.I. diesel combustion based on laser sheet imaging. *Society of Automotive Engineers* , Technical Paper 970873.

Depcik, C., Jacobs, T. J., Hagena, J., & Assanis, D. N. (2005). Instructional use of a single zone, pre-mixed spark-ignition heat release simulation. *Int. J. Mechanical Engineering Education* .

Diesel, R. (1897). *Diesel's Rational Heat Motor.* Progressive Age Publishing.

Dobbins, R. A., Fletcher, R. A., Benner, B. A., & Hoeft, S. (2006). Polycyclic aromatic hydrocarbons in flames, in diesel fuel, and in diesel emissions. *Combustion and Flame , 144*, 773-781.

Duran, A., Monteagudo, J. M., Armas, O., & Hernandez, J. J. (2006). Scrubbing effect on diesel particulate matter from transesterified waste oil blends. *Fuel , 85*, 923-928.

Eastwood, P. (2008). *Particulate Emissions from Vehicles.* John Wiley and Sons.

EPA. (2009). *EPA proposes new regulations for the national renewable fuel standard program for 2010 and beyond*. Retrieved from US-EPA: http://www.epa.gov/otaq/renewablefuels/420f09023.htm

Fang, T., Lin, Y.-C., Foong, T. M., & Lee, C. F. (2008). Spray and combustion visualization in an optical HSDI diesel engine operated in low-temperature combustion mode with bio-diesel and diesel fuels. *Society of Automotive Engineers* , Technical Paper 2008-01-1390.

Fargione, J., Hill, J., Tilman, D., Polasky, S., & Hawthorne, P. (2008). Land clearing and the biofuel carbon debt. *Science , 319* (5867), 1235-1238.

Farrauto, R. J., & Beasley, D. E. (1996). Monolithic diesel oxidation catalysts. *Applied Catalysis B:Environmental , 10*, 29-51.

Figliola, R., & Beasley, D. (2000). *Theory and design for mechanical measurements* (3rd Edition ed.). New York: John Wiley and Sons.

Frank, B. P., Tang, S., Lanni, T., Grygas, J., Rideout, G., Meyer, N., et al. (2007). The effect of fuel type and aftertreatment method on ultrafine particule emissions from a heavy-duty diesel engine. *Aerosol Science and Technology , 41* (11), 1029-1039.

Funkenbusch, E. F., Leddy, D. G., & Johnson, J. H. (1979). The characterization of the soluble organic fraction of diesel particulate matter. *Society of Automotive Engineers* , Technical Paper 790418.

Gail, S., Sarathy, S. M., Thomson, M. J., Dievart, P., & Dagaut, P. (2008). Experimental and chemical kinetic modeling of small methyl esters oxidation: methyl (E)-2-butenoate and methyl butanoate. *Combustion and Flame , 155*, 635-650.

Genzale, C. L., Reitz, R. D., & Musculus, M. P. (2009). Effects of spray targeting on mixture development and emissions formation in late-injection low-temperature heavy-duty diesel combustion. *Proc. Combustion Institiute , 32*, 2767-2774.

Gonzalez, D. M., Piel, W., Asmus, T., Clark, W., Garbak, J., Liney, E., et al. (2001). Oxygenates screening for advances petroleum-based diesel fuels: part 2. the effect of oxygenate blending compounds on exhaust emissions. *Society of Automotive Engineers* , Technical Paper 2001-01-3632.

Greeves, G., & Wang, C. H. (1981). Origins of diesel particulate mass emission. *Society of Automotive Engineers* , Technical Paper 810260.

Grosjean, D. (1975). Solvent extraction and organic carbon determination in atmospheric particulate matter: the organic extraction-organic carbon analyzer (OE-OCA) technique. *Analytical Chemistry , 47* (6), 797-805.

Grosjean, D. (1975). Solvent extraction and organic carbon determination in atmospheric particulate matter: the organic extraction-organic carbon analyzer (OE-OCA) technique. *Analytical Chemistry , 47* (6), 797-805.

Gulder, O., Glavincevski, B., & Burton, G. (1985). Ignition quality rating methods for diesel fuels - a critical appraisal. *Society of Automotive Engineers* , Technical Paper 852080.

Han, M., Assanis, D. N., & Bohac, S. V. (2009). Sources of hydrocarbon emissions from low-temperature premixed compression ignition combustion from a common-rail direct injection diesel engine. *Combustion Science and Technology , 181*, 496-517.

Han, M., Assanis, D. N., Jacobs, T. J., & Bohac, S. V. (2008). Method and detailed analysis of individual hydrocarbon species from diesel combustion modes and diesel oxidation catalyst. *J. Eng. Gas Turbines and Power , 130*.

Hansen, K. F., & Jensen, M. G. (1997). Chemical and biological characteristics of exhaust emissions from a DI diesel engine fuelled with rapeseed oil methyl ester (RME). *Society of Automotive Engineers* , Technical Paper 971689.

Hardy, W. L., & Reitz, R. D. (2006). A study of the effects of high EGR, high equivalence ratio, and mixing time on emissions in a heavy-duty diesel engine for PCCI combustion. *Society of Automotive Engineers* , Technical Paper 2006-01-0026.

Haynes, B. S., & Wagner, H. G. (1981). Soot formation. *Prog. Energy Sci. Combustion , 7*, 229-273.

Herbinet, O., Pitz, W. J., & Westbrook, C. K. (2008). Detailed chemical kinetic oxidation mechanism for a biodiesel surrogate. *Combustion and Flame , 154*, 507-528.

Heywood, J. B. (1988). *Internal Combustion Engine Fundamentals.* New York: McGraw-Hill.

Higgins, B., Siebers, D. L., & Aradi, A. (2000). Diesel-spray ignition and premixed-burn behavior. *Society of Automotive Engineers* , Technical Paper 2000-01-0940.

Hinds, W. C. (1999). *Aerosol Technology.* John Wiley and Sons.

Hoenberg, G. (1979). Advanced approaches for heat transfer calculations. *Society of Automotive Engineers* , Technical Paper 790825.

Huynh, L. K., & Violi, A. (2008). Thermal decomposition of methyl butanoate: ab initio study of a biodiesel fuel surrogate. *J. Organic Chem. , 73*, 94-101.

Ickes, A. M., Assanis, D. N., & Bohac, S. V. (2009). Load limits with fuel effects of a premixed diesel combustion mode. *Society of Automotive Engineers* , Technical Paper 2009-01-1972.

Ickes, A. M., Bohac, S. V., & Assanis, D. N. (2009). Effect of fuel cetane number on a premixed diesel combustion mode. *Int. J. Engine Research , 10*, 251-263.

Jacobs, T. J., & Assanis, D. N. (2007). The attainment of premixed compression ignition low-temperature combustion in a compression ignition direct injection engine. *Proc. Combustion Institute , 31*, 2913-2920.

Jacobs, T. J., Bohac, S. V., Assanis, D. N., & Szymkowicz, P. G. (2005). Lean and rich premixed compression ignition combustion in a light-duty diesel engine. *Society of Automotive Engineers* , Technical Paper 2005-01-0166.

Jacobs, T. J., Knafl, A., Bohac, S. V., Assanis, D. N., & Szymkowicz, P. G. (2006). The development of throttled and unthrottled PCI combusiton in a light-duty diesel engine. *Society of Automotive Engineers* , Technical Paper 2006-01-0202.

Jacobs, T. (2005). *Simultaneous Reduction of Nitric Oxide and Particulate Matter Emissions from a Light-Duty Diesel Engine Using Combustion Development and Diesel Oxidation Catalyst.* Dissertation, University of Michigan, Ann Arbor, MI.

Jacobson, M. Z., Kittleson, D. B., & Watts, W. F. (2005). Enhanced coagulation due to evaporation and its effect on nanoparticle evolution. *Environ. Sci. Technol. , 39*, 9486-9492.

Jung, H., Kittleson, D. B., & Zachariah, M. R. (2006). Characteristics of SME biodiesel-fueled particulate emissions and the kinetics of oxidation. *Env. Science and Technology , 40*, 4949-4955.

Kamijo, M., Kamikubo, M., Akama, H., & Matsushita, K. (2001). Study of an oxidation catalyst system for diesel engine control utilizing HC adsorption. *JSAE Review , 22*, 277-280.

Kamimoto, T., & Bae, M. (1988). High combustion temperature for the reduction of particulate in diesel engines. *Society of Automotive Engineers* , Technical Paper 880423.

Karavalakis, G., Stournas, S., Fontaras, G., Samaras, Z., Dedes, G., & Bakeas, E. (2009). The effect of biodiesel on PAHs, nitro-PAHs and oxy-PAHs emissions from a light vehicle operated over the European and Artemis driving cycles. *Society of Automotive Engineers* , Technical Paper 2009-01-1895.

Karra, K. K., Veltman, M. K., & Kong, S.-C. (2008). Characteristics of engine emissions using biodiesel blends in low-temperature combustion regimes. *Energy and Fuels , 22*, 3763-3770.

Kashdan, J. T., Mendez, S., & Bruneaux, G. (2007). On the origin of unburned hydrocarbon emissions in a wall guided, low NOx diesel combustion system. *Society of Automotive Engineers* , Technical Paper 2007-01-1836.

Kashdan, J., Mendez, S., & Bruneaux, G. (2008). An investigation of unburned hydrocarbon emissions in wall guided, low temperature diesel combustion. *Oil and Gas Science and Tech. , 63* (4), 433-459.

Kennedy, I. M. (1997). Models of soot formation and oxidation. *Prog. Energy and Comb. Sci. , 23*, 95-132.

Kimura, S., Aoki, O., Kithara, K., & Aiyoshizawa, E. (2001). Ultra-clean combustion technology combining a low-temperature and premixed combustion concept for meeting future emissions standards. *Society of Automotive Engineers* , Technical Paper 2001-01-0200.

Kimura, S., Aoki, O., Ogawa, H., Muranaka, S., & Enomoto, Y. (1999). New combustion concept for ultra-clean and high-efficiency small DI engines. *Society of Automotive Engineers* , Technical Paper 1999-01-3681.

Kimura, S., Ogawa, H., Matsui, Y., & Enomoto, Y. (2002). An experimental analysis of low-temperature and premixed combustion for simultaneous reduction of NOx and particulate emissions in direct injection diesel engines. *Int. J. Engine Research , 3* (4), 249-259.

Kitamura, T., Ito, T., Senda, J., & Fujimoto, H. (2002). Mechanism of smokeless diesel combustion with oxygenated fuels based on the dependency of the equivalence ratio and temperature on soot particle formation. *Int. J. Engine Research , 3* (4), 223-247.

Kittleson, D. B. (1998). Engines and nanoparticles: a review. *J. Aerosol Sci. , 29* (5/6), 575-588.

Knafl, A., Han, M., Bohac, S. V., Assanis, D. N., & Szymkowicz, P. (2007). Comparison of diesel oxidation catalyst performance on an engine and a gas flow reactor. *Society of Automotive Engineers* , Technical Paper 2007-01-0231.

Knafl, A., Jacobs, T. J., Bohac, S. V., & Assanis, D. N. (2006). The load limits of low temperature premixed compression ignition diesel combustion. *ISCE 2006, The 2nd International Symposium on "Clean and High-Efficiency Combustion in Engines".*

Knothe, G. (2001). Historical perspectives on vegatable oil-based diesel fuels. *Inform , 12*, 1103-1107.

Knothe, G. (2005). *The biodiesel handbook.* Urbana, IL: AOCS Press.

Knothe, G. (2005). The lubricity of biodiesel. *Society of Automotive Engineers* , Technical Paper 2005-01-3672.

Koci, C. P., Ra, Y., Krieger, R., Andrie, M., Foster, D. E., Siewert, R. M., et al. (2009). Detailed unburned hydrocarbon investigations in a highly-dilute diesel low temperature combustion regime. *Society of Automotive Engineers* , Technical Paper 2009-01-0928.

Kook, S., & Bae, C. (2005). The influence of charge dilution and injection timing on low-temperature diesel combustion and emissions. *Society of Automotive Engineers* , Technical Paper 2005-01-3837.

Krieger, R., & Borman, G. (1966). The computation of apparent heat release for internal combustion engines. *American Society of Mechanical Engineers* , Technical Paper 66-WA/DGP-4.

Lachaux, T., & Musculus, M. (2007). In-cylinder unburned hydrocarbon visualization during low-temperature compression-ignition engine combustion using formaldehyde PLIF. *Proc. Combustion Institute , 31*, 2921-2929.

Lapuerta, M., Armas, O., & Rodriguez-Fernandez, J. (2008). Effect of biodiesel fuels on diesel engine emissions. *Prog. Energy and Combustion Science , 34*, 198-223.

Lapuerta, M., Ballesteros, R., & Rodriguez-Fernandez, J. (2007). Thermogravimetric analysis of diesel particulate matter. *Measurement Sci. Tech. , 18*, 650-658.

Lapuerta, M., Hernandez, J. J., Ballesteros, R., & Duran, A. (2003). Composition and size of diesel particulate emissions from a commercial European engine tested with present and future fuels. *Proc. Instn. Mech. Eng., Part D: J. Automobile Engineering , 217*, 907-919.

Last, R. J., Kruger, M., & Durnholz, M. (1995). Emissions and performance characteristics of a 4-stoke, direct injected diesel engine fueles with blends of biodiesel and low sulfur diesel fuel. *Society of Automotive Engineers* , Technical Paper 950054.

Lea-Langton, A., Li, H., & Andrews, G. E. (2009). Investigation of aldehyde and VOC emissions during cold start and hot engine operations using 100% biofuels for a DI engine. *Society of Automotive Engineers* , Technical Paper 2009-01-1515.

Lechner, G. A., Jacobs, T. J., Chryssakis, C. A., Assanis, D. N., & Siewert, R. M. (2005). Evaluation of a narrow spray cone angle, advanced injection timing strategy to achieve partially premixed compression ignition combustion in a diesel engine. *Society of Automotive Engineers* , Technical Paper 2005-01-0167.

Lewis, S. A., Storey, J. M., Bunting, B., & Szybist, J. P. (2005). Partial oxidation products and other hydrocarbon species in diesel HCCI exhaust. *Society of Automotive Engineers* , Technical Paper 2005-01-3737.

Majewski, A. W., & Khair, M. K. (2006). *Diesel emissions and their control.* SAE International.

Martinot, S., Beard, P., Roesler, J., & Garo, A. (2001). Comparison and coupling of homogeneous reactor and flamelet library soot modeling approaches for diesel combustion. *Society of Automotive Engineers* , Technical Paper 2001-01-3684.

McGill, R., Storey, J., Wagner, R., Irick, D., Aakko, P., Westerholm, M., et al. (2003). Emission performance of selected biofuel blends. *Society of Automotive Engineers* , Technical Paper 2003-01-1866.

McNair, H. M., & Miller, J. M. (1997). *Basic Gas Chromotography.* John Wiley and Sons.

Merritt, P., Huang, Y., Khair, M., & Pan, J. (2006). Unregulated exhaust emissions from alternate combustion modes. *Society of Automotive Engineers* , Technical Paper 2006-01-3307.

Miyamoto, N., Ogawa, H., Nurun, N. M., Obata, K., & Teruyoshi, A. (1998). Smokeless, low NOx, high thermal efficiency, and low noise diesel combustion with oxygenated agents as main fuel. *Society of Automotive Engineers* , Technical Paper 980506.

Mogi, H., Tajima, K., Hosoya, M., & Shimoda, M. (1999). The reduction of diesel engine emissions by using the oxidation catalysts of Japan diesel 13 mode cycle. *Society of Automotive Engineers* , Technical Paper 1999-01-0471.

Monyem, A., & Van Gerpen, J. H. (2001). The effect of biodiesel oxidation on engine performance and emissions. *Biomass and Bioenergy , 20*, 317-325.

Morlang, A., Neuhausen, U., Klementiev, K. V., Schutze, F. W., Miehe, G., Fuess, H., et al. (2005). Bimetallic Pt/Pd diesel oxidation catalysts structural characterization and catalytic behavior. *Applied Catalysis B:Environmental , 60*, 191-199.

Mueller, C. J., Pitz, W. J., Pickett, L. M., Martin, G. C., Siebers, D. L., & Westbrook, C. K. (2003). Effects of oxygenates on soot processes in DI diesel engines: experiments and numerical simulations. *Society of Automotive Engineers* , Technical Paper 2003-01-1791.

Musculus, M. P., Lachaux, T., Pickett, L. M., & Idecheria, C. A. (2007). End-of-injection over-mixing and unburned hydrocarbon emissions in low-temperature-combustion diesel engines. *Society of Automotive Engineers* , Technical Paper 2007-01-0907.

Musculus, M., Pickett, L., & Mikes, P. (2009). In-Cylinder Processes of EGR-Diluted Low-Load, Low-Temperature Diesel Combustion. *DEER - 2009, 15th Directions in Engine Efficiency and Emissions Reduction Research.*

Northrop, W. F., Bohac, S. V., & Assanis, D. N. (2009). Premixed low temperature combustion of biodiesel and blends in a high speed compression ignition engine. *Society of Automotive Engineers* , Technial Paper 2009-01-0133.

Northrop, W. F., Jacobs, T. J., Assanis, D. N., & Bohac, S. V. (2007). Deactivation of a diesel oxidation catalyst due to the exhaust species from rich premixed compression ignition combustion in a light-duty diesel engine. *Int. J. Engine Res. , 8*, 497-498.

Northrop, W. F., Vanderpool, L. M., Madathil, P. V., Assanis, D. N., & Bohac, S. V. (2009). Investigation of hydrogen emissions in partially premixed diesel combustion. *ICEF 2009, Proceedings of the ASME International Internal Combustion Engines Division 2009 Fall Technical Conference.* Lucerne, Switzerland.

Otto, K., Sieg, M. H., Zinbo, M., & Bartosiewicz. (Society of Automotive Engineers). *The oxidation of soot deposits from diesel engines.* 1980: Technical Paper 800336.

Otto, K., Sieg, M. H., Zinbo, M., & Bartosiewicz, L. (1980). The oxidation of soot deposits from diesel engines. *Society of Automotive Engineers* , Technical Paper 800336.

Palmen, N. (2007). *Diesel powering ahead.* Retrieved from bNet: http://findarticles.com/p/articles/mi_m3012/is_1_186/ai_n31061273/

Patterson, J., Hassan, M. G., Clarke, A., Shama, G., Hellgardt, K., & Chen, R. (2006). Experimental study of DI diesel engine performance using three different biodiesel fuels. *Society of Automotive Engineers* , Technical Paper 2006-01-0234.

Payri, F., Bermudez, V. R., Tormos, B., & Linares, W. G. (2009). Hydrocarbon emissions speciation in diesel and biodiesel exausts. *Atmospheric Environment , 43*, 1273-1279.

Peng, C.-Y., Yang, H.-H., Lan, C.-H., & Chien, S.-M. (2008). Effects of the biodiesel blend fuel on aldehyde emissions from diesel engine exhaust. *Atmospheric Environment , 42*, 906-915.

Peterson, A., Lee, P.-I., Lai, M.-C., Wu, M.-C., & Dimaggio, C. (2009). Impact of biodiesel emission products from a multi-cylinder direct injection diesel engine on

particulate filter performance. *Society of Automotive Engineers* , Technical Paper 2009-01-1184.

Plee, S. L., & MacDonald, S. J. (1980). Some mechanisms affecting the mass of diesel exhaust particulate collected following a dilution process. *Society of Automotive Engineers* , Technical Paper 800186.

Plee, S. L., Ahmad, T., & Myers, J. P. (1981). Flame temperature correlation for the effects of exhaust gas recirculation on diesel particulate and NOx emissions. *Society of Automotive Engineers* , 811195.

Polynuclear aromatic compounds part 1: chemical, environmental, and experimental data. (1983). *IARC Monogr. Eval. Carcinog. Risk Humans , 32*.

Purcell, D. L., McClure, B. T., McDonald, J., & Basu, H. N. (1996). Transient testing of soy methyl ester fuels in an indirect injection, compression ignition engine. *JOACS* , 381-388.

Ragauskas, A. J., Williams, C. K., Davison, B. H., Britovsek, G., Cairney, J., Eckert, C. A., et al. (2006). A path forward for biofuels and biomaterials. *Science , 311*, 484-489.

Rakopoulos, C. D., Hountakas, D. T., Zannis, T. C., & Levendis, Y. A. (2004). Operational and environmental evaluation of diesel engines burning oxygen-enriched intake air or oxygen-enriched fuels: a review. *Society of Automotive Engineers* , Technical Paper 2004-01-2924.

Rhead, M. M., & Hardy, S. A. (2003). The sources of polycyclic aromatic compounds in diesel engine emissions. *Fuel , 82*, 385-393.

Scanlon, J. T., & Willis, D. E. (1985). The calculation of FID response factors using the effective carbon number concept. *J. Chromatographic Sci. , 23*, 333-340.

Scholl, K. W., & Sorenson, S. C. (1993). Combustion of soybean methyl ester in a direct injection diesel engine. *Society of Automotive Engineers* , Technical Paper 930934.

Seaton, A., MacNee, W., Donaldson, K., & Godden, D. (1995). Particulate pollution and acute health effects. *The Lancet , 345*, 176-178.

Seinfeld, J. H., & Pandis, S. N. (1998). *Atmospheric Chemistry and Physics.* John Wiley and Sons.

Senatore, A., & Cardone, M. (2000). A comparative analysis of combustion process in D.I. diesel engine fueled with biodiesel and diesel fuel. *Society of Automotive Engineers* , Technical Paper 2000-01-0691.

Sharp, C. A., Howell, S. A., & Jobe, J. (2000). The effect of biodiesel fuels on transient emissions from modern diesel engines, part I regulated emissions and performance. *Society of Automotive Engineers* , Technical Paper 2000-01-1967.

Shimazaki, N., Minato, A., & Nishimura, T. (2007). Premixed diesel combustion using direct injection near top dead center. *Int. J. Engine Research* , 259-270.

Siebers, D. L. (1985). Ignition delay characteristics of alternative diesel fuels: implications on cetane number. *Society of Automotive Engineers* , Technical Paper 852102.

Sluder, S. C., Wagner, R. M., Lewis, S. A., & Storey, J. M. (2004). Exhaust chemistry of low-NOx, low-PM diesel combustion. *Society of Automotive Engineers* , Technical Paper 2004-01-0114.

Solomon, S., Qin, D., Manning, M., Chen, M., Marquis, M., Averyt, B., et al. (2007). *Climate Change 2007: The Physical Science Basis.* Cambridge, UK and New York, NY, USA: Cambridge University Press.

Song, J., Alam, M., Boehman, A. L., & Kim, U. (2006). Examination of the oxidation behavior of biodiesel soot. *Combustion and Flame , 146*, 589-604.

Stanmore, B., Brilhac, J. F., & Gilot, P. (2001). The oxidation of soot: a review of experiments, mechanisms, and models. *Carbon , 39*, 2247-2268.

Stein, H. J. (1996). Diesel oxidation catalysts for commercial vehicle engines: strategies on their application for controlling particulate emissions. *Applied Catalysis B:Environmental , 10*, 69-82.

Stivender, D. L. (1971). Development of a fuel-based mass emission measurement procedure. *Society of Automotive Engineers* , Technical Paper 710604.

Szybist, J. P., Boehman, A. L., Haworth, D. C., & Koga, H. (2007). Premixed ignition behavior of alternative diesel. *Combustion and Flame , 149*, 112-128.

Szybist, J. P., Boehman, A. L., Taylor, J. D., & McCormick, R. L. (2005). Evaluation of formulation strategies to eliminate the biodiesel NOx effect. *Fuel Processing Technology , 86*, 1109-1126.

Szybist, J., Simmons, J., Druckenmiller, M., Al-Qurashi, K., Boehman, A., & Scaroni, A. (2003). Potential methods for NOx reduction from biodiesel. *Society of Automotive Engineers* , Technical Paper 2003-01-3205.

Tat, M. E., Soylu, M., Canckci, M., Monyem, A., & Wormley, S. (2000). The speed of sound and isentropic bulk modulus of biodiesel at 21 degrees C from atmospheric pressure to 35 kPa. *Am. Oil Chem. Soc. , 77* (3), 285-289.

The Official Site of the National Biodiesel Board. (2009). Retrieved from RFS2 Action Center: http://www.biodiesel.org

Theinnoi, K., Rounce, A., Tsolakis, A., Wyszynski, M. L., Xu, H. M., & York, A. P. (2008). Activity of prototype catalysts on exhuast emissions from biodiesel fuelled engines. *Society of Automotive Engineers* , Technical Paper 2008-01-2514.

Thornton, M. J., Alleman, T. L., Luecke, J., & McCormick, R. L. (2009). Impacts of biodiesel fuel blends oil dilution on light-duty diesel engine operation. *Society of Automotive Engineers* , Technical Paper 2009-01-1790.

Tsolakis, A. (2006). Effects on particle size distribution from the diesel engine operating on RME-biodiesel with EGR. *Energy and Fuels , 20,* 1418-1424.

Turns, S. R. (1996). *An Introduction to Combustion.* McGraw-Hill.

U.S. Product Supplied for Crude Oil and Petroleum Products. (2009). Retrieved from Energy Information Administration: http://tonto.eia.doe.gov/dnav/pet/pet_cons_psup_dc_nus_mbbl_m.htm

Ulberth, F., Gabernig, R. G., & Schrammel, F. (1999). Flame-ionization detector response to methyl, ethyl, propyl, and butyl esters of fatty acids. *J. Am. Org. Chem. Society , 76* (2), 263-266.

Upatnieks, A., & Mueller, C. J. (2004). Investigationo of the relationship between DI diesel combustion processes and engine-out soot using an oxygenated fuel. *Society of Automotive Engineers* , Technical Paper 2004-01-1400.

Walker, A. P. (2004). Controlling particulate emissions from diesel vehicles. *Topics in Catalysis , 28* (1-4), 165-170.

Wall, J. C., & Hoekman, S. K. (1984). Fuel composition effects on heavy-duty diesel particulate emissions. *Society of Automotive Engineers* , Technical Paper 841364.

Walton, J. (1938). The fuel possibilities of vegatable oils. *Gas Oil Power , 33,* 167-168.

Wang, H., & Frenklach, M. (1997). A detailed kinetic modeling study of aromatics formation in laminar premixed acetylene and ethylene flames. *Combustion and Flame , 110,* 173-221.

Westbrook, C. K., & Dryer, F. L. (1884). Chemical kinetic modeling of hydrocarbon combustion. *Prog. Energy and Combustion Science , 10,* 1-57.

Yaws, C. L. (2003). *Yaws' handbook of thermodynamic and physical properties of chemical compounds.* Knovel.

Yuan, W., Hansen, A. C., & Zhang, Q. (2003). Predicting the physical properties of biodiesel for combustion modeling. *Transactions of the ASAE , 46* (6), 1487-1493.

Yuan, W., Hansen, A. C., & Zhang, Q. (2005). Vapor pressure and normal boiling point predictions for pure methyl esters and biodiesel fuels. *Fuel , 84,* 943-950.

Zelenka, P., Ostgathe, K., & Lox, E. (1990). Reduction of diesel exhaust emissions by using oxidation catalysts. *Society of Automotive Engineers* , Technical Paper 902111.

Zhang, Y., & Van Gerpen, J. H. (1996). Combustion analysis of esters of soybean oil in a diesel engine. *Society of Automotive Engineers* , Technical Paper 960765.

Zheng, M., Han, X., Tan, Y., Kobler, M. S., Ko, S.-J., Wang, M., et al. (2008). Low temperature combustion of neat biodiesel fuel on a common-rail diesel engine. *Society of Automotive Engineers* , Technical Paper 2008-01-1396.

Zheng, M., Mulenga, M. C., Reader, G. T., Tan, Y., Wang, M., & Tjong, J. (2007). Neat biodiesel fuel engine tests and preliminary modeling. *Society of Automotive Engineers* , Technical Paper 2007-01-0616.

Zheng, M., Mulenga, M. C., Reader, G. T., Wang, M., & Ting, D. S.-K. (2006). Influence of biodiesel fuel on diesel engine performance and emissions in low temperature combustion. *Society of Automotive Engineers* , Technical Paper 2006-01-3281.